

This is an electronic reprint of the original article.

This reprint *may differ* from the original in pagination and typographic detail.

Author(s): Anuj Kumar, Tuula Jyske and Marko Petrič

Title: Delignified Wood from Understanding the Hierarchically Aligned Cellulosic Structures to Creating Novel Functional Materials: A Review

Year: 2021

Version: Published version

Copyright: The Author(s) 2021

Rights: CC BY 4.0

Rights url: <http://creativecommons.org/licenses/by/4.0/>

Please cite the original version:

Kumar, A., Jyske, T., Petrič, M., Delignified Wood from Understanding the Hierarchically Aligned Cellulosic Structures to Creating Novel Functional Materials: A Review. *Adv. Sustainable Syst.* 2021, 2000251. <https://doi.org/10.1002/adsu.202000251>

All material supplied via *Jukuri* is protected by copyright and other intellectual property rights. Duplication or sale, in electronic or print form, of any part of the repository collections is prohibited. Making electronic or print copies of the material is permitted only for your own personal use or for educational purposes. For other purposes, this article may be used in accordance with the publisher's terms. There may be differences between this version and the publisher's version. You are advised to cite the publisher's version.

Delignified Wood from Understanding the Hierarchically Aligned Cellulosic Structures to Creating Novel Functional Materials: A Review

Anuj Kumar,* Tuula Jyske, and Marko Petrič

Utilization of hierarchically aligned natural cellulosic structures has become a leading natural template scaffold for a diverse range of functional applications. This natural scaffold derived from wood by partial or full removal of lignin without altering or disturbing the hierarchically aligned cellulosic structure is known as delignified wood (DW). Over the past five years, various types of functional materials for diverse applications have been fabricated using DW. This review aims to highlight the significance of DW in functional material development by discussing the delignification impacts on the wood cell wall properties and review the different strategies used in functional materials fabrication. The first part of this review discusses the fundamental aspects of wood cell wall structure in relation to wood chemistry and lignin biosynthesis. The second part focuses on the different delignification methods used in partial and full lignin removal from wood cell walls and the fundamental properties (i.e., physical, mechanical, and chemical) of DW. The third part of this review discusses the strategies and the detailed current literature regarding the development of diverse functional materials based on DW. A greater understanding of DW provides the potential for further development of DW-based functional materials for a diverse range of future applications.

1. Introduction


The future of sustainable development depends on how humans will transfer their dependability from finite fossil-based materials to sustainable and renewable materials. Scalable assembly methods are and will be imperative in designing high

performance environmentally friendly materials. This is because new processes will be required that allow control on all hierarchical levels. Wood is well defined as a biological engineering material with a complex hierarchical structure of organic material based on cellulose fibrils embedded in a matrix of hemicelluloses and lignin.^[1,2] Wood has long been used as a construction material, as well as for pulp and paper production. These applications are highly dependent on the properties of lignin in wood. Removal of lignin is the key step in pulp and paper production, in addition to the conversion of biomass to liquid biofuels. Lignin was first discovered in wood by Anselme Payen in 1839,^[3] as the incrusting material that must be removed to isolate the useful fibers in wood. Research pertaining to wood nanotechnology or functional wood materials is a rapidly emerging field. Functional wood materials are mostly fabricated by treating hierarchical natural templates (wood cell wall) by chemical and thermal means. These treatments selectively modify the wood cell wall structure (fine pore spaces and inner lumen surface area) for different applications.^[4] The pore region and inner lumen surface have actively been modified to enhance the bulk properties of wood using organic chemicals,^[5] inorganic chemicals, organic–inorganic chemicals,^[6,7] and thermal methods.^[8] Hybrid wood scaffolds have been prepared for diverse applications such as magnetic wood,^[9,10] as well as wood–mineral and wood–metal hybrids.^[11]

Recent research on delignified wood (DW) has emerged from the classical pulp production method. In the preparation of DW, the embedded lignin is removed from the wood cell wall structure, while maintaining the natural hierarchical cellulosic structure.^[12] Initially, DW was prepared in order to understand the unknown ultrastructure of wood cell walls. However, since 2015, research in this area has rapidly expanded to focus on the development of wood-based functional scaffolds. Within the literature, DW is predominantly prepared using alkaline delignification methods such as Kraft pulping (a mixture of sodium hydroxide (NaOH) and sodium sulfite (Na₂SO₃)) heated to boiling temperature, followed by bleaching using hydrogen peroxide (H₂O₂) to remove the lignin. DW is chemically hydrophilic due to the presence and exposure of hydroxyl groups and possible sites for DW functionalization. DW scaffolds have been functionalized

Dr. A. Kumar, Dr. T. Jyske
 Natural Resources Institute Finland
 Production Systems
 Tietotie 2, Espoo 02150, Finland
 E-mail: anuj.kumar@luke.fi

Prof. M. Petrič
 Department of Wood Science and Technology
 Biotechnical Faculty
 University of Ljubljana
 Jamnikarjeva, 101, Ljubljana 1000, Slovenia

 The ORCID identification number(s) for the author(s) of this article can be found under <https://doi.org/10.1002/adsu.202000251>.

© 2021 The Authors. Advanced Sustainable Systems published by Wiley-VCH GmbH. This is an open access article under the terms of the Creative Commons Attribution License, which permits use, distribution and reproduction in any medium, provided the original work is properly cited.

DOI: 10.1002/adsu.202000251

for various applications such as transparent wood,^[13,14] high performance thermal insulators,^[15] energy generation systems,^[16] nanostructured wood membranes,^[17,18] carbonized wood nanocomposites,^[19] and other bioinspired woods.^[20]

In the last decade, regenerated cellulose materials have been thoroughly investigated. In particular, this research has focused on creating microcellulose and nanofibrillar cellulose-based components for functional applications such as packaging materials, optical/electrical devices, cellulose textiles, and wastewater treatment.^[21] Several recent review articles focused on the extraction, fabrication, and applications of cellulose and cellulose-based nanomaterials.^[21–33] Yang et al.^[34] recently published a review on ionic cellulose-based compounds with diverse functional moieties either along the cellulose chains or on the surface of nanocellulose for biomedical applications. Research on bioinspired and biomimetic wood-based nanotechnologies has mainly focused on harnessing hierarchical or naturally aligned cellulose for functional materials fabrication.^[32] Jiang et al.,^[35] Burgert et al.,^[36] and Berglund and Burgert^[37] have published review articles on functional material fabrication using aligned cellulose via chemical modification. These reviews presented several wood-based functional materials such as transparent wood, polymer infiltrated wood, superstrong wood, hybrid wood, water-based energy storage devices, and wastewater treatment materials. Li et al.^[13] published a review article focusing on recent progress (data collected up to 2017) regarding the opportunities and challenges in the fabrication and applications of optically transparent wood. Zhu et al.^[38] discussed the latest developments in the area of wood-based functional materials for electronic, biological, and energy storage device applications. In 2018, Huang et al.^[39] and Chen and Hu^[40] reviewed the potential applications of wood-based materials in electrochemical energy storage devices and many other areas.

In recent years, fabricating functional materials using DW has become an area of extensive research within the field of wood materials science and engineering. Consequently, this has led to significant progress in several bottom-up approaches. However, recent review articles have only briefly discussed DW-based functional materials (e.g., transparent wood)^[37,13] and their potential applications (e.g., membranes for electronics, biological applications, and wastewater treatments).^[24,35,39] Some other recent review articles have focused on environmentally friendly wood modifications,^[41] and wood–carbides composites,^[42] and other biopolymeric based processing of wood.^[43] Rongpipi et al.^[44] reviewed the latest developments and techniques used for cellulose characterization of structure and interactions of cellulose in plant cell walls, particularly cellulose crystallinity, microfibril size, and spatial organization along with cellulose–cellulose and cellulose–matrix interactions. The research on DW has progressed very significantly in the last five years. However, there is a need for systematic reviews that broaden the understanding of the scientific community and discuss all the latest developments in DW and its functional materials. A recent review article by Chen et al.^[45] focused on the material and structural perspectives on how wood can be redesigned via structural engineering. This involved the chemical and/or thermal modification of wood to alter its mechanical, fluidic, ionic, optical, and thermal properties. Furthermore, they reviewed the diverse applications of redesigned wood materials.

This review focuses on a wide range of relevant topics beginning with wood cell wall structure and chemistry, in addition to the lignification processes (see **Figure 1**). This is followed by reviewing the delignification processes and the impact of delignification on the basic properties of wood (physical, mechanical, chemical, and thermal) including wood cell wall microstructure. Further, this review covers the latest

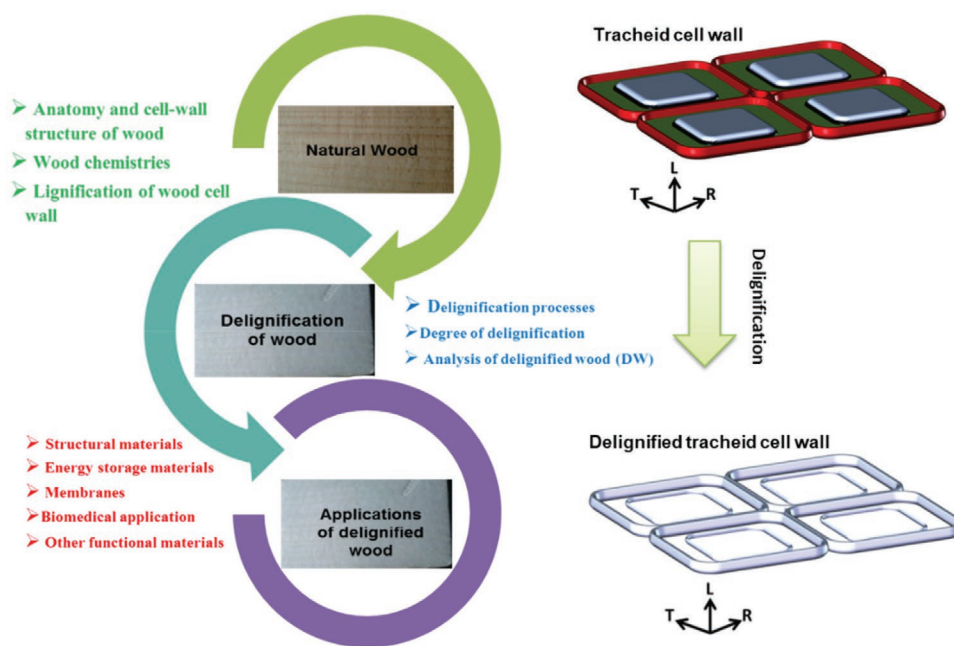


Figure 1. Schematic summary of the focus areas of this review, wherein we cover the current development and applications of DW, which has a hierarchical cellulosic structure. This review is divided into three main sections, which focus on native wood, the delignification process of wood, and the functional applications of DW.

developments of DW-based functional material applications such as transparent wood, bulk wood materials, membranes, thermal insulators, phase-change materials (PCMs), solar cells, tunable wood, self-luminous wood, superflexible wood, energy storage materials, wood to textile, and many more applications, where DW-based materials could replace synthetic plastics. Finally, we present the conclusions and prospects of DW-based functional material innovations.

2. Hierarchical Microstructure of Wood

2.1. Cell Wall Structure of Wood

2.1.1. Cell Wall Structure of Softwood Tracheids

As described in the previous section, tracheids are the main component of softwood. The tracheid wall comprises a middle lamella (ML), a primary wall, a multilayered secondary wall, and open lumen spaces as shown in **Figure 2**. The thickness of the cell walls varies with the wood species, in addition to the thickenings and depositions of the growth rings.^[2,46] ML is an intercellular amorphous region that primarily adheres the walls of neighboring cells together during the enlargement and differentiation of the cells. ML is composed of pectic compounds but gradually becomes highly lignified; the lignin has an important role as a cementing compound for cell wall structural stability.^[47] The outermost layer of tracheids primary cell wall is very thin (0.1–0.2 μm) but stronger in nature to withstand the tensile forces arising from turgor pressure, extensible to allow wall stress relaxation, which motivates cell water uptake and physical enlargement of the cell.^[48] It is difficult to distinguish between ML and the primary wall and thus, the layers are also known as compound middle lamella (CML). Random distribution of cellulose fibrils in the primary cell wall is a result of cell expansion during growth.^[49]

The secondary wall of softwood tracheids is formed after the primary wall formation and consists of three distinct layers

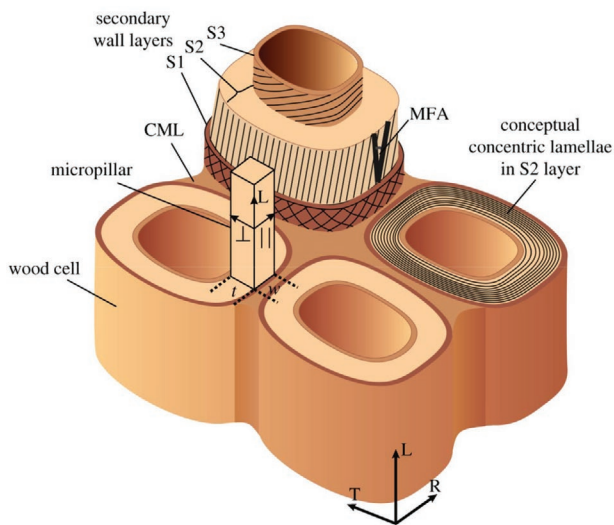


Figure 2. Schematic diagram of softwood cell wall layers. Reproduced with permission.^[51] Copyright 2014, the Royal Society.

(S_1 , S_2 , and S_3) with highly ordered cellulose microfibrils. The thicknesses of the S_1 , S_2 , and S_3 layers are 0.1–0.3, 1–5, and 0.1 μm , respectively. According to S–Z–S helical structure, the S_1 layer's cellulose microfibrils are arranged in the S-helix (transversely oriented microfibrils) between angles of 50° and 75° to the long axis of the cell. In the S_2 layer, the microfibrils are arranged in the Z-helix (axially oriented microfibrils) at angles of 10° – 30° . In the S_3 layer, the cellulose microfibrils form an S-helix at angles of 60° – 90° .^[49,50] The S_2 layer is considered to be the most important layer for providing structural properties to a living tree. It is also responsible for the strength properties of wood because it carries most of the axial loading in tracheids of softwood. The pits (small openings in the walls of adjacent cells) provide a passageway for water flow between the tracheids. The pits of softwood tracheids are bordered, which means that the secondary wall overarches the pit membrane. The tracheids have highly specialized pit membrane with central thickened torus and surrounding margo.^[49]

2.1.2. Cell Wall Structure of Hardwood Vessel Elements and Fibers

The fibers in hardwood are solely responsible for providing mechanical support to wood. Hardwood fibers are 0.2–1.2 mm in length and their lumens are smaller than those of softwood tracheids. The cell walls of hardwood fibers have a greater thickness compared those of softwood's earlywood tracheids. This is because the fibers do not conduct water, and thus their pits are also smaller in size compared to softwood. Some hardwood fibers differ from softwood tracheids in their ability to form an extra gelatinous wall layer as a substitute to a normal S_3 layer.^[49] The cell wall structure of hardwood vessels differs from that of softwood tracheids and hardwood fibers. Microfibrils in the S_2 layer form a Z-helix ($<90^\circ$) with average orientation varying from 1° to 59° among tracheids.^[52,53] It is postulated that this is an adaptation of the vessel structure due to internal water tension. Perforation plates enable end-to-end connections between the individual vessel elements to facilitate waterflow from cell-to-cell. In hardwood species, these interconnected vessel elements have been reported to form long pipeline structures up to several meters. Vessel elements also exhibit intervessel pitting, which facilitates long-distance water transportation.

2.1.3. Importance of Microfibril Orientation

In wood-based product manufacturing, the strength, stiffness, appearance, dimensional stability, and treatability of timber are important factors that affect both the processing and end-product properties. These characteristics, with respect to wood and cellular properties, are related to various factors such as the orientation of cellulose microfibrils (MFA) with respect to the longitudinal axis of the cell, wood density, spiral grain angle, proportions of juvenile and reaction wood, and growth stresses within wood. Juvenile wood typically has a higher MFA than mature wood, and consequently a high proportion of juvenile wood lowers the strength, stiffness, and dimensional stability of timber. Compression wood (i.e., reaction wood of conifers) is also characterized by a higher MFA than normal wood.

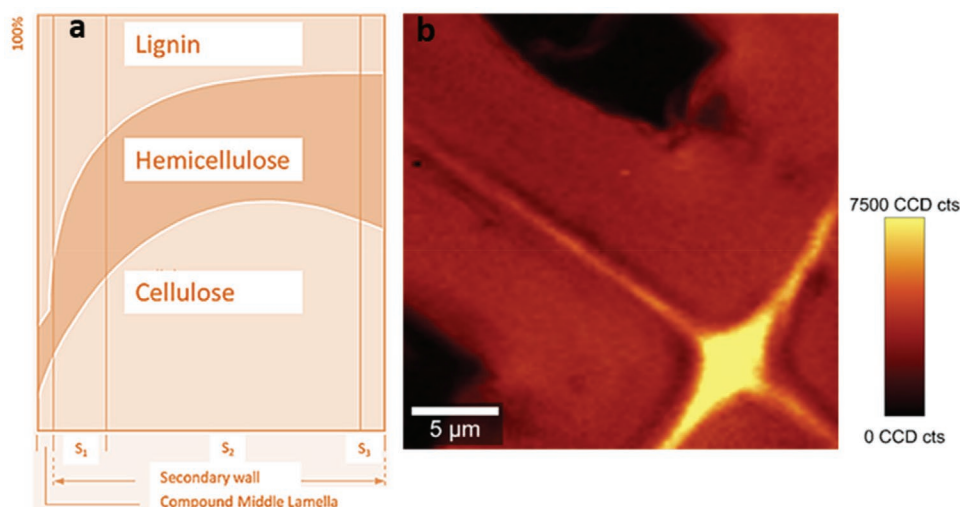


Figure 3. a) Distribution of the main biopolymers of wood within cell wall layers. This image is redrawn from Panshin and de Zeeuw.^[57] b) Confocal Raman spectrometry image of a cell wall (latewood tracheid in sapwood) of pine (*Pinus sylvestris* L.). The image is produced by integrating the spectrum in the wavenumber range 1550–1700 cm^{-1} . This spectral range contains strong lignin-derived bands. The image was captured using a WITec alpha 300 RA Raman microscope, using a 532 nm laser and 0.3 s integration time.

3. Chemical Composition of Wood

Wood is a complex 3D composite of biopolymers composed of an interconnected network of cellulose, hemicelluloses, and lignin, as well as various amounts of extractives and inorganics within different wood species.^[53,54] To fully comprehend the chemistry of wood, the location of the major chemical constituents of the wood cell walls must be first understood. **Figure 3a** schematically shows the location and distribution of the main chemical constituents of the tracheid cell wall of softwood composed of ML primary and secondary cell wall layers. **Figure 3b** shows the lignin distribution in cell wall mainly in the corners of ML. In primary and secondary walls, cellulose acts as a framing material. Cellulose microfibrils are arranged within a hemicellulose matrix, marginally covered by lignin, which acts as incrusting material. The intercellular regions between cell walls (i.e., ML) are composed of 70–80% lignin by weight and act as a cementing material to provide cell wall rigidity against growth stresses and other external loads.^[55] The elementary compositions of wood polymers are principally composed of carbon (≈ 49), hydrogen (≈ 6), and oxygen (≈ 44) on a dry weight basis.^[54] The chemical components of wood are mainly cellulose, hemicelluloses, and lignin, which comprise $\approx 40\%$, 15–35%, and 20–30% of the mass of wood, respectively.^[56]

3.1. Cellulose

Cellulose microfibrils form the structurally strong framework of the cell wall.^[58] This framework is embedded within the matrix polymers (hemicellulose and pectin) and encrusted with lignin. The pectin is located only in the ML and in the primary wall in regular cells. Cellulose provides high tensile strength for the cell wall. Cellulose is a linear polymer chain of β -D-glucose molecules linked together by β -(1-4) glycosidic bonds.^[59] Two bonded glucose molecules form an anhydroglucose unit, as

shown in **Figure 4**. The pair of units is called cellobiose, which is the repeating chemical entity of the cellulose polymer.^[60] Several chains of cellulose are linked by hydrogen bonding and van der Waals forces to form microfibrils, which include both crystalline and amorphous cellulose.^[61] Microfibrils are further combined to form larger fibrils and lamellae.

3.2. Hemicelluloses

Hemicelluloses are heteropolysaccharides that comprise various types of sugar units (see **Figure 4**).^[62] They are usually amorphous and branched-chain polymers that form the link between cellulose and lignin. Hemicelluloses permeate water and thus, provide flexibility and support in the cell wall. Galactoglucomannans and xylans are the main hemicelluloses in conifers.^[63]

3.3. Lignin

Lignin (from the Latin *lignum* that means wood) is a phenylpropanoid polymer present in the wood cell wall. It is primarily derived from three cinnamyl alcohols: *p*-coumaryl, coniferyl, and sinapyl alcohol (molecular structure in **Figure 4**) (termed monolignols).^[64–70] Lignin is a crucial structural component of secondarily thickened plant cell walls, which preserve structural integrity by providing stiffness and strength. This enables the transport of water and solutes through the tracheary elements in the vascular systems^[66] and provides a barrier against phytopathogens and environmental stresses.^[69] Lignin can either be defined chemically (i.e., chemical composition and structure of lignin) or functionally (i.e., the role of lignin within the plant).^[71]

The cell wall lignification has been a critical innovation in the evolution of terrestrial plants from aquatic ancestors over

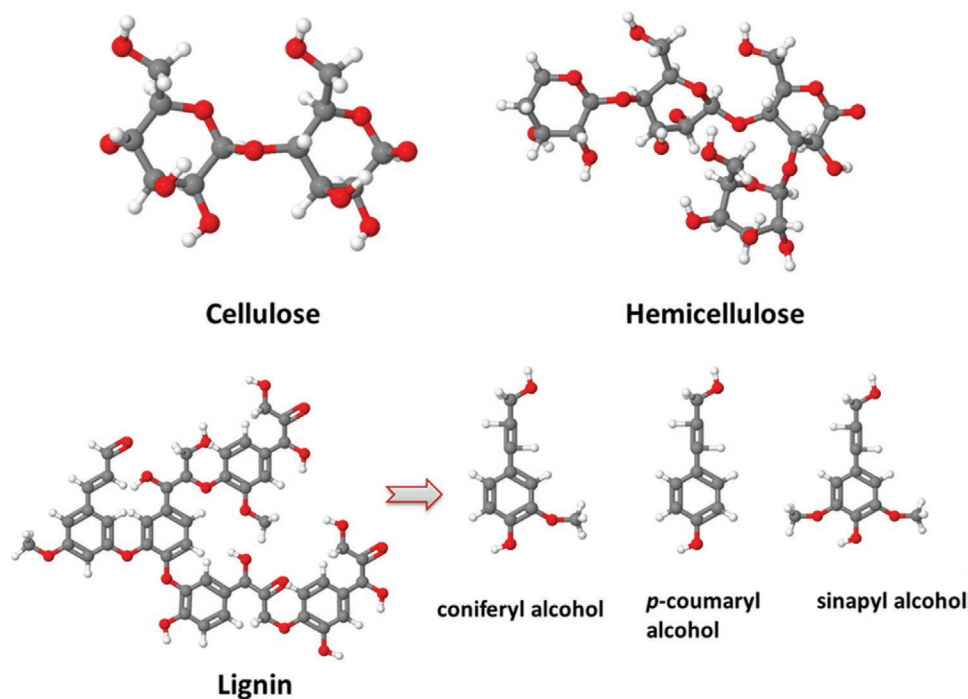


Figure 4. Molecular structure of wood biopolymers.

450 million years ago.^[72,73] According to biochemical understanding, lignin forms in the spaces between cellulose microfibrils by the oxidative coupling of free monolignols secreted directly into the plant cell wall.^[64,69,74–76] Lignification involves three stages: the biosynthesis of monolignols in the cytosol, their transportation to the cell wall, and their subsequent oxidative dehydrogenation, and polymerization to form the heterogeneous macromolecules.^[64,66,77] The inclusion of detailed lignification description is slightly diverting the main focus of present review; however, one can refer the old and latest review articles lignin biosynthesis in woody plants.^[69,70,78]

3.4. Chemical Interactions between Wood Biopolymers

The secondary wall of wood cells forms a laminated filamentary composite, in which cellulose molecules form the supporting network that is embedded within a matrix composed of hemicelluloses and lamellar lignin “sheets.” These are partly bound to each other via chemical bonds. Hemicelluloses selectively connect with cellulose molecules through hydrogen bonding and cover the microfibrillar bundles of cellulose. Hemicelluloses also interact with lignin macromolecules, thus maintaining a consistency between the main components of the wood cell wall. However, scientists still have disputatious views on how lignin is incorporated into the cell wall.

4. Delignification of Wood

Liberation of lignin from woody biomass is usually termed as delignification and it is one of the primary fractionation

approaches used in traditional paper making and biorefineries.^[79,80] As discussed in the section above, lignin’s main function is to strengthen wood in vascular plants as it is mainly composed of xylem cells and lignified sclerenchyma fibers. Fractionation based on delignification is mainly distributed into alkaline delignification, acidic delignification, reductive catalytic fraction, and other lignification techniques.^[79] In the following section, classical delignification processes are discussed briefly. **Table 1** demonstrates the delignification processes currently used in the paper industry and their experimental conditions are also mentioned.

Delignification via alkaline conditions is the most frequently used method to remove lignin from biomass, such as in traditional pulping processes.^[81–83] Lignin solubility is significantly higher in alkaline media compared to (neutral) water media, where it is insoluble. This is due to the phenolic OH-groups deprotonation present in lignin.^[79] The cleavage of lignin–carbohydrate bonds and β -O-4 motifs is initiated in alkaline media, which leads to increase in the fragmentation and lignin degradation, or depolymerization from or in the wood cell walls. Alkaline delignification comprises seven different pulping processes as shown in Table 1. Kraft pulping is the leading alkaline pulping process due to its high quality pulp production, integrated recovery system of used chemicals, and its self-sufficiency in terms of energy demands.^[84]

Depending on the desired applications of prepared DW, various wood species have been used as a source for delignification. For instance, when DW is utilized in the preparation of transparent wood, the most frequent wood species to be delignified have been balsa wood (*Ochroma pyramidale*), various poplar species, basswood species (*Tilia*), beech wood, and pine wood. In addition, reports on the utilization of chemically modified

Table 1. Different delignification processes used in pulp and paper manufacturing and biorefinery industries.^[82]

Delignification techniques		Experimental conditions
Alkaline	Kraft pulping ^{a)}	Temp: 140–170 °C Aq. mixture of NaOH, Na ₂ S, and H ₂ O
	Sulfite pulping ^{a)}	Temp: 140–170 °C Aq. mixture of H ₂ O, Na, NH ₄ , Mg, or Ca salts of SO ₃ ²⁻ or HSO ₃ ⁻
	Soda pulping ^{a)}	Temp: 160–170 °C Aq. mixture of H ₂ O, NaOH, and C ₁₄ H ₈ O ₂ [(AQ) anthraquinone]
	Aq. alkaline pretreatment ^{a)}	Temp: 40–160 °C Aq. mixture of H ₂ O, NaOH, Ca(OH) ₂ , and AQ
	Aqueous fiber explosion + extraction ^{a)}	Temp: 100–130 °C Aq. mixture of H ₂ O, NH ₃ , and fast decomposition
	Anhydrous ammonia pretreatment + extraction ^{a)}	Temp: 60–160 °C Anhydrous NH ₃ and dry biomass
	Ammonia recycle percolation ^{b)}	Temp: 150–210 °C Aq. NH ₃
Acidic	Flow-through dilute acid pretreatment ^{b)}	Temp: 120–210 °C H ₂ O, mineral acid (e.g., H ₂ SO ₄ , HCl)
	Flow-through hot water pretreatment ^{b)}	Temp: 160–240 °C H ₂ O
	Steam explosion pretreatment + extraction ^{a)}	Temp: 100–210 °C H ₂ O, (SO ₂), fast decomposition
	Organosolv pulping ^{a)}	Temp: 120–210 °C Organic solvents: • MeOH, EtOH, BuOH, etc. • EtGly, glycerol • THF, dioxane, Me-THF • Formic acid, acetic acid, (H ₂ O), mineral acid: H ₂ SO ₄
Formaldehyde-assisted fractionation ^{a)}	Temp: 80–100 °C H ₂ O, dioxane, formaldehyde, HCl	
	Reductive catalytic fractionation ^{a)}	Temp: 180–250 °C Redox catalyst, H ₂ (–donor) Organic solvents (+H ₂ O): • MeOH, EtOH, iPrOH, etc. • Ethylene glycol, glycerol • THF, dioxane
Other	Ionic liquid dissolution organosolv pulping ^{a)}	Temp: 90–170 °C IL: e.g., [C ₄ C ₁ im][MeCO ₂], [C ₄ C ₁ im][HSO ₄], [C ₄ C ₁ im][Cl][H ₂ O], (H ₂ SO ₄)
	Mechanical pretreatment + extraction ^{a)}	Room temperature + extensive ball milling

^{a)}Batch process; ^{b)}Flow-through process.

acetylated wood as a substrate in preparation of transparent wood can also be found.^[85] Delignification and bleaching chemicals (bleaching is sometimes also a step in the production of transparent wood) are most often NaClO₂ (sodium chlorite)

or NaClO (sodium hypochlorite), NaOH, and Na₂SO₃ (sodium sulfite). These chemicals are sometimes used in combination with acetic acid and the (additional) bleaching agent is by majority H₂O₂. We have prepared a comparative table (Table 2) of different wood delignification processes that includes the types of wood species, sample thickness, delignification details, lignin percentage, and target functional applications.

An example of the typical delignification process used within the literature is presented as followed. First, basswood (*Tilia*) was dried at 103 °C for 24 h before chemical extraction. The delignification solution was then prepared through mixing 2 wt% NaClO₂, 0.1 wt% acetic acid glacial, and 97.9 wt% ultrapure water.^[86] The dried wood samples were then submerged in the delignification solution in a water bath oscillator at 80 °C with an oscillation frequency of 40 rpm. The five levels of DW were obtained through adjusting the treatment time (30, 60, 90, 120, and 150 min).^[87] Longitudinally cut basswood (*Tilia americana*) veneers with a thickness of 1.6 mm were delignified by oxidation to remove lignin at 80 °C with NaClO₂ at a concentration of 0.5 g g⁻¹ of wood in a 1 N acetate buffer solution (sodium acetate and acetic acid to maintain a pH ≈4.6). The DW template was then dehydrated via sequential solvent exchanges from ethanol to ethanol/acetone (1:1 by volume) to acetone. Optimization of the delignification process was carried by Qin et al.^[88] Specifically, the optimum conditions for the two-step delignification of low-density balsa wood (*O. pyramidale*) and of high-density basswood (*Tilia tuan*) were studied. The two-step delignification method of NaClO₂ and H₂O₂ was adopted. In the preparation of highly anisotropic transparent wood composites,^[89] they performed the delignification by immersing and boiling the wood in a solution consisting of NaOH (2.5 mol L⁻¹) and Na₂SO₃ (0.4 mol L⁻¹) in deionized water. Afterward, the wood blocks were placed in the bleaching solution (H₂O₂ (2.5 mol L⁻¹) in deionized water) and boiling was maintained without stirring. When the yellow color of the sample disappeared, the samples were removed and rinsed with cold water.^[90] The longitudinal-cut poplar veneer was delignified and bleached in a boiling solution of potassium hydroxide (2.7 mol L⁻¹) in deionized water for 8 h at 120–130 °C. This was followed by immersion in NaClO (0.81 mol L⁻¹) solution in deionized water for ≈24 h. Ethyl alcohol absolute was used to improve the limited swelling of the cellulose fiber network.

In order to simplify the delignification process, a green and universal H₂O₂ or H₂O₂/acetic acid steam-modified delignification approach was developed. This process removes more lignin, thereby generating a greater number of pores to be conveniently backfilled by epoxy resin for highly transparent wood composites.^[91] Heating the H₂O₂ solution generates vapor, which penetrated the wood cell walls and removed lignin. The excellent penetration ability of steam allowed DW to be created from various wood species (e.g., basswood and pine) with different cutting directions, as well as the thickest (40 mm) and largest (210 mm × 190 mm) wood samples investigated.

Bi et al.^[92] used deep eutectic solvents (DESs) in wood delignification. In this work, balsa wood chips (200 mm × 200 mm × 1 mm) were mixed with choline chloride/oxalic acid DES at a ratio of 20:1 w/w. The mixture was heated through microwave-assisted heating (800 W) for 10 min, followed by rinsing thoroughly with distilled water three times to remove most of the

Table 2. Different wood delignification methods used in selected literatures from the past four years with experimental details such as wood species, sample thickness, the type of delignification process, lignin content, and applications.

Wood species	Sample thickness [mm]	Delignification process (chemical composition, temperature, and time)	Lignin content [%]	Applications	Refs.
Chinese fir	0.1	Aqueous solution of 0.3% NaClO ₂ buffered with glacial acetic acid at pH 4.4–4.8 for 4 h and 8 h at 80 °C.	29.76	Analyzing the mechanical properties of DW	[94]
		Aqueous solution (pH 2.7) of 150 mL of distilled water, 1.0 g NaClO ₂ , and 2.0 mL of glacial acid for 8 h at 80 °C.	25.37		
Balsa wood	0.6, 1.0, 2.5, 5.0, 8.0	1 wt% of NaClO ₂ with acetate buffer solution (pH 4.6) at 80 °C.	2.9	Transparent wood	[95]
		Reaction time of 6 h for samples with thicknesses below 3 mm and 12 h for samples with thicknesses from 5 to 8 mm.			
Balsa wood	0.8	Bleaching of wood in 5% NaClO solution for 3, 8, 12, and 24 h at room temperature.	0.8	Transparent wood (epoxy, polyvinyl alcohol (PVA)) and thermal insulators	[96]
Basswood	0.1–1	NaOH (2.5 mol L ⁻¹) and sodium sulfite (Na ₂ SO ₃ , 0.4 mol L ⁻¹) solutions in deionized water boiling for 12 h. Bleaching solution (H ₂ O ₂ , 2.5 mol L ⁻¹ in deionized water) with maintained boiling without stirring.	–	Transparent wood for solar cells (polyvinylpyrrolidone, PVP)	[97]
Norway spruce	0.02	Acidic bleaching with H ₂ O ₂ /HAC (acidic acid): 1:1 H ₂ O ₂ /HAC solution and treatment was conducted for 0.5, 2, and 4 h at 40 and 80 °C, and for 0.25, 0.75, 1, 1.5, and 3 h at 60 °C. Soda pulping with sodium hydroxide (NaOH): NaOH (10 wt%), wood samples heated to 40 and 80 °C for 4, 6, and 8 h.	–	Tunable wood and functional materials	[98–101]
Balsa wood	1	Partial delignification: 1 h boiling in an aqueous solution of NaOH and Na ₂ SO ₃ , and quickly transferring into a vacuum chamber.	19.7	Superflexible wood for wearable medical membranes	[102]
Poplar wood	4	Hot water extraction: mixture of ethanol and benzene (1:2v/v) for 48 h then subjected to a water bath at 60 °C for 3 h to remove soluble extractives. Delignification: a mixture of 967 mL distilled water, 20 g NaClO ₂ , and 13 mL acetic acid under a vacuum of –0.1 MPa for 5 h. Afterward, the specimens were placed in a water bath at 40 °C for 30 h.	–	Wood furfurylation	[103]
Balsa wood	10	2 wt% NaClO ₂ solution buffered with acetic acid at pH 3.8 for 12 h at 105 °C, and the solution was refreshed every 2 h. Then, the obtained DW samples were transferred into an 8 wt% NaOH solution at 80 °C for 12 h to remove hemicellulose fraction.	–	F-rGO@wood (magnetic wood) sponge for clean-up of viscous crude oil via electrothermal processes	[104]
Basswood	10	Bleached in an aqueous solution containing 2 wt% NaClO ₂ buffered with acidic acid at pH 3.5 for 12 h at 70 °C. This process was repeated three times. The bleached wood pieces were further treated in a 5 wt% NaOH solution at 90 °C for 7 h to remove hemicellulose, followed by two more bleaching steps with acidic NaClO ₂ solution (2 wt%).	2.3	Ultrastrong and tough bulk materials via hydrogen-bonding	[105]
Birch wood	1.5 ± 0.1	1 wt% NaClO ₂ in acetate buffer solution (3 L, pH 4.6) at 80 °C for 12 h.	9.3	Bulk hot-pressed high-performance wood after surface dissolution in ionic liquids	[106]
Basswood	5 (4 h)	H ₂ O ₂ steam delignification: wood samples were steamed by placing them on grids above (distance of ≈2 cm) a boiling H ₂ O ₂ aqueous solution (30 wt%). When the yellow color of the samples disappeared (≈2–12 h), they were removed and rinsed with ultrapure water and ethanol.	0.84	Transparent wood (MMA and epoxy polymer infiltration)	[91]
	10 (5 h)		0.96		
	20 (12 h)		0.94		
Basswood	20 (4 h)	H ₂ O ₂ /acidic acid steam delignification: thick wood samples were steamed by placing them on grids above (distance of ≈2 cm) a boiling H ₂ O ₂ /acidic acid solution (5:4 v/v).	1.03	Transparent wood (MMA and epoxy polymer infiltration)	[91]
	40 (20 h)		1.16		
Basswood	–	H ₂ O ₂ bleaching: wood blocks immersed in the bleaching solution (H ₂ O ₂ , 2.5 mol L ⁻¹ in deionized water) and boiled at mild conditions until they turned white. The blocks were then rinsed in ethanol/water solution three times to remove the residual chemicals. The DW samples were then preserved in ethanol/water overnight and left to air-dry.	0.6	Bulk materials by stacking the DW blocks together via hot pressing	[107]

Table 2. Continued.

Wood species	Sample thickness [mm]	Delignification process (chemical composition, temperature, and time)	Lignin content [%]	Applications	Refs.
Bamboo	5	Aqueous solution of 2.5 M NaOH and 0.4 M Na ₂ SO ₃ for 12 h and washed with boiling water to remove residual lignin, hemicellulose, and waxy compounds. This created a fully aligned cellulosic structure.	5	Bamboo-based bulk structural materials via delignification and densification	[108]
Hybrid poplar	2 × 2 (cross-section)	The delignification treatment used a dissociation solution of 1:1 configuration of 30% H ₂ O ₂ and glacial acetic acid. The solution was boiled in a water bath at 40 °C for 0, 1, 6, 10, 32, and 34 h.	27.3 22.6 14.8 5.6 1.4 0.2	To study the effect of delignification on the mesopore structure in poplar cell walls by the nitrogen absorption method	[109]
Poplar wood flour	10 mesh size	NaClO ₂ (2 wt%) was dissolved in buffer (pH 4–5) composed of acetic acid and NaOH to prepare the etching solution for lignin. The wood flour (WF) was then immersed and dispersed into this solution, which was kept boiling at 130 °C until the WF turned from brown to white.	-	Phase-change materials	[110]

chemicals. The bleaching solution utilized in the preparation of the DW substrate for transparent wood was prepared by mixing deionized water, sodium silicate (3 wt%), sodium hydroxide solution (3 wt%), magnesium sulfate (0.1 wt%), ethylenediaminetetraacetic acid (EDTA) (0.1 wt%), and H₂O₂ (4 wt%). The wood substrates were immersed in the boiling bleaching solution until the yellow color of the wood chip had disappeared. The wood substrates were then thoroughly rinsed with ultrapure water and preserved in ethanol until use. Although this review's primary aim is to compile and characterize the state-of-the-art literature within in the field of DW, it should be mentioned that delignification of other lignocellulosic materials has also been the focus of extensive investigation. Furthermore, potential applications of other delignified lignocellulosic materials are often similar to those of DW. For instance, Feng et al. developed a transparent material that was similar to transparent wood.^[93] As the first step, they delignified the jute fiber with surface-knitting densities of 190 and 340 g m⁻². This was followed by impregnation under vacuum with epoxy resin. The jute fibers were then washed, dried, and placed in a bottle before NaClO₂ (5 wt%, pH 4.6) was added to dissolve the fibers. The reactor was placed in an oil bath to remove the lignin from the jute fibers. The reaction times were 6 and 8 h, and the lignin was heated to 80 °C. After the reaction, the delignified jute fibers (DJFs) were removed and heated to boiling with 5 mol L⁻¹ alkaline H₂O₂ solution. After 1 h, the solution was cooled to room temperature and the delignified lignocellulosic samples were freeze-dried.

5. Influence of Delignification on Wood Properties

Wood cell wall is mainly composed of three biopolymers: cellulose, hemicellulose, and lignin. The chemical interactions, functions, and arrangement in the cell wall of these biopolymers significantly influence the overall chemical, physical, microscopic, and mechanical properties of wood. Delignification treatment rearranges the cell wall biopolymers by altering the chemical composition of wood cell wall by removing the target percentages of lignin and in some cases by hemicellulose.

Removal of lignin, partially or completely, from wood via chemical processes can significantly modify the cell wall structure at the microscopic level and simultaneously affect the wood's physical, chemical, and mechanical properties. In this section, we will discuss the influence of delignification on the physical, chemical, mechanical, and microscopic properties of wood.

5.1. Mechanical Properties

Results from literature have demonstrated that strong interactions occur between hemicelluloses (viz xylan and glucomannan) and other wood biopolymers (cellulose and lignin).^[94,111–113] Hemicelluloses act as a crosslinking agent between cellulose and lignin in the cell wall, which influences its mechanical properties.^[114] Any type of thermal, chemical, or other treatment alters the cell wall biopolymer arrangement. Consequently, this impacts the physical and chemical properties of the wood cell wall and its service life.^[37,115] As aforementioned, lignin is a structural component with a cementing function in the wood cell wall that provides stability, protection against biological deterioration and provides mechanical support to cell wall particularly under compressive loading. Zhang et al.^[94] has analyzed the mechanical function of lignin and hemicelluloses in a single wood fiber cell wall. They removed different percentages of lignin using three delignification processes described in Table 2. **Figure 5** shows that as the lignin percentage is reduced in single wood fibers, their tensile strength increases but their tensile modulus decreases. The tensile strength of wood fibers increases with reducing lignin content and has values of 729, 775, and 815 MPa for lignin contents of 29.76%, 25.37%, and 0.4%, respectively, from 577.43 MPa of original wood fibers. The increase in the tensile strength is due to the increased proximities (or aggregation) of cellulose fibrils upon removal of lignin from the cell wall.^[111,116] Conversely, hemicellulose removal causes the mechanical properties of wood to decrease. A recently conducted study.^[117] found that cellulose microfibrils are partially coated with xylan chains viz galactoglucomannan and lignin. After delignification and hemicellulose removal, it was found that this coating was

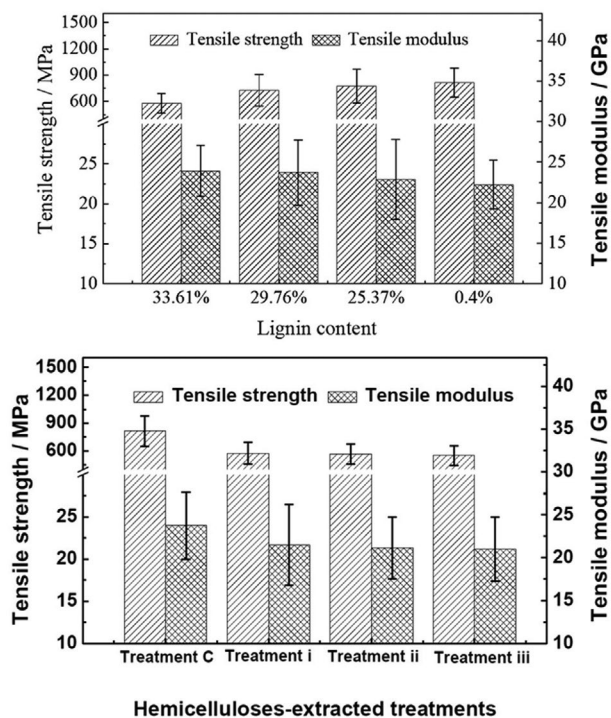


Figure 5. Tensile properties of single wood fibers with lignin and hemicellulose treatments. Adapted with permission.^[94] Copyright 2013, North Carolina State University, USA.

removed, which loosened the arrangement of cellulose fibrils. It was deduced that this was the main reason for the observed reduction in mechanical properties.

5.2. Microstructure, Moisture Sorption Behavior, and Porosity of DW

It is very important to understand how delignification alters the wood cell wall. **Figure 6** shows scanning electron microscopy (SEM) images of native wood (Figure 6a–c), partially DW (Figure 6d–f), and fully DW (Figure 6g–i). It is clear from the images that the thick-walled and thin-walled (tube-like vessels) fibers of the beech wood are aligned in the longitudinal direction and cells are connected via pits for transportation of liquid between cells. The vessels elements, aligned end-to-end with the next vessel element and separated by perforation plates, are visible in Figure 6b,c. After mild delignification, several changes took place in the wood cell wall. The fibers were partially detached, and the vessels were also fragmented from assembly but kept the cell wall stable without any apparent fracturing. However, voids are visible in the ML of the secondary wall due to the partial delignification (see Figure 6d–f). After harsh or complete delignification, the wood cell wall was fractured and showed clear disassembly in the vessels and fibers (see Figure 6g–i) of oven-dried DW. Upon drying, the softened cell wall was more likely to collapse, promoting a “compacting” of the entire structure.^[118] However, after freeze-drying of DW, scaffolds of the cellular structure were relatively stable as they did not show collapsing behavior and maintained a porous structure

(see Figure 6j–l). Further, they studied the influence of different drying on the porosity of DW. Figure 6m,n is histograms that show the cumulative and relative pore volume of DW as a function of the pore radius and a comparison of oven- and freeze-dried DW, respectively. Complete or harsh delignified samples show a peak region in the range of 10–100 μm pore sizes after oven-drying, while freeze-dried samples exhibit two peaks centered around 4 and 35 μm in the macropore region.

It is well known that lignin provides stability and protection to the wood cell wall against external factors. However, it is essential to remove the lignin from the cell wall to explore the vast potential of hierarchical-cellulosic materials. Delignification of wood provides a favorable environment to create free hydroxyl groups for cellulosic structures, which are arranged naturally as a potential functionalization site. Wood becomes very sensitive to moisture or water upon the removal of the hydrophobic structural polymer lignin from the cell wall and the opening of the cellular structure. Therefore, estimating the mesoporosity and moisture behavior of DW is essential for determination of the functionalization ability for development of value-added materials. Grönquist et al.^[119] studied the water affinity and cell wall porosity of native spruce wood, as well as partially and fully delignified spruce wood by means of water vapor sorption isotherms and estimated the pore size distribution (see **Figure 7**). They also used the deuteration experiments to estimate the number of available OH groups in the wood samples. In this work, spruce wood cubes (5 × 5 × 5 mm³) were delignified in a H₂O₂/HAc mixture at 80 °C for 10, 15, 30, 60, 120, and 360 min. The wood was partially delignified at each interval from 10 to 120 min, and fully delignified at 360 min. They found that partial delignification up to 120 min significantly changed the water vapor sorption behavior and pore size distribution. Figure 7a,b shows the volume of water adsorbed and pore size distribution in natural wood, in addition to partially and fully DW scaffolds. The partial delignification up to 120 min increased the water absorption and pore size of the wood scaffolds due to changes in the structure of the wood cell wall caused by lignin removal from the ML between cells. However, fully DW showed similar behavior to natural wood because harsh delignification appeared to collapse the cell walls upon drying, as well as close the open spaces and pores of the fully DW. Subsequently, this reduced the water vapor adsorption and pore size distribution. Further, they estimated the amount of OH groups in the different wood scaffolds by deuteration using heavy water (D₂O). The results demonstrated that the number of OH groups increased significantly from 8.5–9 mmol g⁻¹ in natural wood to 10–10.5 mmol g⁻¹ in partially DW due to chemical changes of the cell wall (see **Figure 7c**). They also concluded that cellulose crystallinity may have been affected due to delignification and played a role in the water vapor absorption behavior.

In a recent study, Vitas et al.^[118] evaluated the porosity and pore size distribution of natural and delignified beech wood using mercury intrusion porosimetry. The microstructure of the native and DW was also investigated using SEM. Furthermore, the influence of different drying techniques (e.g., oven- and freeze-drying) on the porosity and pore size of different wood scaffolds was investigated (see **Figure 6**). The results demonstrated that mildly DW or lignin retaining samples provided more reactive

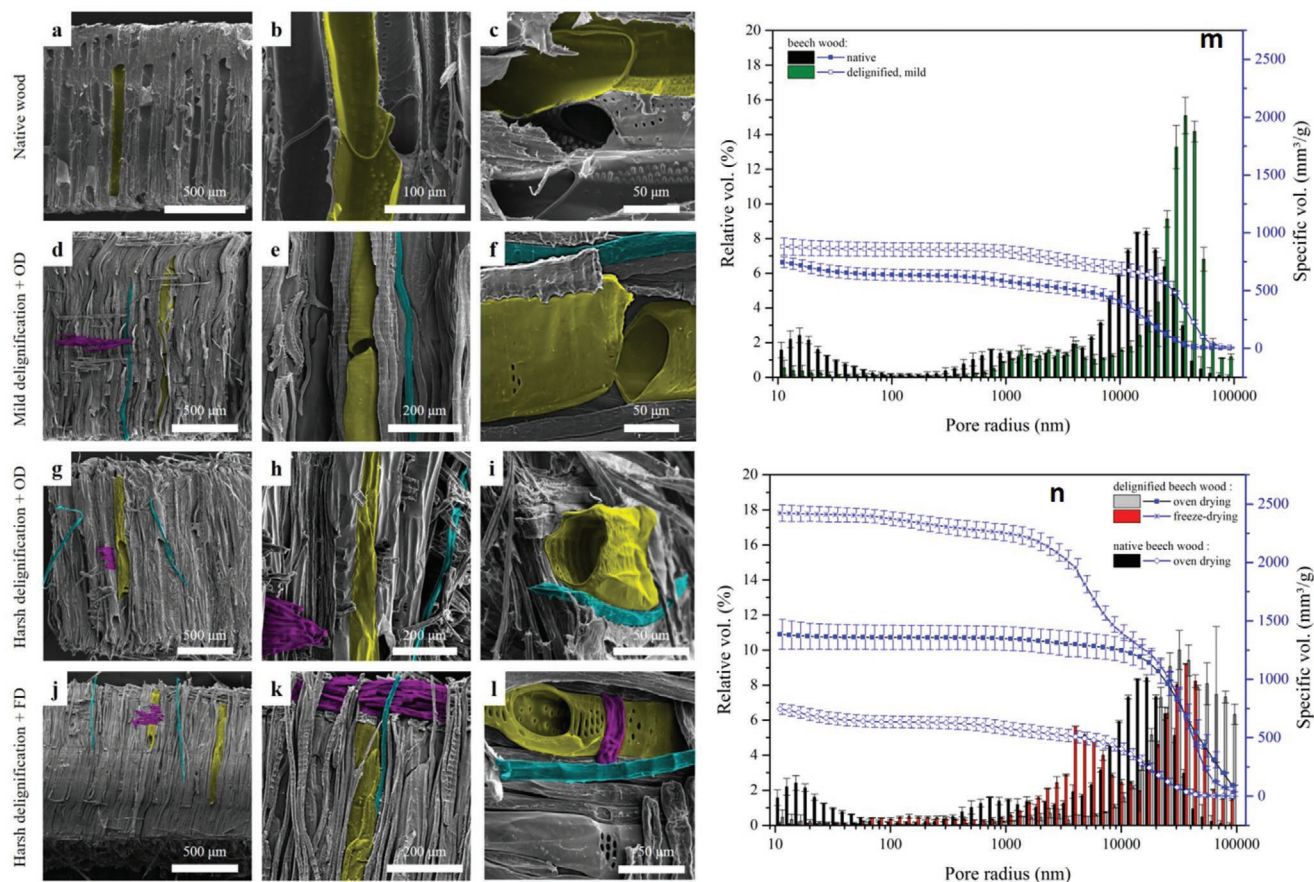


Figure 6. SEM images of a–c) native wood, d–f) beech wood after mild delignification and oven-drying, g–i) beech wood after harsh delignification and oven-drying, and j–l) beech wood after harsh delignification and freeze-drying, and m, n) effect of the extent of delignification (mild (60 °C, 8 h) and harsh (80 °C, 4 h)) and drying process (freeze-drying and oven-drying) on the porosity of beech wood expressed as cumulative pore volume and a histogram of the relative pore volume as a function of the pore radius. Reproduced with permission.^[118] Copyright 2019, Multidisciplinary Digital Publishing Institute.

hydroxyl groups compared to fully DW (see Figure 7). It is very important to freeze-dry the DW to maintain the stability of the naturally aligned cellulosic structure and the natural porosity and pore size for the development of various functional materials. In another study, Han et al.^[105] investigated the water vapor sorption behavior in a desiccator containing saturated potassium sulfate (K_2SO_4) solution ($97.6 \pm 0.5\%$, under relative humidity at 20 °C) of DW samples that were dried in three different conditions (air-drying, solvent exchange-drying, and freeze-drying). All three types of dried DW samples showed gradually increased water vapor uptake over 96 h and followed a decreasing trend for freeze-dried ($19.4 \pm 0.1\%$), solvent exchange-dried ($18.3 \pm 0.6\%$), and air-dried ($16.8 \pm 0.3\%$).

Liang et al.^[109] evaluated the effects of increasing the percentage of lignin removal on the mesopore structure in poplar cell walls by the nitrogen adsorption method. First, DW strips were ground and passed through a 150-mesh screen. Approximately 1.5 g of the ground samples were successively dehydrated to 30%, 50%, 70%, 90%, and 100% gradient dehydration displacements with ethanol, and then dried using the supercritical drying method for nitrogen adsorption measurements. In the nitrogen adsorption experiments, the specific surface area, pore volume, and mesoporous distribution were measured

using the Brunauer–Emmett–Teller (BET) and Barrett–Joyner–Halena (BJH) models. **Figure 8** demonstrates the pore size distribution in wood samples with different delignification stages, the control wood sample have two separate pore size distribution size ranges: 10–50 nm (81%) and >50 nm (19%). After 22% delignification, the pore size distribution into four ranges where $\approx 64\%$ of the pores are in the mesopores range of 1.97–2 nm. After $\approx 95\%$ delignification, the pore size distribution is separated into four ranges but more than half (56%) of the pores are in the range of 10–50 nm. The formation of a large number of mesopores (1.97–2 nm) was due to the removal of lignin. As previously discussed in Section 3, lignin is distributed throughout different locations in the wood cell wall, such as the compound ML and cell corners. Due to the delignification treatment of the wood cell wall, the lignin created holes of different pore sizes in the ML and cell corners.

5.3. Influence of Different Drying Conditions on the Properties of DW

Han et al.^[105] investigated how aligned cellulose fibrils interact with each other via hydrogen bonding to form compressed

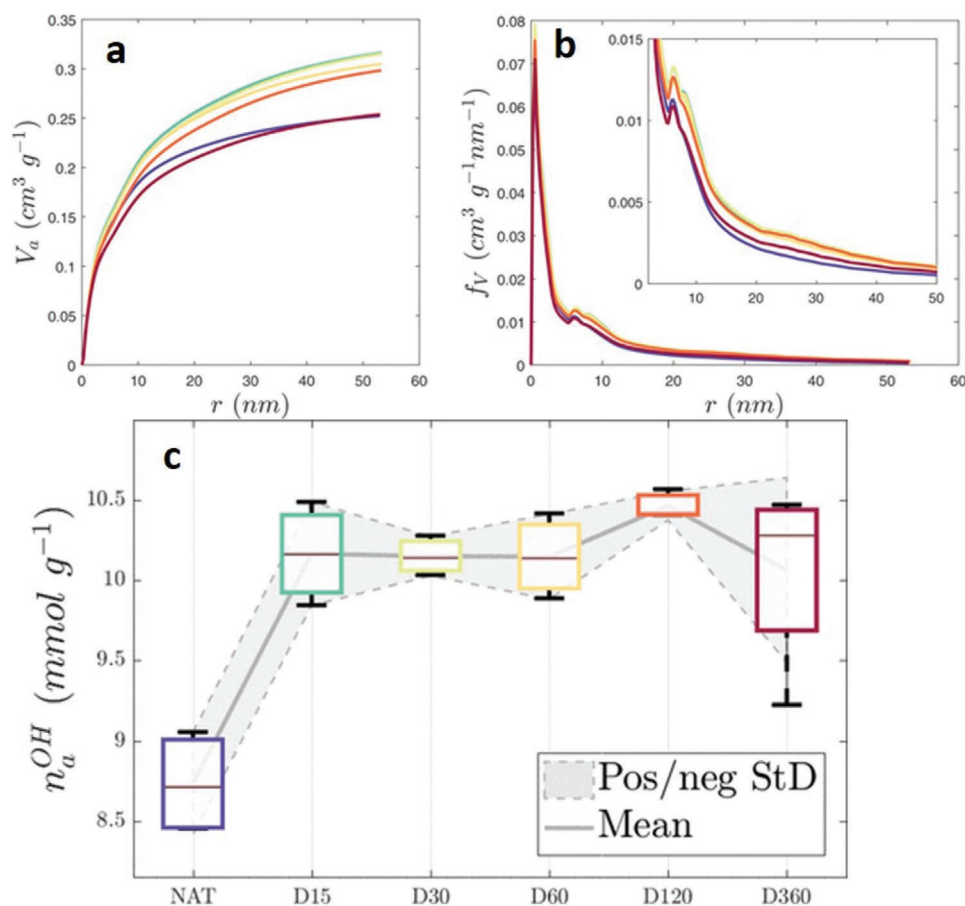


Figure 7. a) Cumulative adsorbed water (V_a) in theoretical pores of cylinder radius r from adsorption curves, b) pore volume distribution (f_v), and c) number of available OH groups by deuteration with D₂O. Adapted with permission.^[119] Copyright 2019, American Chemical Society.

ultrastrong bulk materials based on DW. They applied three different drying methods (air-drying, solvent exchange-drying, and freeze-drying) to manipulate the hydrogen bonding formation. Furthermore, they investigated the effects of drying conditions on the mechanical properties and water vapor sorption behavior of prepared bulk materials. **Figure 9** compares the influence of the three different drying conditions on the chemical and physical properties, as well as the microstructure of the DW samples. The air-dried sample experienced a $\approx 62\%$ loss in volume, had a

density of 0.5 g cm^{-3} , and 66.1% porosity. The solvent exchange-dried sample experienced a $\approx 20\%$ loss in volume, had a lower density of 0.22 g cm^{-3} , and 85.5% porosity. The freeze-dried sample exhibited very different properties and experienced a volume increase of $\approx 15\%$, had a density of 0.15 g cm^{-3} , and $\approx 90\%$ porosity. Figure 9e,h clearly demonstrates that the aligned nanocellulose structure of DW collapsed due to air-drying. Furthermore, freeze-drying stabilized the structural integrity of the DW scaffolds, as well as the porous structure formed due to lignin removal.

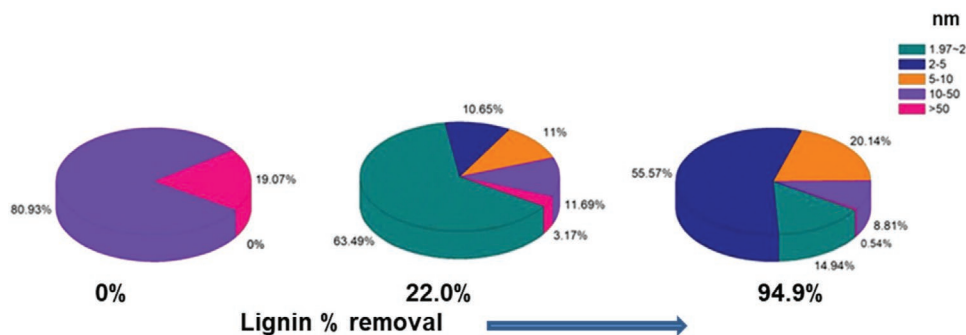


Figure 8. Pore size distribution pie charts for wood samples with varying percentages of lignin removal, estimated by the nitrogen absorption method (BET + BJH). Adapted with permission.^[109] Copyright 2020, Springer Nature.

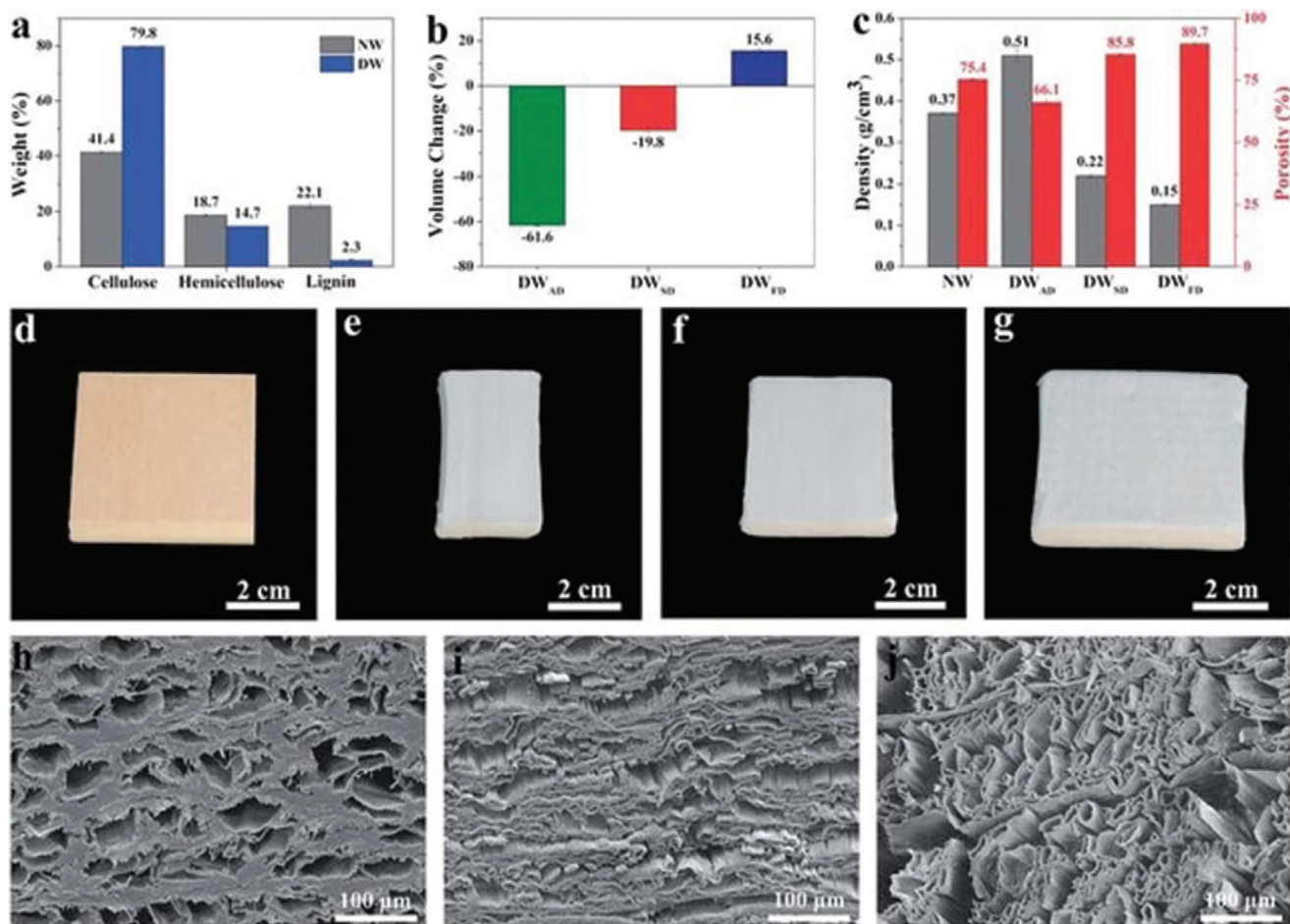


Figure 9. a) The composition of cellulose, hemicellulose, and lignin in natural wood and DW. b) Volume change caused by different drying methods. c) Densities and porosities of natural wood, air-dried DW, solvent exchange-dried DW, and freeze-dried DW. Photographs of d) natural wood, e) air-dried DW, f) solvent exchange-dried DW, and g) freeze-dried DW. SEM cross-section images of h) air-dried DW, i) solvent exchange-dried DW, and j) freeze-dried DW. Adapted with permission.^[105] Copyright 2019, Royal Society of Chemistry.

5.4. H-Bond Formation between Free OH Groups in Aligned Cellulose

As discussed in Section 5.2, the delignification treatments improved the wood cell wall accessibility toward the moisture uptake due to the removal of hydrophobic lignin and which also creates the voids in cell wall. In wet conditions, DW is extremely flexible and can be easily molded into different

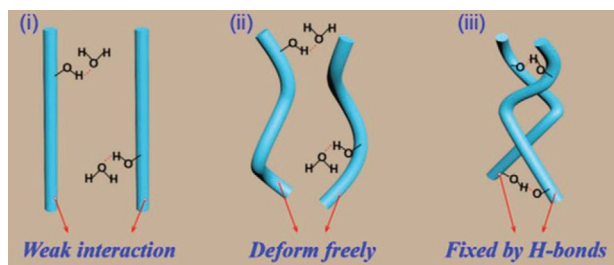


Figure 10. Schematic diagram showing the possible H-bond formations due to the mechanical pressing of DW. i) Without mechanical pressing, ii) with mechanical pressing in wet conditions, and iii) with mechanical pressing in dry conditions. Adapted with permission.^[102] Copyright 2019, Wiley-VCH.

shapes. After drying, free OH groups form H-bonds with one another to fix the DW into a molded shape. After delignification, the fibril aggregates in DW maintain their cell configurations due to the complex nanofibril structure.^[102] **Figure 10** shows the H-bond formation by the mechanism of free OH groups. Immediately after delignification, OH groups exhibit weak interactions (Figure 10i). During pressing in wet conditions, cellulose is easily deformed (Figure 10ii), and once the water is removed from the pressed wood, the cellulose fibrils form fixed H-bonds (Figure 10iii). This phenomenon is essential in order to fabricate the densified bulk materials using DW as a base material. Furthermore, it can be assumed that most functional materials can be fabricated using DW in wet conditions. However, this preparation is not suitable for all functional materials.

6. Functional Materials Derived from Delignified Wood

The process of delignification makes wood highly hydrophilic with an aligned cellulose structure and free OH groups. These

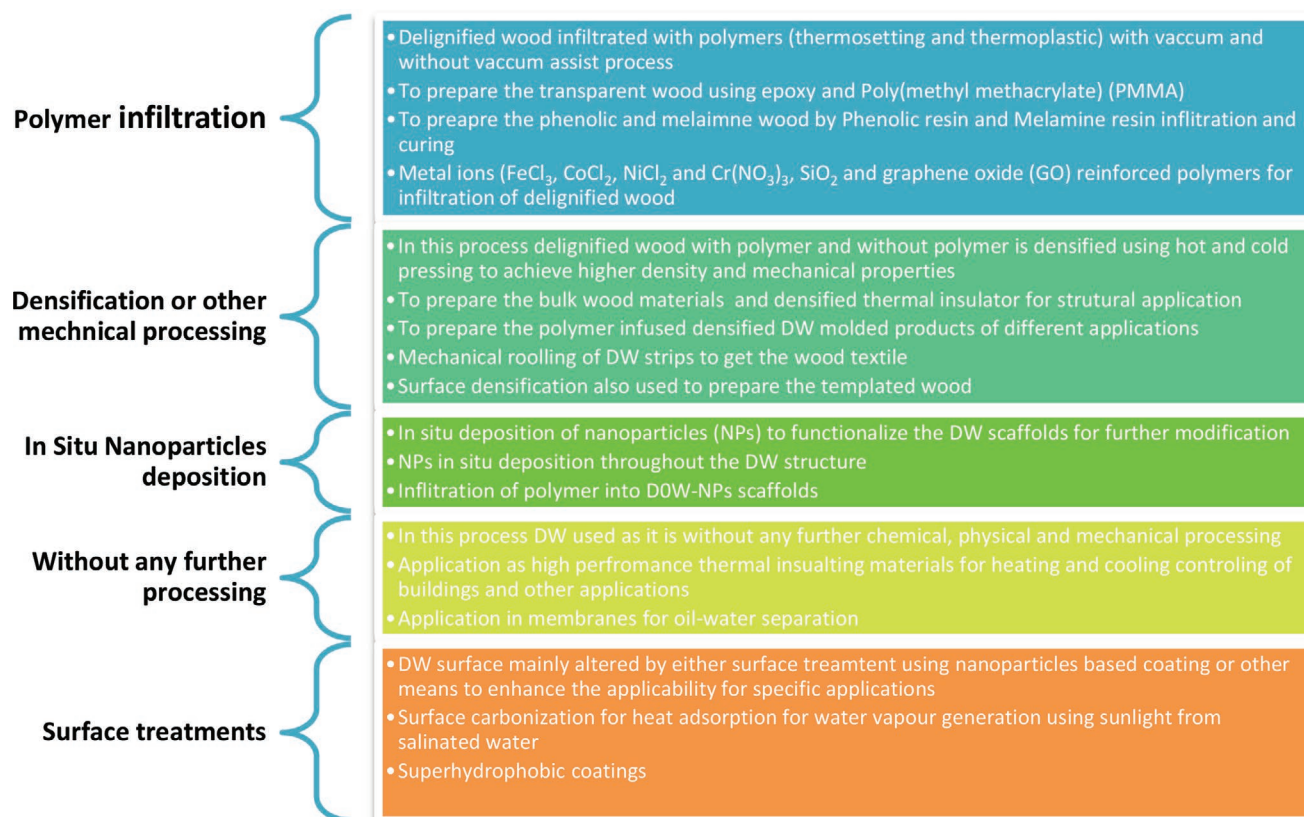


Figure 11. Strategies utilized in the preparation of DW-based functional materials.

free reactive OH groups and the hierarchically aligned cellulose structure allow DW to be used as a biotemplate for the development of various functional materials. **Figure 11** shows the different strategies utilized to prepare functional materials based on DW. During the last four years, DW was used as a base material in the fabrication of transparent wood, bulk wood materials, membranes, thermal insulators, phase-change materials, solar cells, tunable wood, self-luminous wood, superflexible wood, energy storage materials, textile fibers from wood, and many more applications related to replacing synthetic plastics. In the present review, we have categorized DW-based functional materials according to their applications into six different areas: 1) structural materials, 2) membranes, 3) energy storage materials, 4) electronics/optoelectronics/solar cells, 5) biomedical applications, and 6) other functional applications. However, transparent wood is one of the most broadly researched topics regarding the applications of DW. This review covers the introduction, preparations, property evaluations, and diverse applications of each of the above mentioned categories separately.

6.1. Transparent Wood

6.1.1. Introduction

Transparent wood is a topic that has gained considerable attention in recent years and the first study in this field was performed by Fink in 1992.^[12] Transparent materials and especially

films made from lignocellulosic materials (mainly nanocellulose) have been the focus of earlier research from approximately 2000 to 2010 onward. Some examples of scientific publications on the topic of nanocellulose-based transparent materials are those of Endo et al.,^[120] Nogi and Yano,^[121] Okahisa et al.,^[122] Moon et al.,^[125] Zhu et al.,^[97] or Abiral et al.^[123] However, only transparent wood and not nanocellulose-based transparent material is covered within this review.

Although transparent wood has only been extensively investigated in recent years, some reviews have been published, which solely focus on this subject area.^[124] Furthermore, in some broader reviews, transparent wood has been the topic of an individual chapter.^[37,125] In a condensed state, the preparation of transparent wood and its possible applications were described in the introduction of an article by Feng et al.,^[97] which focused on utilizing transparent jute fiber to replace transparent wood. In 2018, two comprehensive reviews on the preparation and properties of transparent wood were published by a group of researchers from the KTH Royal Institute of Technology, Stockholm, Sweden.^[126,13] The reviews summarize transparent wood preparation methods, optical and mechanical performance, functionalization routes, and potential applications. The basics regarding the interactions between light and wood were also covered. The applications of transparent wood include smart buildings and load-bearing structures with a photonic function, luminescent materials, devices for lasing emission, smart windows with heat-shielding properties, magnetic switches, and electromagnetic interference shielding. A review focusing

on the current state of research on transparent wood, with a particular focus on its optical properties, was published by the same group of authors.^[13,127]

As aforementioned, several reviews have been published on the subject of transparent wood. Consequently, the aim of this chapter is not to compete with these reviews or to highlight recent novel findings. Instead, the purpose of the chapter is to amend this general review about DW as a future material with a hierarchical aligned cellulosic structure. It is simply impossible to write about DW without mentioning transparent wood. Therefore, this chapter brings the author's critical views on the very propulsive topic of transparent wood to provide a more complete picture about the current research status of DW.

6.1.2. Preparation of Transparent Wood

In general, transparent wood is prepared in several steps. First, the wood is cut into thin specimens (≈ 1 mm thickness). Subsequently, delignification of the substrate is executed, which leads to a decreased light absorption in the wood and a refractive index mismatch in the cell wall. Bleaching of the delignified substrate is achieved simultaneously with the delignification step, or it is carried out as an additional or amending phase after delignification. This is followed by infiltration of a polymer with a refractive index matching the wood substrate. The final step involves curing the wood substrate into a solid state in wood cell lumens. The reported procedures differ in their chosen wood types, delignification and bleaching chemicals, and impregnation polymer of the DW structure. As the substrate, balsa wood (*O. pyramidale*), various poplar species, and basswood species (*Tilia*) are commonly utilized. Beech wood and other species, such as pine, are less frequently used. In addition, reports that use chemically modified acetylated wood as a substrate can also be found. These chemicals are sometimes used in combination with acetic acid and the (additional) bleaching agent is by majority H_2O_2 . The most commonly utilized polymers for infiltration are epoxy resins, poly(methyl methacrylate) (PMMA), and polyvinyl alcohol (PVA). If particular effects need to be achieved, for instance, luminescence, various additives may be dispersed within the resin.

The preparation methods of transparent wood are described in more detail in numerous papers. For example, the general description of transparent wood preparation was provided in one of the earliest reports within the field by Li et al.^[128] Optically transparent wood with transmittance and haze as high as 85% and 71%, respectively, was obtained using a delignified nanoporous wood template. The template was prepared by removing the light absorbing lignin component from balsa wood (*O. pyramidale*) by extraction with $NaClO_2$, which led to nanoporosity in the wood cell wall. Transparent wood was prepared by successful impregnation of refractive index matched prepolymerized MMA into lumens and the nanoscale cellulose fiber network in the cell wall. During the process, the hierarchical wood structure was preserved. It was shown that optical transmittance decreased as wood thickness and cellulose volume fraction increased, whereas haze increased for the same changes. The cellulosic wood template could be compressed in order to control the volume fraction of the reinforcement. The

mechanical properties of the transparent wood revealed synergies between DW and PMMA as both components showed lower mechanical properties compared to the optically transparent wood. Using very similar methods described above, transparent wood was prepared from beech wood by Yaddanapudi et al.^[129]

Delignification is the first step in the preparation of transparent wood. However, we have already described the processes of delignification in detail within a previous section. Hence, in the following paragraphs, only details of delignification that are specifically related to the preparation of transparent wood are described. How the degree of delignification prior to polymer impregnation influences the properties of transparent wood is very relevant and significant. This topic was addressed by the group of researchers led by Wu et al.^[86] The five levels of delignified Basswood were obtained through adjusting treatment time (30, 60, 90, 120, and 150 min). Transparent wood was then prepared by applying the prepolymerized MMA mixed solution. An impregnated wood sample was sandwiched between two pieces of glass and wrapped with aluminum foil, then heated to 70 °C for 5 h. The optical (e.g., surface color, optical transmittance, and optical haze) and mechanical properties of natural wood and each transparent wood product were measured in order to better understand the influence of delignification. The transparent wood exhibited a maximum optical transmittance of 61% at 800 nm with 9% lignin content and also possessed enhanced visual optical haze at different levels of delignification. In addition, transparent wood had a higher tensile strength than natural wood and displayed a maximum tensile strength up to 171.4 MPa with 15% lignin content among these transparent wood products pretreated with delignification.

Optimization of the delignification process for preparation of transparent wood was also studied by Qin et al.^[88] Specifically, the optimum conditions for two-step delignification of low density balsa wood (*O. pyramidale*) and high density basswood (*T. tuan*) were studied. In order to simplify the delignification process of the transparent wood with a thickness greater than 2 mm, the veneers were laminated together at the cross direction ($0^\circ/90^\circ$) and the same direction ($0^\circ/180^\circ$). The vacuum laminating method retained the porous structure and thickness of the samples and filled additional cell lumens with epoxy resin. The direct light was dispersed into a fuzzy-looking halo that dispersed sunshine. This showed that the transparent wood had a good light management effect, which distributed the light more evenly throughout the room and saved energy. The results demonstrated that the lamination method reduced the delignification time by $\approx 50\%$ and improved the dimensional stability of the transparent wood. Optical testing showed that the maximum transmittance of the same direction laminated transparent wood was similar to the single layer transparent wood with the same thickness. The general conclusions of the authors were that optimizing the preparation process of transparent wood could greatly reduce preparation time and energy consumption.

Highly anisotropic transparent wood composites were reported by Zhu et al.^[89] The DW was immersed in liquid epoxy resin and the impregnation of cell lumens was achieved by alternating the exposure of the blocks in the resin to vacuum and atmospheric pressure several times. Finally, the

dish containing the wood sample and resin was kept static at 30 °C for 12 h. Two types of transparent wood were fabricated in which the original channels in the wood aligned either perpendicularly to the wood plane or along the wood plane. The resulting anisotropic wood composites maintained the original wood micro and nanostructures, including the aligned cell walls and internal cellulose fibers. The composite displayed highly favorable anisotropic optical and mechanical properties. The steam-modified delignification method has also been reported for the preparation of thick highly transparent wood composites.^[95] The higher the lignin removal from the wood skeleton, the lower the absorbance of visible light, the higher the porosity in the DW, and the more space there is to be backfilled with polymer to eliminate the interface debonding gap between the cell walls and filled polymer. Consequently, this leads to both high optical and mechanical properties of the transparent wood composites. After the infiltration of epoxy resin, the mechanical strength of the 5 mm thick transparent wood composite increased from 12.5 to 20.6 MPa. Furthermore, the transmittance (550 nm wavelength) also increased from 80% to 87% due to the lower absorbance of visible light by lignin and the suppression of the interface debonding gap between the cell walls and the backfilled epoxy resin.

The majority of articles utilize delignification as the first step in the preparation of transparent wood. However, a report has also prepared lignin-retaining transparent wood.^[130] The reasons for this alternative approach is because lignin removal is time consuming, not environmentally benign, and it also weakens the wood structure, which leads to limitations in the fabrication of large structures made of transparent wood. In the study, up to 80 wt% of lignin was preserved, leading to a stronger wood template compared to the delignified alternative. After polymer infiltration, a high-lignin content transparent wood was obtained with a transmittance, haze, thermal conductivity, and work-to-fracture of 83%, 75%, 0.23 W m K⁻¹, and 1.2 MJ m⁻³ (a magnitude higher than glass), respectively. The approach was based on the chemical modification of lignin rather its removal. The modification of the balsa wood with the chlorine free alkaline reagent H₂O₂ led to removal of chromophoric groups in the lignin system. The resulting transparent wood demonstrated high optical performance. The optical transmittance and haze of the balsa transparent wood lignin (550 nm wavelength) were 83% and 75%, respectively, for a specimen thickness of 1.5 mm. Since haze is the ratio of diffused light transmittance to total transmittance (diffused transmittance + direct transmittance), this meant that diffused transmittance dominated, despite the high optical transmittance. High haze is favorable for applications such as solar cells since the light path in the active layer can be drastically increased.

In another study, transparent wood was prepared by directly impregnating the wood cell wall and cavity with index matched prepolymerized MMA. When compared to the previous preparation methods of transparent wood, this process retained lignin, which made the production faster and more energy efficient. The innovation of this method is that the prepared transparent wood retains the natural color and texture of natural wood while transmitting light. This is particularly apparent under the illumination of a specific light source that exists as the special visual effect.^[131] Before impregnation, the dried

wood was placed in an ethanol absolute solution to displace the moisture inside, which greatly enhanced the permeability of the wood. NaOH solution was used to remove the polymerization inhibitor inside the pure MMA monomer. The lignin was retained during the experiment so that the transparent wood had the color and texture of natural wood, in addition to obtaining faster and more energy-efficient production.^[131] However, it is not just the delignification preparation step that influences the properties of transparent wood. The H₂O₂ bleaching step also has an important effect on the final properties of transparent wood.^[132] Transparent wood samples were fabricated from a H₂O₂ bleached basswood (*Tilia*) template using polymer impregnation with PMMA. Experimental results showed different decreases in cellulose, hemicellulose, and lignin content with increasing bleaching time. This allowed for successful impregnation of the polymer into the bleached wood template and strong transparent wood products. The transparent wood possessed a maximum optical transmittance up to 44% (800 nm wavelength) at 150 min bleaching time. Moreover, the transparent wood displayed a maximum tensile strength up to 165.1 ± 1.5 MPa at 90 min bleaching time. The elastic modulus (*E_r*) and hardness (*H*) of the transparent wood samples reduced with increasing H₂O₂ bleaching treatment time. Consequently, the transparent wood at 30 min bleaching time exhibited the highest *E_r* and *H* values of 20.4 and 0.45 GPa, respectively.

In the aforementioned report by Bi et al.,^[92] DESs were used in the preparation of transparent wood for applications as white light-emitting diodes (LEDs). The experimental method used for this research was somewhat different to other works within the literature (see Section 5 for comprehensive details regarding the wood substrate preparation). Once the wood substrates were prepared, polymer infiltration into the wood cells was performed by diluting acrylic acid with deionized water to a concentration of 40 wt% and then adding ammonium persulfate (1 wt%) to the mixture. After complete dissolution, the lignin-removed wood was placed at the bottom of a beaker and immersed in a poly(acrylic acid) (PAA) solution. The solution was then degassed under 200 Pa for ≈10 min to ensure full infiltration of the solution into the wood. Finally, the monomer-infiltrated wood sample was sandwiched between two glass slides, wrapped with aluminum foil, and heated in an oven at 75 °C for 4 h in air for the polymerization.

The most commonly used polymers for the bulking of delignified and bleached wood cell lumens are epoxy resins and PMMA. However, within the literature, some other polymers have also been utilized for these procedures. For example, Rao et al.^[133] fabricated transparent poplar wood by utilizing PVA. The obtained transparent veneers were highly flexible and the optical and mechanical properties of the wood–PVA composite were significantly influenced by the addition of polyethylene glycol (PEG) as a plasticizer. The wood–PVA composites plasticized with 0.0 wt% (TPW-PG-00) and 50 wt% (TPW-PG-50) PEG exhibited high rigidity and brittleness. The optical transmittance of TPW-PG-00 and TPW-PG-50 samples were 65% and 69%, respectively, while the haze of the TPW-PG-00 and TPW-PG-50 samples were 80% and 85%, respectively. As the PEG content in PVA was increased to 100 wt% (TPW-PG-100), the optical transmittance and haze increased to 80% and 90%, respectively. Finally, the potential applications of TPW-PG-100

for diffused light shaping, decorative lighting, optoelectronics, and display devices were successfully demonstrated.

Wang et al.^[134] demonstrated in situ photopolymerization with polymerizable deep eutectic solvents (PDESs) in the preparation of transparent wood. In this case, PDES, acrylic acid, and choline chloride were used as backfilling agents and were in situ photopolymerized in the DW. This provided the materials with high transparency (transmittance of 90%), good stretch-ability (strain up to 80%), and high electrical conductivity (0.16 S m^{-1}). The PDESs utilized for infiltration were prepared by mixing choline chloride and acrylic acid at a 1:2–1:6 molar ratio. Before being mixed, choline chloride in the form of ammonium salt was dried under vacuum at $60 \text{ }^\circ\text{C}$ for 2 h. Furthermore, acrylic acid, which acted as the hydrogen bond donor molecule, was dried over 4 \AA molecular sieves. The mixed solution was heated with stirring at $90 \text{ }^\circ\text{C}$ in a closed flask for around 4 h until a homogenous transparent liquid solution was formed. To initiate the polymerization, the prepared PDES was mixed thoroughly under ultrasonication with crosslinkers, PEG (200) diacrylate (DA), and a photoinitiator. In this work, the prepared PDES, PEG (200) DA, and photoinitiator were mixed at a weight ratio of 100:3.5:1, while stirring for a few minutes. The delignified wood samples were placed at the bottom of a dish and immersed in the liquid-prepared PDES, which was preheated in an oven at $90 \text{ }^\circ\text{C}$. Subsequently, the lignin-removed wood template was infiltrated in prepolymerized PDES solution under vacuum for 5 min, and this process was repeated five times to ensure full infiltration. The polymerization process was completed by passing the solution through an ultraviolet (UV) light source (major wavelength of 365 nm) for seconds. The poly(PDES)-infiltrated wood sample was peeled off the glass slides after the poly(PDES) had solidified completely. In addition to high transparency, stretch-ability, and electrical conductivity, the prepared transparent material exhibited excellent sensing behaviors to strain/touch, even at low strains. Therefore, the authors believe that these materials can be used to detect weak pressure, such as the subtle bending-release activities of humans. This means that the materials have promising potential for electronic applications in flexible displays, tactile skin sensors, and other fields.

Within previous research studies, prepared transparent wood structures were either thin and highly anisotropic, or thick and isotropic but weak. Therefore, transparent plywood (TPW) laminates were also investigated as loadbearing bio-composites with tunable mechanical and optical properties.^[135] This study utilized NaClO_2 and MMA as the delignifying and polymer media, respectively. The plies of transparent balsa wood were laminated with controlled fiber directions and predetermined stacking sequences in order to control the directional dependence of modulus and strength. Consequently, this provided improved properties in the weakest direction. The five impregnated delignified veneers were then assembled with their grains perpendicular ($0^\circ/90^\circ/0^\circ/-90^\circ/0^\circ$) to each other or laminated with a quasi-isotropic structure by increasing their angle by 45° ($0^\circ/45^\circ/90^\circ/-45^\circ/0^\circ$). The laminated wood was sandwiched between two glass slides and packaged with aluminum foil. The polymerization process was then performed by oven heating at $70 \text{ }^\circ\text{C}$ for 4 h. In addition, the quantum dots (QDs) CdSe/ZnS were embedded in the transparent wood to

make luminescent TPW. This was achieved by dispersing the QDs in a prepolymerized MMA solution. The wood templates were then infiltrated into the dispersed QD/PMMA solution. After complete infiltration, the wood templates were assembled and sandwiched between glass for further polymerization. Due to the lamination, the ultimate strength in the “transverse” direction increased from 15 to around 45 MPa. Light was transmitted through TPW and subjected to isotropic angular spreading. From an engineering standpoint, the TPW can be designed with higher strength and larger dimensions. Foster et al.^[87] also prepared plywood from transparent wood using similar methods. Furthermore, Li et al.^[130] utilized the same approach of infiltrating a wood template with MMA containing CdSe QDs to produce luminescent transparent wood.

6.1.3. Short Overview of Transparent Lignocellulosic Materials

Transparent or semitransparent wood-based products have also been prepared without using a DW matrix.^[136] The authors introduced pieces of walnut wood into a mixture of hydroxypropyl acrylate and/or MMA, 2-hydroxyethyl methacrylate monomers, and a plasticizer (dioctyl phthalate) in the presence of a chemical initiator (benzoyl peroxide). Through bulk free-radical polymerization, they obtained a transparent polymeric matrix containing dispersed wood. The exact size of the wood pieces embedded within the $0.4 \times 27 \times 12 \text{ cm}$ plates was not mentioned in the paper. However, from the figures, it can be assumed that they had a relatively small size. Although it is difficult to decipher exactly how the transparent wood was produced in the study, the results still demonstrate that the bulking of wood cells with a polymer is a useful method for the preparation of transparent wood-based materials. The sheets produced were characterized by tensile testing, dynamic mechanical thermal analysis, thermal gravimetric analysis, and heat deflection temperature. Good thermal stability up to temperatures of around $200 \text{ }^\circ\text{C}$ was presented.

Additional studies have also prepared similar transparent wood-based materials. However, within the context of this chapter, they cannot be classified as transparent wood. In a particular study, a novel transparent flat woody film was developed by direct dissolution of finely divided Japanese beech wood in formic acid at room temperature for 4–7 days.^[137] A mixture of 0.2 g of the ball-milled wood and 3.8 g of formic acid was stirred at room temperature for 5 days. A 5 wt% solution was obtained when the ball-milled wood was fully dissolved. The solutions were cast onto a flat suitable substrate to prepare the films. Films were formed by evaporating the formic acid at room temperature in a fume hood, which led to slow evaporation of the solvent on the substrate. The obtained woody films were considered to be molded wood. The woody films were transparent and foldable without breaking, and could also be utilized below $180 \text{ }^\circ\text{C}$. Furthermore, the films had relatively high Young’s moduli and tensile strengths. Moreover, the films exhibited very high biodegradability, which is comparable to that of cellulose. It is expected that this highly biodegradable and sustainable molded wood will be used for various applications in which cellulose acetate is currently utilized.

Transparent wood is a relatively new yet extremely active area of research. However, some reports have appeared that highlight the drawbacks of this material and its preparation, in addition to providing subsequent solutions to overcome these issues. For example, Feng et al.^[97] believe that wood is an anisotropic heterogeneous material and various defects easily form during the growth process. Some shortcomings exist for large-scale preparation of transparent wood such as difficult production, easy warping, and poor crossgrain properties. Moreover, the original 3D structure of transparent wood needs to be retained and the process of delignification needs to be precisely controlled to prevent disintegration of large-scale wood, which increases cost. Consequently, Feng et al. proposed replacing transparent wood with transparent DJFs within the production industry. The preparation of DJFs within this study has been explained in detail in Section 5. Once the DJFs were prepared, an electronic balance was immersed in anhydrous ethanol solution for 6 h after loading. Epoxy resin and the curing agent were then disposed of separately and the DJFs were mixed with the resin by vacuum impregnation for 2 h. The completely impregnated but not cured DJFs were sandwiched between two silica gel pads. More than 2 kg of weight was placed on the top silica gel pad to ensure smoothness of the transparent DJFs. The DJFs were dried at room temperature for 24 h. The mechanical and optical properties were compared with transparent coir fiber and transparent balsa wood. The experimental results showed transparency of 51% even for dense DJF cloth and a maximum transmittance as high as 60% at a low surface density. DJF had similar tensile strength to transparent balsa wood with a maximum value of 43.25 MPa at a surface density of 340 g m⁻³. These results suggested that transparent DJF material has the potential to match the optical and mechanical properties of transparent wood, while facilitating a simpler and cheaper preparation process.

Transparent paper is also a relevant product as it is prepared directly from transparent wood.^[138] A top-down method was developed to fabricate isotropic transparent paper directly from anisotropic wood. It included two steps: a delignification process to bleach the wood by lignin removal and a pressing process for removing light reflecting and scattering sources. The resulting isotropic transparent paper had high transmittance and haze of ≈90 and >80%, respectively, and its potential was demonstrated as a natural disposable substrate for electronic/optical devices.

6.1.4. Properties of Transparent Wood

Optical Properties: The optical properties of transparent wood are probably the most important characteristics in terms of its potential utilization in various applications. Hence, it is useful to provide an overview of the definitions of the most relevant optical properties:

Scattering is defined as the deviation of a beam of light from a straight path after interaction with an object.^[139] In this sense, refraction and reflection (in addition to many other optical phenomena) can correctly be regarded as scattering. However, generally speaking, scattering tends to refer to the interaction of light with small particles, often distributed at random in a

continuous medium, such as small dust particles in air. Elastic scattering is a complex process that generally refers to the interaction of a light beam with objects such as smoke, dust, or water droplets, in which little or no energy is exchanged. To a reasonable approximation, elastic scattering simply involves the redirection of light from its original trajectory. Inelastic scattering describes the complex process occurring when there is a significant energy exchange with the object so that the scattered radiation generally has a lower energy than the incoming radiation.^[139]

Optical transmittance: As an optical beam travels through a material—in this case, transparent wood—it loses part of its energy and changes its structure due to several factors: 1) back reflection at the front and back planes, 2) scattering inside the material (backward and forward scattering), and 3) absorption inside the material. All these processes depend on the physical properties of the transparent wood. Some properties that influence light scattering include the quality of the sample facets, refractive index mismatch between the wood and polymer, the presence of voids, and the anisotropic structure. Residual absorbents from the original wood and the introduced polymer are responsible for light absorption.^[136] Physically, the transmittance is the total amount of light energy transported through the sample into forward half-space, including both scattered (diffused) light and part of the beam going without noticeable disturbance. Effectively, it equates to the energy of the input beam subtracted by the reflection, absorption, and scattering in the backward half-space.

Haze phenomenologically describes the relative amount of forward scattered or diffused light that results in decreased image contrast observed through the material. In this case, it can be defined as the ratio between the forward scattered light and transmittance.^[136] Similarly, Preston et al.^[140] define haze as the ratio between forward scattered light and the sum of forward nonscattered and forward scattered light.

Transport mean free path is an established term in the theory of optical scattering that is defined as the distance after which the photon direction of propagation is fully randomized. It is not related to the initial direction.^[141]

From an application standpoint, the production of transparent wood with a larger thickness than the typically manufactured veneers would be of a great interest. Chen et al.^[142] carried out an extensive investigation on the thickness dependence of optical transmittance of transparent wood. Unlike non-scattering absorbing media, the thickness dependence of light transmittance of transparent wood is complex because optical losses are also related to increased photon path length from multiple scattering. The study used both acetylated and non-acetylated balsa wood templates that were delignified, bleached, and impregnated with prepolymerized MMA. Using the photon diffusion equation, they found that the angle-integrated total light transmittance of transparent wood has an exponentially decaying dependence on sample thickness. The key parameter of the photon diffusion equation is the attenuation coefficient that characterizes a certain material. According to the model, the attenuation coefficient encompasses both light absorption and scattering effects to light transmittance. Therefore, it can serve as a primitive material property inherent to a particular type of transparent wood prepared by a certain process. The

total transmittance and thickness values were measured for a range of transparent wood samples and were fitted according to the derived relationship. With regard to optical transmittance, the attenuation coefficient can facilitate crosscomparison of different sample types and thicknesses. The model was verified with two other types of transparent wood (ash and birch) and was found to be generally applicable to other scattering media.

The optical and mechanical properties of acetylated transparent wood composite laminates were investigated by Foster et al.^[87] The authors stressed the importance of multiply composite laminates due to their mechanical advantages compared to single-ply. The detailed description of the DW template preparation in this study is provided in Section 5. Using the DW template samples, a base-catalyzed acetylation was completed using acetic anhydride and triethylamine in dimethylformamide. One- and two-ply laminate transparent wood composites were fabricated using the DW and acetylated templates and a clear photocurable methacrylate-based resin. The optical and mechanical properties of the prepared transparent laminates made both from unmodified and acetylated wood were determined using ultraviolet–visible (UV–vis) spectroscopy and tensile testing, respectively. It was shown that acetylation of the DW template influenced both its mechanical and optical responses. In addition, the ability of the classical lamination plate theory and the simple rule of mixtures to predict multiply tensile modulus and strength, respectively, were investigated using the ply-level mechanical properties. Experimental results highlighted tradeoffs between the mechanical and optical responses of both unmodified and chemically modified transparent wood composites. Template acetylation reduced the stiffness and strength in the 0° fiber direction by 2.4 GPa and 58.9 MPa, respectively, compared to the unmodified samples. At high wavelengths of light (>515 nm), composites made of acetylated wood exhibited higher transmittance than the samples from unmodified wood. Above wavelengths of 687 nm, the 2-ply acetylated wood sample exhibited a higher transmittance than the 1-ply unmodified wood sample, indicating that thickness-dependent optical constraints can be overcome with improved interfacial interactions.

The scattering of light when transmitted through transparent wood is an important characteristic that was studied by Vasileva et al.^[152] They investigated the relationship between anisotropic scattering and the internal structure of transparent wood. In the study, acetylated transparent wood was prepared in four main steps. First, a balsa wood template was cut from a tangential section of the tree and was delignified using NaClO₂. The sample was then acetylated by acetate anhydride to reduce the interfacial gaps between the polymer and cell wall by improving the surface compatibility between the wood template and polymer. The acetylated balsa was then delignified again to remove its color, and finally it was infiltrated with prepolymerized MMA. Using the samples, the authors measured the angular distribution of scattered light. They stated that the anisotropy of the light scattering was attributed to the structural anisotropy of the material introduced by coaligned vessels and fibers, as well as perpendicularly oriented rays. It was demonstrated that in order to characterize the scattering properties of transparent wood, the haze (commonly used for the analysis of isotropic scattering media) should be applied with certain restrictions: the sample thickness should be smaller than the

transport mean free path and the detector aperture should be considerably limited.

Wu et al.^[131] prepared transparent wood from six species using a method that retained the natural color and texture of the wood while transmitting light. The difference in color and light transmittance of transparent wood of dark and light tree species may be caused by different factors such as lignin content, pigment group, and extract type. Consequently, the authors believe that transparent wood also has significant potential as a functional decorative material.

Mechanical Properties: Some mechanical properties of transparent wood were discussed in the review article by Keplinger et al.^[143] It has been demonstrated that cellulose scaffold–PMMA composites with a cellulose volume fraction of 5% have an elastic modulus and tensile strength of 2 GPa and 40 MPa, respectively. The direct comparison of transparent wood showed that an increase in the cellulose volume fraction from 5% to 19% increased the strength and elastic modulus values by a factor of two. Upon compressing the transparent wood, the cellulose volume fraction was increased to 19% and the tensile strength (90 MPa) and elastic modulus (3.6 GPa) were improved. However, it was demonstrated that the density as a single parameter was not useful for a general comparison of composites with different matrices and degrees of densification as it is not necessarily correlated with cellulose volume fraction. For instance, transparent wood has a high density but comparably low strength and stiffness because PMMA, which has the largest volume fraction in these composites, possesses a density of 1150 kg m⁻³.

Transparent wood based on delignified birch veneer and thermoplastic PMMA was investigated by uniaxial tensile tests and full-field strain analyses based on digital image correlation techniques.^[144] It was stated that the delignified birch veneer provided unexpectedly strong reinforcement effects in transparent wood/PMMA biocomposites due to the high cellulose content and favorable stress transfer mechanisms. Four in-plane elastic constants along the material axes were reported to enable the use of continuum mechanics and lamination theory. The longitudinal composite strength was as high as 270 MPa at a reinforcement content of only 25 vol%. The failure behavior was interpreted based on strain field development.

As described previously, Zhu et al.^[97] prepared anisotropic transparent basswood composites. They prepared radially and longitudinally oriented transparent wood pieces and demonstrated that the properties are strongly dependent on the type and orientation of the transparent wood. In particular, the light scattering and mechanical properties were shown to be dramatically different. The transparent wood with lumina in the plane was mechanically stronger and tougher. Further, while the light scattering effect was isotropic in the light propagation cross-section plane for radial transparent wood, the light scattering in longitudinal wood was highly anisotropic.

6.1.5. Applications of Transparent Wood

Applications in Energy Efficient Buildings and Windows: An interesting and condensed review of the possible utilization of transparent wood in the building and architecture industry was

presented in 2019 by Karl.^[124] One particular study cited within this review demonstrated a novel process to prepare transparent wood. This method left the lignin inside the wood cells by modifying its structure and only removing chromophoric structures. As mentioned in Section 6.1.2, the mechanical and optical properties of the lignin-modified wood proved to be better than delignified samples. The favorable properties of lignin retaining transparent wood can be useful for transparent wood beam applications. Various types of such beams can be created. For example, transparent wood “I” beams are the best option to maximize transparency. Box beams are relatively similar to “I” beams but they contain two parallel webs, which makes them less transparent but stronger. Another option is to create trusses or façade materials from lignin retaining transparent wood. Finally, TPW was discussed for potential use in the building industry as semitransparent nonbearing partition walls or as load bearing solid beams for short bridges, stairs, or railings. If thicker TPW materials were created, they could be arranged similarly to crosslaminated timber and would be able to span even further distances.

For transparent wood to be successfully utilized for building materials, and in particular load bearing structures, the thickness of the wood would need to be substantial.^[142] Li et al.^[145] addressed this issue by preparing 2–5 cm thick translucent (rather than transparent) basswood composites as the wall material for a house model. The composites were prepared by H₂O₂ steam delignification and infiltration with epoxy resin. Although the transmittance of these materials was only 40%, the light intensity inside the house model with 2 cm thick translucent wood walls was more uniform and higher compared to the model with a 0.5 cm thick transparent wood rooftop. This remained the case in both the morning and afternoon of a sunny day, as well as throughout overcast days. Moreover, unlike transparent wood rooftops, the light intensity inside the house model with translucent wood walls increased from the rooftop to the ground. It was deemed that this increasing light intensity was beneficial to daily life. Finally, a light intensity of 600 lux could be attained at a spot 10 cm from the 5 cm thick translucent wall although the transmitted light intensity of the wall was only 20% of the environmental light.

Another attempt to produce thicker transparent wood specimens was reported by Li et al.^[146] The study prepared highly transparent balsa and birch wood (thickness of 1.5 mm) with a transmittance of 92%, which is close to that of pure PMMA (95%). The high transmittance was achieved by interface manipulation through acetylation of the wood template. For example, the presence of interface debondings introduced greater optical heterogeneity due to the low refractive index of air 1) in the debonding gap. Consequently, this led to stronger light scattering, and thereby decreased transmittance. The interface gap is mainly caused by poor compatibility between the more hydrophilic wood cell wall and the more hydrophobic infiltrated polymers (PMMA, epoxy resin, polystyrene, vinyl carbazole, iso-bornyl methacrylate, etc.). Moreover, polymer volume shrinkage occurs during polymerization, further promoting the formation of interface gaps. Surface manipulation is a common and useful strategy to solve the compatibility issues, including the use of compatibilizer and surface modification. It is well documented that acetylation is an efficient method

to hydrophobize wood or lignocellulose pulp. Therefore, the authors of this research applied surface acetylation on DW substrates before PMMA infiltration to improve compatibility between the wood template and PMMA. This led to reduced interface debonding and improved optical transmittance. Both experimental and electromagnetic modeling results supported that the improved transmittance is mainly due to the elimination of the interface debonding gap. By applying this method, a centimeter thick transparent wood structure was obtained.

Within the architecture and building industry, transparent wood has great potential to be utilized for windows. For example, Lang et al.^[147] assessed the favorable properties of transparent wood composites (high strength and toughness, thermal insulation, and excellent transmissivity) and presented a route to replace glass for diffusely transmitting windows. Furthermore, transparent wood could be used as a material for smart windows, such as in the form of electrochromic devices that switch on-demand. Compared to glass, transparent wood has lower thermal conductivity and density, and better impact strength. Therefore, transparent wood could be used to produce windows or rooftops, which would reduce the energy consumption of air conditioning and lighting, especially during the daytime. The current approach for the preparation of transparent wood is based on delignification of the wood substrate followed by infiltration of a polymer with a refractive index that matches the wood substrate. However, the residual lignin and resin in transparent wood are sensitive to UV light, resulting in discoloration and aging. Furthermore, near infrared (NIR) light easily passes through transparent wood, which is disadvantageous when maintaining a constant indoor temperature.^[148]

Mi et al.^[149] developed thermally insulated transparent wood for potential application in energy efficient windows. The delignified wood slice was infiltrated by PVA and heated at 60 °C to dry and solidify for about 48 h. The transparent wood simultaneously exhibited low haze (≈15%) and high transmittance (≈91%). Furthermore, it had a high toughness of 3.03 MJ m⁻³, which is 3 orders of magnitude higher than standard glass (0.003 MJ m⁻³), and a low thermal conductivity (0.19 W m⁻¹ K⁻¹), which is more than five times lower than that of glass. Hence, the authors suggested that the prepared transparent wood could be employed as energy efficient and sustainable windows.

In order to improve the UV resistance and increase the IR heat shielding of transparent wood, it was prepared by delignification of the wood substrate and infiltration of prepolymerized MMA with modified antimony-doped tin oxide (ATO) nanoparticles.^[148] The ATO nanoparticle addition enhanced the interfacial bonding among the compounds, which improved the fracture strength. This led to a high fracture strength and modulus of 96.4 MPa and 4.27 GPa, respectively, with the addition of 0.3% ATO. The obtained ATO/transparent wood exhibited high transparency, excellent NIR heat shielding performance, and UV shielding properties. The transparent wood treated with 0.3% ATO maintained a very low thermal conductivity of ≈0.2 W m⁻¹ K⁻¹. After addition of 0.7% ATO, the obtained transparent wood had a quite low UV transmittance of <20%.

A similar approach for obtaining transparent wood with heat shielding properties for windows was reported by Yu et al.^[150] However, instead of ATO nanoparticles, Cs_xWO₃ nanoparticles

were dispersed in prepolymerized MMA and filled the nanopores of DW to prepare transparent wood. High optical transmittance and haze of 86% and 90%, respectively, were achieved for 5 mm thick transparent wood. These properties are suitable for windows with requirements of day lighting and privacy. The Cs_2WO_3 /transparent wood displayed excellent mechanical properties with a fracture strength and modulus up to 59.8 MPa and 2.72 GPa, respectively, which are much higher than those of neat PMMA. Further, the wood-based composite showed outstanding NIR (780–2500 nm) shielding ability.

The high haze (>40%) of transparent wood is a major obstacle preventing it from effectively replacing glass in windows.^[151] In the work of Jia et al.,^[151] fabrication of a clear wood material with a maximum optical transmittance of 90% and a very low haze of 10% was performed using a delignification and polymer infiltration method. The significant removal of wood components from basswood with NaClO , NaClO_2 , and acetic acid resulted in a highly porous microstructure, thin wood cell walls, and large voids among the cellulose fibrils. As a polymer (e.g., epoxy resin) could easily enter these voids, the clear wood had a very dense structure. The separated cellulose fibrils that resulted from the removal of the wood components weakened light scattering in the clear wood. The combination of weak light scattering and the highly dense structure of the wood produced both high transmittance and extremely low haze. In addition, the clear wood exhibited excellent thermal insulation properties with a low thermal conductivity of $0.35 \text{ W m}^{-1} \text{ K}^{-1}$ ($\approx 33\%$ of ordinary glass).

Utilizing transparent wood as an energy-saving building material was also considered by Wang et al.^[152] In particular, they addressed the difficult problem of fabricating larger (thickness and size) transparent wood samples. Within the study, an efficient large-scale production method for manufacturing transparent wood with the same advantages as smaller-sized transparent wood was presented. In the study, transparent wood ($300 \times 300 \times 10 \text{ mm}$) was prepared by infiltrating the prepolymerized MMA solution into DW fibers rather than the intact wood template. Poplar (*Populus* sp.) wood was pulverized into particles, following delignification with NaOH and Na_2SO_3 and bleaching with H_2O_2 . Further, the DW fibers were infiltrated by using the prepolymerized MMA solution. The prepolymerized MMA solution with infiltrated fibers was then decanted into prepared molds where the additional polymerization was carried out. It is important to mention that this work produced a transparent wood fiber/polymer composite rather than a true transparent wood. However, regardless of this, the transmittance, haze, mechanical properties, and thermal conductivity of the obtained transparent composite were investigated. A 10 mm thick transparent composite sample exhibited high optical transmittance and haze of 68% and 90%, respectively. Furthermore, the sample had excellent mechanical properties with a maximum rupture strength and modulus of 46.8 MPa and 2.2 GPa, respectively. These mechanical property values were much higher than that of natural wood and neat PMMA. Real-environment simulation tests showed that the transparent fiber wood provided excellent thermal insulation. The authors of the paper believe that the transparent fiber wood could be a desirable material for energy-saving building applications.

Thermal Energy Storage: Utilizing transparent wood as a functional load-bearing material for thermal energy storage applications can be further improved by the inclusion of phase-change materials.^[16] A shape-stabilized phase-change material based on PEG was encapsulated into a delignified silver birch wood substrate and the transparent wood obtained was fully characterized. The thermal energy storage wood was prepared by impregnation with a liquid PEG/MMA blend, followed by MMA polymerization. The large latent heat ($\approx 76 \text{ J g}^{-1}$) of the material was combined with switchable optical transparency. The researchers believe that the prepared transparent wood is superior to normal glass as a thermal storage material because of the combination of good heat-storage and thermal insulation properties.

Magneto-Optical, Luminescent, Electroluminescent, and Electrochromic Applications and Devices: Gan et al.^[153] highlighted that optically transparent magnetic materials have attracted increasing attention in the materials science community because of their numerous potential applications including information storage, magneto-optical switches, bioanalysis, optical isolators, and modulators. Therefore, they prepared and characterized transparent magnetic wood (TMW) based on filling the DW template with index matching MMA and magnetic Fe_3O_4 nanoparticles. Transparent Cathay poplar (*Populus cathayana* Rehd) wood was prepared by conventional methods of delignification and bleaching but impregnation was executed using MMA and Fe_3O_4 nanoparticles. Light transmittance of the transparent wood decreased from 90.4% to 19.5% with the increasing concentration of magnetic particles. The tensile strength and elastic modulus were also affected by the Fe_3O_4 nanoparticles but still remained outstanding. Conversely, the obtained magnetic properties were described as excellent and the authors believed that the material is an outstanding candidate for light transmitting magnetic buildings and magneto-optical devices.

LEDs based on transparent wood have also been prepared.^[92] Multiple-color-emission carbon dots (CDs), serving as trichromatic systems in white-LEDs, were synthesized by tuning the extent of graphitization and surface function of the nanoparticles using citric acid and urea as feedstocks. The ultrafast removal of lignin from wood using DESs (oxalic acid and choline chloride) under microwave-assisted treatment was then performed. After this, carbon dots and PAA were filled into the DW through an in situ polymerization. The transparent wood film embedded with multicolor CDs showed white light emission under UV light excitation and enhanced mechanical tensile strength (60.92 MPa). Simultaneously, the as-prepared film could be used as an encapsulation film for white LEDs, which exhibited excellent color characteristics.

Tang et al.^[154] prepared a conductive film of silver nanowires with an optimal area density of 341 mg m^{-2} . The prepared film showed outstanding synergistic properties, with a transmittance and sheet resistance of 80% and $11 \Omega \text{ sq}^{-1}$, respectively, which is equal to the conductivity of indium tin oxide. Poplar (*Populus*) slices ($9.0 \text{ cm} \times 5.5 \text{ cm} \times 180 \mu\text{m}$) were delignified with NaClO_2 and glacial acetic acid, and the DW was then impregnated with the flexible resin mixture of epoxy and polyurethane. Electrical conductance was assured by direct deposition of silver nanowire ink on the surface of the flexible wood film. The morphologies

of the DW and silver nanowires were characterized by SEM, the transmittance spectrum and haze were measured by UV–vis spectrophotometry, and the mechanical properties were measured with an electronic testing machine. Furthermore, the sheet resistances of the wood films were determined. The natural cell structure in the wood was well preserved during the delignification and polymer impregnating processes. The alignment of the cell structure in the transparent films led to highly anisotropic transmittance. It was also demonstrated that a conductive film with high transparency could light up an LED. The conductive film was quickly assembled from the wood film as a flexible substrate and silver nanowire ink as conductive filler. Silver nanowires were thereby encapsulated into the matrix and uniform multiscale electrical network architecture was ultimately established. The conductive film showed high optical transmittance, low sheet resistance, strong adhesion, and mechanical flexibility. Consequently, it could be used to fabricate efficient, flexible, and printable paper electronic devices for future applications. The transparent wood film exhibited outstanding mechanical flexibility and it was suggested to be used as a screen protector film for cell phones. In general, it was concluded that transparent conductive wood films may potentially replace plastic for flexible green electronics in the same way that plastic had previously replaced glass.

Transparent wood can also be used in the production of lasers.^[155] In a particular study on this topic, the authors used a PMMA filling polymer that was mixed with Rhodamine 6G (Rh6G) laser dye before impregnation into the DW matrix. Polymerization occurred after the polymer/dye solution was already infiltrated into the transparent wood material. With optical pulses (4 ns, 40 mJ at 532 nm wavelength) and a side-transversal pumping scheme, they obtained laser radiation from the transparent wood sample. The lasing transparent wood had radiation of relatively narrow linewidth and low spatial coherence simultaneously. The transparent wood was classed as a “quasi-random laser” since it had a somewhat ordered structure (neither totally regular nor random) but did not contain any external cavities providing optical feedback for the whole system. Such a material could be interesting for the practical development of “quasi-random lasers” since it provides high spectral brightness with simultaneous absence of the speckle pattern. These characteristics are very desirable for many applications such as illumination, lighting, and projector design. A quasi-random laser from dye-doped transparent wood was also reported by the same group of coauthors.^[156,157] They utilized a quasi-random laser based on transparent wood as a semioordered host matrix, which was doped with Rh6G dye as the gain medium.

Sliced veneers of transparent birch wood (delignified, bleached, and epoxy resin treated) were used to produce intrinsically high-temperature and high-humidity resistant alternating current electroluminescent (ACEL) devices.^[158,159] The ACEL devices were fabricated by sandwiching an elastic ZnS:Cu/epoxy resin luminescent layer between two silver nanowires/transparent veneer electrodes. The advantage of the novel device compared to classic plastic-based electroluminescent devices was its low coefficient of thermal expansion (3.94×10^{-6} K) and good antideformation capabilities. Consequently, the preparation of flexible and high temperature resistant ACEL

devices was demonstrated.^[158,159] Zhang et al.^[159] showed that the total transmittance of the ACEL device (up to 86%) was larger than cellulose-based transparent films. Furthermore, the prepared ACEL device possessed waterproofing properties without the need for additional sealing. The luminance of the device approached a maximum value of 18.36 cd m^{-2} at a voltage of 220 V (frequency at 1 kHz), demonstrating its great potential for applications in signal expression and ambient lighting. The preparation of luminescent TPW has also been reported in the literature.^[160]

Gan et al.^[161] produced another relevant report on the preparation of luminescent and transparent wood composites. The luminescent effect was obtained by introducing luminescent $\gamma\text{-Fe}_2\text{O}_3@Y\text{VO}_4:\text{Eu}^{3+}$ nanoparticles in the prepolymerized polymer solution. First, the delignified Cathay poplar (*Populus cathayana* Rehd) wood template, which was used as a support for the transparent polymer and nanoparticles, was obtained from natural wood through a lignin removal process. The functionalization then occurred in the lumen of the wood as the PMMA filled the cell lumen and enhanced cellulose nanofiber interaction. This led to wood composites with excellent thermal and mechanical properties, in addition to dimensional stability. More importantly, the wood composite displayed a high optical transmittance in a broad wavelength range (350–800 nm), magnetic responsiveness, and brightly colored photoluminescence under UV excitation at 254 nm. The authors suggested that luminescent wood composites with these unique properties have great potential in applications including green LED lighting equipment, luminescent magnetic switches, and anti-counterfeiting facilities.

Transparent wood was exhibited to be a very interesting material in the production of electrochromic devices.^[147] There are three main classes of electrochromic materials that have been studied for smart windows and mirrors: metal oxides (WO_3 , NbO_x , VO_x), molecular electrochromes (e.g., viologen derivatives), and electrochromic polymers.^[147] The working principle for electrochromic materials is the generation of new electronic states resulting from a redox reaction. These states give rise to new electronic transitions, which cause a shift in the absorption profile providing light modulation over wavelengths from UV to IR.^[147] In the work of Lang et al.,^[147] a simple and relatively benign process of generating highly conductive poly(3,4-ethylenedioxythiophene):poly(styrene sulfonate) (PEDOT:PSS)/transparent wood electrodes for electrochromic devices was demonstrated. The transparent substrates derived from birch wood incorporated 30% cellulose fibers by volume and exhibited improved strength and toughness compared to neat PMMA. Transparent birch wood (NaClO_2 was used for delignification and as a bleaching agent and PMMA for the polymer filler) was coated with PEDOT:PSS as a transparent conducting electrode. The coating exhibited a magenta-to-clear color change that resulted from a colorless bleached state. Low energy power inputs of 3 mW h m^{-2} at 2 W m^{-2} were required to switch due to a high coloration efficiency (590 C cm^{-2}) and low driving voltage (0.8 V). Therefore, it was shown that transparent wood has a great potential in smart windows to replace glass because of its high strength (140 MPa), excellent work of fracture (3.2 MJ m^{-3} , 30 times higher than glass), low thermal conductivity (0.23 W m K^{-1}), diffuse transmittance (80%), and haze (70%).

Another interesting property of transparent wood, which may be very significant to potential applications, is photochromism. For instance, the photochromic characteristics of transparent wood might be highly desired in the production of smart windows. Wang et al.^[134] obtained photochromic transparent wood with photo switching of transmittance in the visible light region by infiltrating the lignin modified wood template with a mixture of photochromic material (30,30-dimethyl-6-nitro-spiro[2H-1-benzopyran-2,20-indoline]-10-ethanol) and prepolymerized MMA. The material exhibited a vibrant purple-to-colorless color change under the illumination of light.

Applications in Solar Cells: Transparent wood has also been used as a substrate for solar cells.^[136] Perovskite solar cells with a power conversion efficiency up to 16.8% were successfully assembled on optically transparent Balsa wood (*O. pyramidale*) substrates using a low temperature process below 150 °C. The devices also showed good long-term stability. These results suggest that transparent wood is a potential candidate for replacing glass as a substrate in the assembly of sustainable solar cells. This would lower the overall carbon footprint of the devices.

Zhu et al.^[97] produced another report regarding the application of transparent wood in solar cells. Lignin removal of basswood was performed using NaOH and Na₂SO₃, and PVP was used for infiltration. Transparent wood elements were then attached to GaAs solar cells and a drop of ethanol was deposited on the surface of the existing solar cell. The transparent wood was then placed on top of the cell to form intimate contact. The sandwich structure was allowed to dry at room temperature until the wood was firmly attached to the surface of the bare GaAs solar cell. The morphologies of wood were characterized by SEM and the lignin contents were measured using standard methods. Transparency and haze were also determined, in addition to the electrical properties of GaAs solar cells before and after the attachment of the transparent wood composite. The transparent wood displayed a high optical transmittance and haze simultaneously in a broad wavelength range (400–1100 nm). It was demonstrated that the novel transparent wood composite can function as a broad range light management layer and substantially improve the overall energy conversion efficiency by as much as 18% when simply coated with a GaAs thin film solar cell.

Consequently, the literature demonstrates that transparent wood is an emerging material with great potential to replace conventional materials. However, we believe that some significant technological challenges still need to be overcome before transparent wood can be considered for regular production and find its position on the market. Further, its environmental impact, in addition to cost analysis should be examined.

6.2. Structural Materials

6.2.1. High Performance Structural Wood Materials

Wood is generally modified to improve its undesirable properties via chemical, thermal, and mechanical methods. Wood materials with increased density can be an alternative to other structural materials because the mechanical properties and hardness of wood are mostly dependent on its density. Through

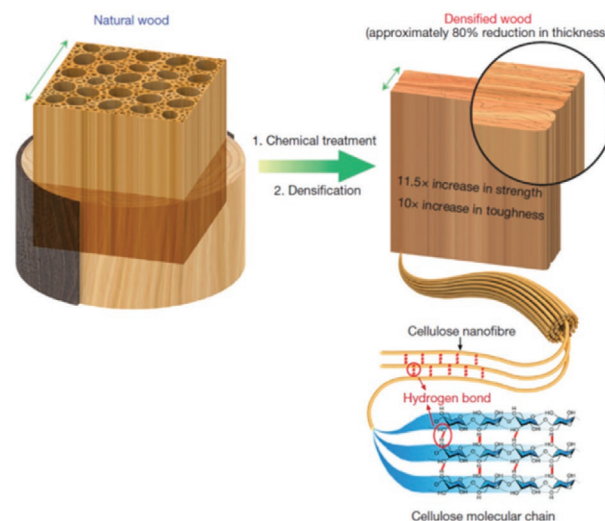


Figure 12. Schematic representation of the bulk densified wood material fabrication process. Adapted with permission.^[162] Copyright 2018, Nature Publishing Group.

densification, low-density medium-rotation wood species (e.g., hybrid aspen) can be converted into commercially high-value high-density products with better resistance to moisture and biological degradation. The densification of wood is achieved through compression, which reduces its pore space. The greatest problem encountered in compressed densified wood materials is that they tend to return to their initial dimensions due to spring-back, when used in high moisture conditions or exterior applications. The cell wall of densified wood swells and the compressed cells recover to their original position. Recently, several methods such as heat and vapor treatment have been developed to control this spring-back issue.

Song et al.^[162] explored the potential of H-bonding between cellulosic groups in the wood cell wall by controlling the removal of hemicellulose and lignin to prepare the densified bulk wood materials with high specific strength (see Figure 12). They removed different percentages of lignin from the wood cell wall (0%, 23.6%, 27%, 30%, 32.5%, 45%, 60%, and 100%; see Table 3) and DW samples were pressed at 100 °C under a pressure of ≈5 MPa for ≈1 day to obtain the densified wood. Table 3 demonstrates that 45% lignin removal from wood achieves the highest density, strength, toughness, and work fracture of densified bulk wood material. The densification of DW helps to form stronger H-bonding between OH groups available on adjacent cellulose nanofibrils. Further, they performed the scratch hardness test, hardness modulus test, Charpy impact test, Ballistic test, and accelerated test against moisture for prepared bulk materials. It can be concluded from this study that densified wood (after delignification) is mechanically superior to natural wood and many other widely used structural materials, as well as being more sustainable.

The same research group recently fabricated high quantity and thicker bulk wood materials via the delignification-densification process.^[107] In this work, wood blocks were first delignified and then stacked and hot-pressed together to achieve densification. The prepared bulk wood showed a high tensile strength of 161.3 MPa, which is threefold higher

Table 3. Summary of the cellulose/hemicellulose/lignin content of densified wood, as well as strength, work of fracture, and density under various degrees of lignin removal.^[102,162]

Lignin content removed [%]	Cellulose [%]	Hemicellulose [%]	Lignin [%]	Strength [MPa]	Work of fracture [MJ m ⁻³]	Density
0 ^{a)}	44.01	19.5	20.8	51.6	0.43	0.46
0 ^{b)}	44.01	19.5	20.8	175	1.1	1.04
23.6 ^{b)}	42.2	10.6	15.9	325.6	1.6	1.13
27 ^{b)}	40.02	9.2	15.1	386.6	2.1	1.20
30 ^{b)}	38.2	7.2	14.7	425.6	2.3	1.23
32.5 ^{b)}	38.1	6.8	14.3	488.8	2.9	1.25
45 ^{b)}	38.7	5.2	11.3	586.8	4	1.3
60 ^{b)}	35.4	3.8	8.2	319	1.48	1.15
100 ^{b)}	31.2	1.89	0.13	12.5	0.02	1.06

^{a)}Natural wood; ^{b)}Compressed/densified samples.

than natural wood. Similarly, a high compressive strength of 64.4 MPa was exhibited, which is approximately two times higher than natural wood. In another study, it was shown that DW–lignin hot-pressed composite materials could be potentially utilized as scalable functional materials with high strength properties.^[163]

A similar approach of delignification-densification was used to fabricate bamboo-based bulk material.^[108] In this work, linear cut bamboo was first softened with high-pressure steam (140 °C, 8 min) and flattened into bulk bamboo using a horizontal pressing apparatus (125 kg cm⁻² pressure). The sample was then delignified in aqueous solutions of 2.5 M NaOH and 0.4 M Na₂SO₃ for 12 h. Subsequently, it was washed with boiling water to remove residual lignin, hemicellulose, and waxy compounds in order to obtain a fully aligned cellulosic structure. Mechanical densification of delignified bamboo was performed at 150 °C under a pressure of 5 MPa for ≈24 h. The densified bamboo exhibited a record high tensile strength up to 1 GPa and a maximum tensile modulus of 75 GPa. Furthermore, this work demonstrated the top-down scalable method. The same research group reported^[164] the fabrication of lightweight densified bamboo structural materials with an additional step of microwave treatment after delignification to drive water out of the delignified bamboo structure without altering the aligned nanocellulose's structural integrity. After hot densification, the modified bamboo reached a density of 1.0 g cm⁻³ with exceptionally high specific tensile strength of 560 MPa cm³ g⁻¹.

Han et al.^[105] prepared bulk materials by compressing them with 0%, 5%, and 18% moisture content. They were then dried at three different conditions (air-dried, solvent exchange-dried, and freeze-dried). The densification formed close H-bonding between the adjacent OH groups. Essentially, they rehydrated DW at different relative humidities and mechanical compression was performed to introduce more hydrogen bonding to improve mechanical properties. The air-dried samples without rehydration and compression showed better mechanical properties (tensile strength, Young's modulus, and toughness) than the solvent exchange-dried samples. The freeze-dried samples exhibited the lowest mechanical properties.

Khakalo et al.^[106] prepared hot-compressed delignified birch wood-based bulk materials. The birch wood samples

were first delignified and the DW template (moisture content of 8.6%) was then infiltrated by the ionic liquid (IL) 1-ethyl-3-methylimidazolium acetate ([EMIM]OAc, >95% purity, ≤15 mbar) for 30 min. The IL infiltrated DW template was washed and then passed through the nip between these rolls at a temperature of 130 °C, speed of 1 m min⁻¹, and a line load of ≈30 kN m⁻¹. Dissolution of DW with IL increases flexibility in the sample by forming a gel-type layer on DW surfaces, which keeps the inner fiber structure intact. This is because the gel layer likely promotes better interconnection between fibers during pressing. During densification by hot-pressing, the pure DW was compressed from 560 to 1170 kg m⁻³. However, the IL dissolved DW was compressed up to 1347 kg m⁻³ due to the increased flexibility in the sample, which promoted more pronounced folding of the cells. The tensile strength of DW was increased from ≈75 to ≈300 MPa and had a maximum of ≈430 MPa for the IL-treated samples. This is because IL-treated DW has greater consolidation between cellulosic fibers and better H-bonding was achieved.

6.2.2. High Performance Thermal Insulators

Insulation materials are extensively used to reduce heat losses (or gains) from thermal systems in buildings.^[165] The ideal thermally insulating materials should possess a complex combination of properties such as low thermal energy absorbance/emissivity, low mass density, and good mechanical strength. Furthermore, they should be sustainable, renewable, degradable, and cost-effective.^[166,167] Various types of thermally insulating materials such as mineral wool, extruded and expanded polystyrene, polyurethane, and natural fibrous insulators (hemp and wood fibers) are commonly used in buildings.^[165,166] **Table 4** demonstrates the required properties of thermal insulators and provides a comparison between existing and recently developed thermally insulating materials. All existing thermal insulators have certain disadvantages such as excessive dependency on fossil fuels and high energy consumption in production (mineral wool). Furthermore, the performance of current biobased thermal insulators is not adequate to fulfil the present scenarios of the circular bioeconomy. All existing insulators

Table 4. Comparison of the thermal conductivities of existing thermally insulating materials and recently evolved high-performance thermal insulators.

Thermally insulating materials	Apparent density [kg m ⁻³]	Thermal conductivity (λ) [mW m ⁻¹ K ⁻¹]	Refs.
Mineral wool	30–180	30–45	[177]
Expanded polystyrene	18–50	29–41	[177]
Extruded polystyrene	20–80	25–35	[177]
Fiberglass or glass wool	13–100	30–45	[177]
Polyurethane	30–80	20–27	[177]
Cellulose fiber	50	40	[176]
Silica aerogels	13	15	[178]
Freeze-dried nanocellulose foam (aerogels)	12–33	24–28	[179]
Nanocellulose/graphene oxide/boric acid/sepiolite (freeze-dried)	7.5	15 (radial direction) 170 (axial direction)	[168]
Nanocellulose/silica nanoparticles (freeze-dried)	19–21	21–33 (radial direction) 77–132 (axial directions)	[180]
DW	13	30 ≈60	[15]
Transverse direction			
Axial direction			
NaOH-treated and freeze-dried delignified balsam wood	25	31	[181]

also have thermal conductivities that are too high for retrofitting or building new surface-efficient passive houses.^[168] In recent years, nanocellulose-based thermal insulators such as cellulose aerogels or foams have been extensively studied for the fabrication of sustainable and renewable high performance thermal insulators with ultralow thermal conductivities.^[169–176] However, cellulose-based aerogels or foam insulators still cannot be effectively scaled up to explore their full potential in building systems or other applications. This is due to their complex fabrication process that includes extracting nanocellulose from wood and then processing it into foams or aerogels via methods such as freeze-casting. In addition, the hierarchical cellulosic fibril arrangement of the samples is lost, resulting in a random orientation of fibrils. Consequently, poor mechanical properties are often exhibited. DW-based thermal insulators have the potential to overcome these issues and disadvantages. Li et al.^[15] prepared DW (they referred to it as nanowood) samples (12 × 30 × 120 mm) by preserving the hierarchical arrangement of cellulose and characterized its mesoporous–microporous structure, as well as bulk material properties including thermal conductivity, mechanical strength, porosity, density, and anisotropic behavior. The prepared DW exhibited anisotropic and transverse thermal conductivities of 30 and 60 mW m⁻¹ K⁻¹, respectively, in the axial direction of the cellulose fiber arrangement, as shown in **Figure 13**. The density of the DW was 13 kg m⁻³ and the compressive strength was 13 and 20 MPa in the axial and transverse directions, respectively. Therefore, DW has the potential to meet all the desired

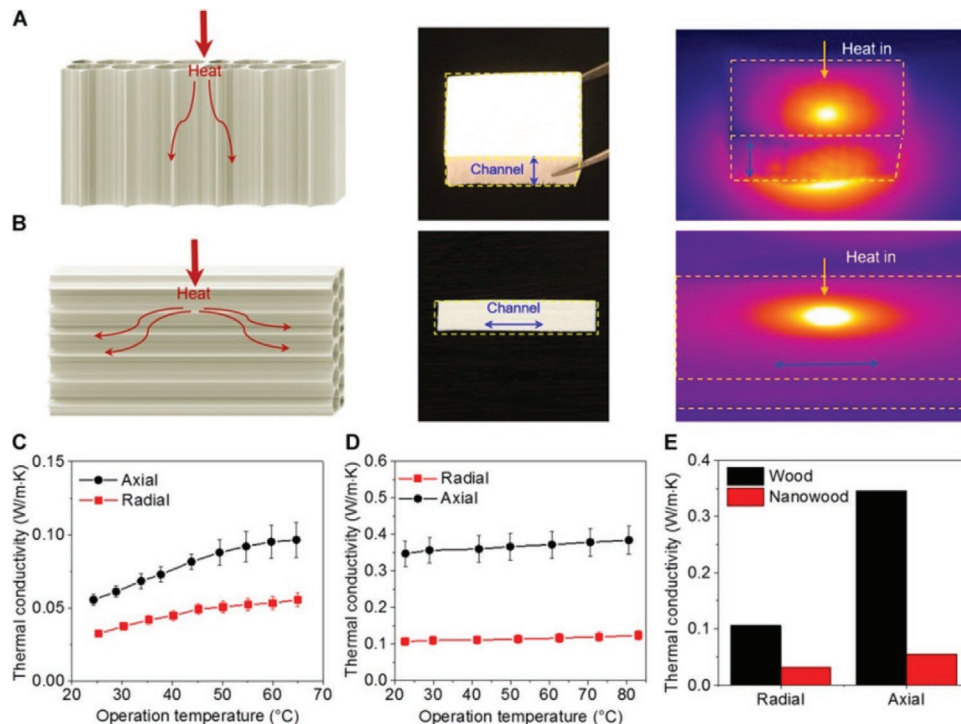


Figure 13. A) Schematic representation of heat conduction along the wood cell walls as axial heat transfer. B) Heat conduction across the wood cell walls and hollow channels (i.e., the lumen and the nanosized pores inside the fibril walls) as transverse heat transfer. C) Measured thermal conductivity of the nanowood (i.e., DW) from room temperature to 65 °C. D) Measured thermal conductivity of the original wood from room temperature to 80 °C. E) Comparison of the thermal conductivity of the natural wood and nanowood at room temperature. Adapted with permission.^[15] Copyright 2018, American Association for the Advancement of Science.

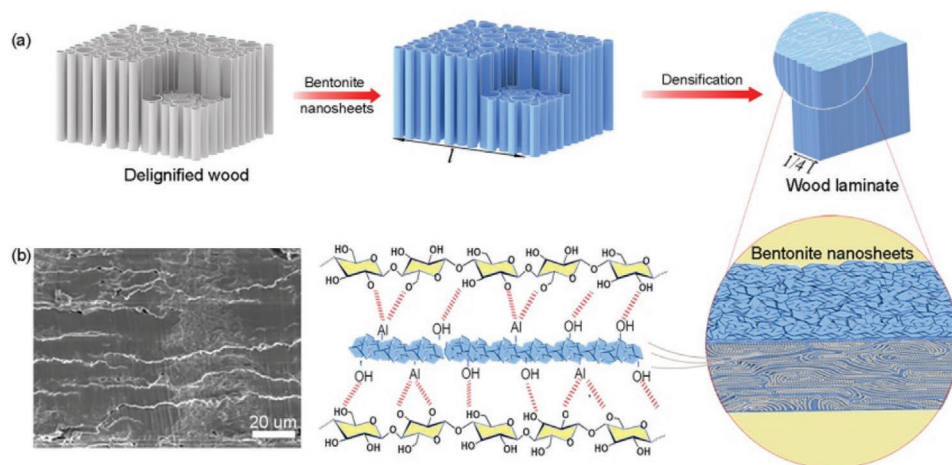


Figure 14. a) Bentonite nanosheets were infiltrated into DW before hot-pressing. The resulting densified wood laminate consisted of cellulose nanofibers and compatible bentonite nanosheets throughout. b) SEM image of the densified wood laminate and diagrams showing the formation of hydrogen and Al–O–C bonds between the cellulose nanofibers and bentonite nanosheets. Adapted with permission.^[182] Copyright 2019, Elsevier Ltd.

properties of an ideal thermally insulating material for use in energy-efficient buildings or other advanced applications such as light-weight materials for space programs.

In another study, a DW-based thermal insulator was prepared with flame-retardant and exceptionally high mechanical properties.^[182] **Figure 14** presents a schematic representation of the flame-retardant thermal insulator preparation. Bentonite nanosheets were infiltrated into delignified basswood to achieve flame-retardant characteristics. The sample was then densified by hot-pressing to improve its mechanical properties. The prepared thermal insulators exhibited 50% less peak heat release during a flame test, a tensile strength of 330 MPa, and thermal conductivities of 0.2 and 0.18 W m⁻¹ K⁻¹ in the axial and radial directions of fiber alignment, respectively. The infiltration of bentonite nanosheets into DW not only provided flame-retardant properties, it also enhanced the mechanical properties of the wood laminate through strong hydrogen bonds and increasing Al–O–C bond formation between the wood laminate cellulose and bentonite nanosheets.

Li et al.^[183] prepared radiative cooling structural materials using DW. Compressed DW was obtained by hot-pressing with ethanol. A hydrophobic treatment based on fluorosilane was also applied to the prepared multifunctional structural material to enhance its durability and applicability in exterior conditions. The mechanical (tensile strength and hardness), thermal (thermal conductivity), and optical properties of the sample were measured. Furthermore, a theoretical building model for measuring the radiative performance of DW-based cooling wood was designed and applied in 30 different US cities with various climatic conditions. The prepared densified DW was characterized as a structural cooling material for buildings and the radiative cooling properties were measured in real-time. **Figure 15** shows the comparative properties of natural wood and DW-based cooling wood. It was concluded that cooling wood is superior to natural wood for building efficiency due to its superior mechanical strength, continuous energy savings, and cooling behavior.

An attempt was made to fabricate a multifunctional structural material with desirable thermally insulating and mechanical

properties.^[111] In this work, fully DW was partially densified via humidity-assistance to reduce its thickness from ≈18.2 to ≈9.1 mm (≈50% reduction). During densification, the reactive OH groups formed strong hydrogen bonds, which contributed to a high tensile strength of ≈161 MPa (≈3.4 times higher than natural wood) and toughness of ≈1.31 MJ m⁻³ (≈3.2 times higher than natural wood). In addition to the exceptional mechanical properties, the prepared delignified-densified wood exhibited very low thermal conductivity of ≈0.09 W m⁻¹ K⁻¹ in the transverse direction. These exceptional properties demonstrated that the prepared structural material was ideal for utilization in energy-efficient buildings.

6.2.3. DW Reinforced Polymers

Polymers that are reinforced with synthetic (e.g., glass, carbon, and aramid) and natural fibers (e.g., flax and hemp) are termed as fiber reinforced polymers (FRPs). These materials have been utilized for many years in various applications such as strengthening materials for structural membranes in buildings and bridges, car parts (doors, sheets, etc.), wind turbine blades, and compressed molded products for day-to-day use. DW can provide a hierarchical cellulosic structure for future FRP material development and the fabrication process is also very similar to the preparation of transparent wood using DW (as discussed in Section 6.1). About two decades ago, Yano^[184] had produced the PF resin impregnated delignified spruce wood veneer and hot compressed to get densified wood, the Young's modulus and bending strength of prepared-treated samples showed 50% higher compared to nontreated samples. In this work, density of 1.4 g cm⁻³ was achieved and got 62 GPa Young's modulus and 670 MPa bending strength.

Frey et al.^[98,103] prepared a DW-polymer interpenetrating composite for high performance load-bearing wood components. In this work, different fiber volume contents (FVCs) were achieved by controlling the densification of the DW and polymer. This allowed the fabrication of a product with a specific desired stiffness and comparable properties to glass fiber

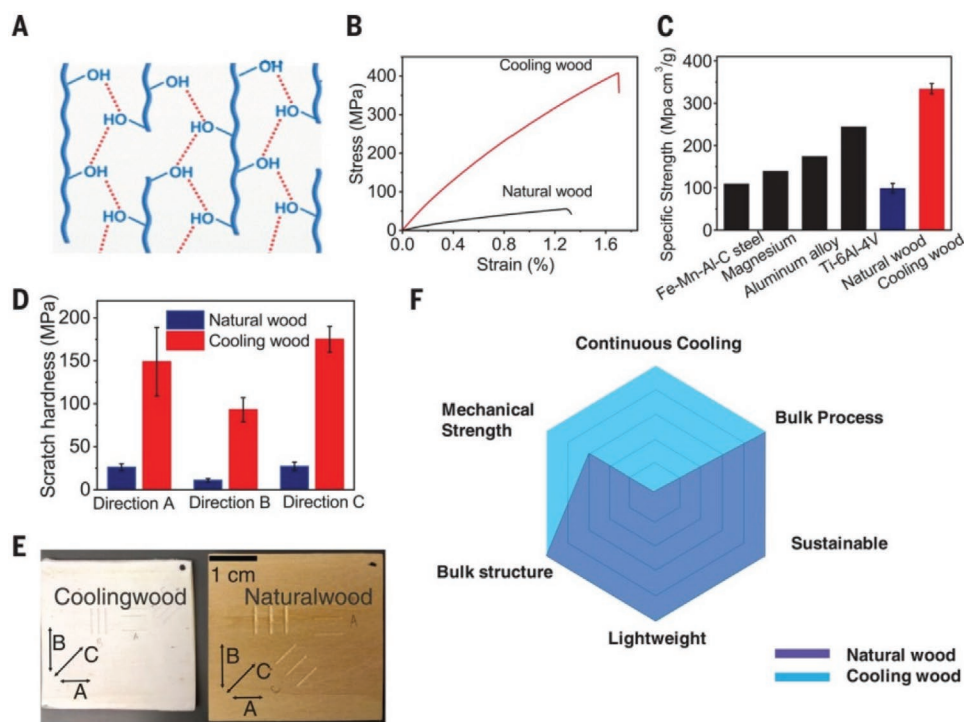


Figure 15. A) Schematic showing molecular bonding of the aligned cellulose nanofibers, which is responsible for the high mechanical strength of the DW-based cooling wood. B) The tensile strength and C) the specific ultimate strength of the cooling wood compared with natural wood and some common metals and alloys. D, E) Scratch-hardness characterization of natural and cooling wood in three different directions. A, B, and C denote directions parallel, perpendicular, and at 45° to the tree growth direction, respectively. F) Performance comparison of natural and cooling wood. Adapted with permission.^[183] Copyright 2019, American Association for the Advancement of Science.

reinforced polymer, as shown in **Figure 16a**. The prepared DW reinforced polymer (DWRP) material with an 80% FVC exhibited an extremely high tensile stiffness and strength of up to 70 GPa and 600 MPa, respectively. This was due to the combination of interlocks between cells and the reinforcing polymer matrix phase connecting fibers through lumen and pits.

Yu et al.^[20] utilized the bulk cellulosic structure of wood to fabricate artificial polymeric wood by replacing lignin with phenol formaldehyde (PF) and melamine formaldehyde (MF) resin. Similarly to various nanomaterials (e.g., cellulose nanofibers), SiC nanofibers, metal ions (FeCl₃, CoCl₂, NiCl₂, and Cr(NO₃)₃), SiO₂, and graphene oxide (GO) were mixed into PF and MF resins in different weight percentages and infiltrated into DW. The samples were then freeze-dried and thermally

cured as demonstrated in **Figure 17**. The prepared polymeric and composite wood showed exceptionally high mechanical strength, favorable corrosion resistance, fire retardancy, and low thermal conductivities.

6.3. Membranes

6.3.1. Membranes for Oil Spillage Cleaning

The frequency of oil spill accidents has increased, resulting in severe environmental and ecological consequences.^[185,186] Therefore, there is an urgent need to develop effective technologies to clean oil spills and solve the subsequent ecological problems, such as long-term effects from environmental pollution and the increasing release of oily industrial wastewater. The three most important strategies for cleaning up oil spills are natural degradation with dispersant agents of oil in water, in situ burning, and the use of absorbents for recovery of oils spills.^[187,188] Among the available techniques, the cleanup and subsequent recovery of oil spills using a wide range of absorbent materials seems to be the most efficient. When absorbents are applied to remove and transfer the oil (including organic contaminants) from water, they can exhibit the characteristics of higher efficiency and recyclability. Various types of absorbents are suitable for the cleanup of oil spills from water and they can be classified into three main categories: inorganic mineral materials, synthetic polymers, and organic natural materials.

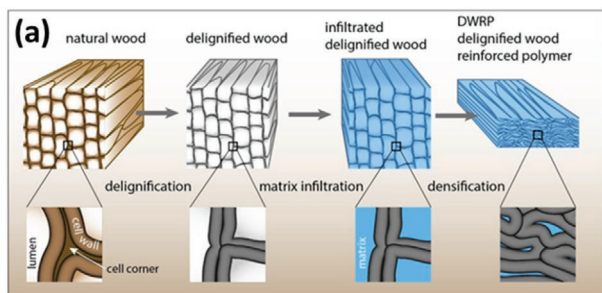


Figure 16. a) Schematic illustration of DWRP composite fabrication. Adapted with permission.^[99] Copyright 2019, American Chemical Society.

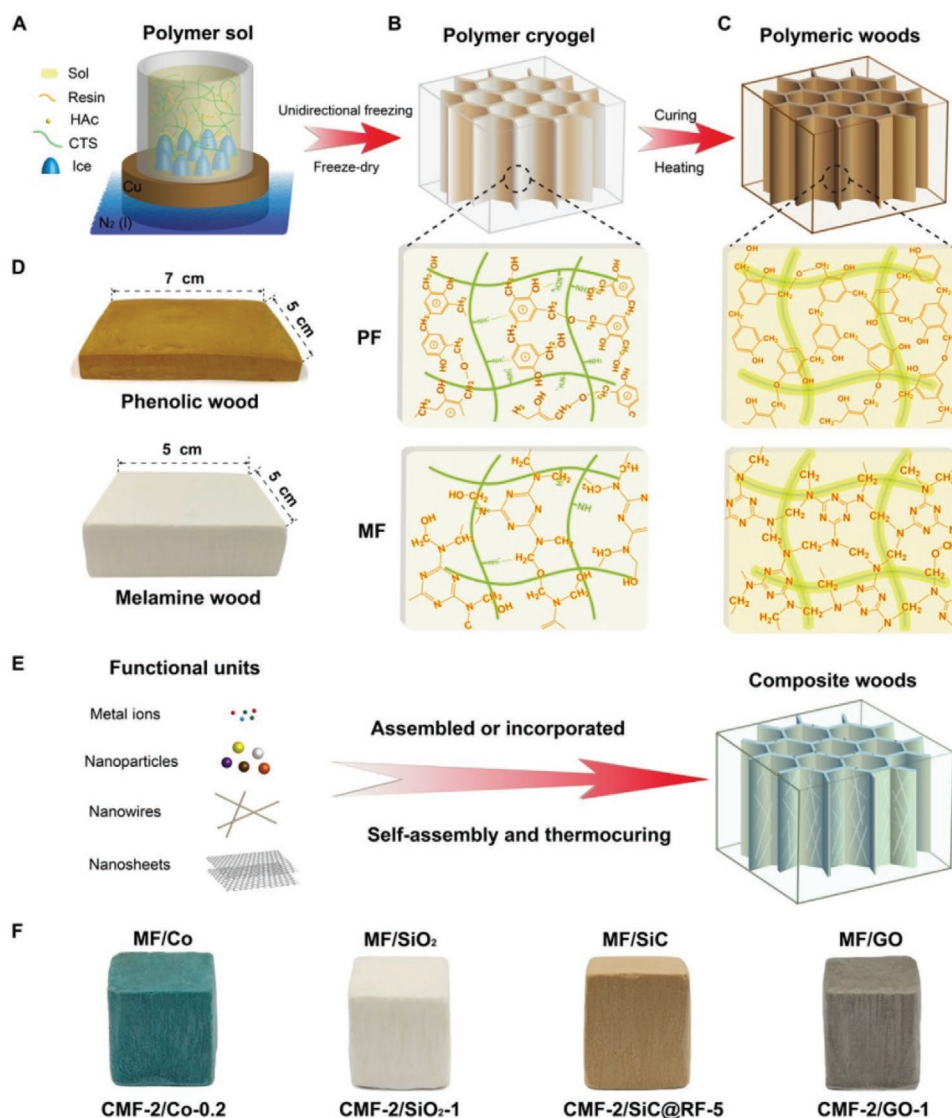


Figure 17. Schematic showing the preparations of functional polymeric wood. A) The starting solution (sol) including water-soluble thermoset resins, chitosan, and acetic acid forming a homogeneous polymer solution. B) Predesigned matrix prepared by the ice template-induced self-assembly and freeze-drying process. C) The final polymeric wood after thermocuring the predesigned matrix where the resins are completely crosslinked. D) Photographs of the artificial polymeric wood based on phenolic resin or cellular polymeric wood with PF (top, cellular (C, PF-4-5) and melamine resin; bottom, cellular (C, MF-3-5)). E) Scheme illustration showing the fabrication of various composite woods by adding ions or functional nanomaterials into the polymer solution, followed by the self-assembly and thermocuring process. F) Photographs of various composite woods based on melamine resin, including MF/Co (CMF-2/Co-0.2), MF/SiO₂ (CMF-2/SiO₂-1), MF/SiC (CMF-2/SiC@RF-5), and MF/GO (CMF-2/GO-1). The size of the composite woods was $\approx 1 \times 1 \times 1$ cm. Adapted with permission.^[20] Copyright 2018, American Association for the Advancement of Science.

Synthetic polymeric sponges such as polyurethane,^[189,190] melamine,^[191] PVA formaldehyde,^[192] polystyrene,^[193] and carbon/polymer materials^[194,195] have been developed for efficient removal of oil spills from water. However, the fabrication process of synthetic polymeric absorbent sponges is very complex and involves many steps. Consequently, this limits the large-scale fabrication for practical applications; further, their non-biodegradability is a critical issue. Organic natural cellulosic materials might be a sustainable solution for these oil spillage problems. Many types of cellulosic materials such as corn straw,^[196] cotton,^[197,198] and nanocellulose-based sponges^[206–201] are currently used for oil spillage removal from water.

Cellulosic materials have a low absorption capacity of oil and extremely high water absorption due to presence of free OH groups.^[206] An effective oil-absorbing material should: 1) have excellent hydrophobic–oleophilic properties to draw the oil into the material matrix.^[202] 2) Demonstrate fast absorption kinetics to facilitate the easy recovery of oil spills and less leakage. 3) Exhibit high buoyancy and durability in water, which is beneficial for collection. 4) Be recyclable and biodegradable, which will benefit the environment. Some cellulosic materials were prepared with extreme wettability exhibiting both superhydrophobicity (contact angle of $>150^\circ$ and sliding angle of $<5^\circ$) and superoleophilicity (oil contact angle of $<5^\circ$). For instance,

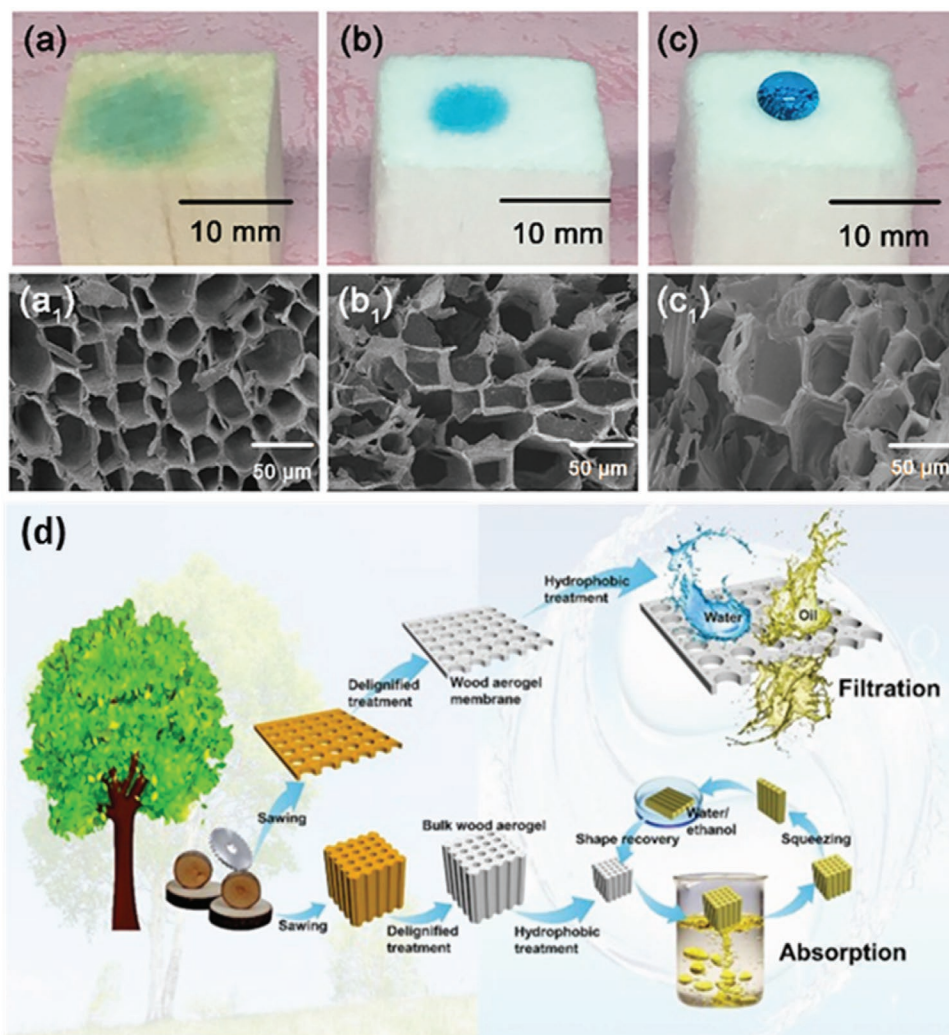


Figure 18. Characterization of the microscopic structures of the wood samples. a–c) Photographs of the spreading behavior of water droplets on natural balsa wood, DW (wood aerogel), and a DW/PDMS composite, respectively. a₁–c₁) Field-emission SEM images of the cross-section of natural balsa wood, DW, and a DW/PDMS composite at different degrees of magnification, respectively. d) Schematic outlining the preparation of DW materials for multibehavioral oil/water separation. Adapted with permission.^[204] Copyright 2019, Elsevier Ltd.

superhydrophobic wood fibers^[179] were prepared by orthodecyltrichlorosilane (OTS) treatment, where the superhydrophobic/superoleophilic cotton was prepared using sol–gel SiO₂ and simultaneous treatment with OTS.^[203] OTS (CH₃(CH₂)₁₇SiCl₃) is the most extensively used surface-active reagent for generating self-assembled monolayer films on a variety of substrates by the solution method. The currently available organic materials for removal of oil spillage from water such as cotton fibers, coir fibers, kenaf fibers, or other organic fibrous materials are not very efficient due to their low oil absorption capacities, structural instabilities, and reusability. Other materials such as nanocellulose-based aerogels have good overall properties, but their high production cost makes them difficult to manufacture at industrial scale.

DW with an inbuilt hierarchical cellulosic porous structure could be a potential substitute for all existing materials used in the cleaning of oil spills. Wang et al.^[204] prepared a 2D membrane and 3D bulk aerogel using DW-based multibehavioral

and reusable materials for oil/water separation (see **Figure 18d**). First, the partially delignified highly hydrophilic 2D membrane (wood veneer sample) and 3D aerogel (thicker wood sample) were prepared from balsa wood. The prepared 2D and 3D samples were then impregnated with polydimethylsiloxane (PDMS) with toluene as a curing agent to develop the superhydrophobic/superoleophilic DW. Figure 18a–c shows photographs of the spreading behavior of water droplets on the surfaces of natural balsa wood, delignified balsa wood, and PDMS modified DW. Figure 18a₁–c₁ shows the porous structure and cell lumen of natural wood, DW, and PDMS/DW. It is clearly visible from the microscopic images that the honeycomb-like cell wall structure was preserved even after delignification and PDMS modification. **Table 5** demonstrates the comparative properties of nanocellulose sponges (NCSs, amphiphilic) and DW (amphiphilic). As prepared (without hydrophobic treatment) NCSs and DW show a strong hydrophilic behavior due to the presence of OH groups, as well as their zero adsorption

Table 5. Comparative properties of natural wood, nanocellulose aerogels/sponges, and DW-based aerogels used in oil/water separation.

Sample	Density [kg m ⁻³]	Porosity [%]	Water contact angle [°]	Shape recovery after stress [%]	Adsorption capacity [g g ⁻¹]
Balsa wood ^{a)}	135.2 ± 12.5	91.4 ± 0.8	Hydrophilic	–	–
NCS ^{b)}	7.70	99.6	Strong hydrophilic	61	–
NCS + Si (3.5 wt%) ^{b)}	5.56	99.6	115	76	55
NCS + Si (9.1 wt%) ^{b)}	9.20	99.4	132	78	55
Delignified balsa wood ^{a)}	52.4 ± 8.70	96.7 ± 0.5	Strong hydrophilic	–	–
DW ^{a)} (aerogel)/PDMS	74.8 ± 11.3	95.3 ± 0.3	<150	97–100	13
DW sponge ^{c)}	29.8 ± 3.8	98.1 ± 0.12	Strong hydrophilic	–	16–41
Silylated delignified balsa wood sponge ^{c)}	30.1 ± 2.6	97.8 ± 0.10	151	–	–
Delignified balsa wood ^{d)}	–	–	Strong hydrophilic	–	–
Reduced graphene oxide (rGO)-coated DW	–	–	Strong hydrophilic	–	–
Hydrophobic rGO-coated DW	–	–	145	–	3.63–16.73

^{a)}Ref. [204]; ^{b)}Ref. [207]; ^{c)}Ref. [205]; ^{d)}Ref. [104].

capacity of oil from water because free OH groups interact with water molecules. However, after hydrophobic (PDMS) treatment, both superhydrophobicity (contact angle of >150° and sliding angle of <5°) and superoleophilicity (oil contact angle of <5°) were achieved for the DW aerogels and their oil adsorption capacity significantly improved. Therefore, in conclusion, the DW materials could be useful as an alternative to fossil-based materials for cleaning oil from water but they require additional hydrophobic treatment. A similar study was carried out by Guan et al.^[205] However, they used methyltrimethoxysilane to prepare the hydrophobic silylated wood sponge for oil/water separation. The prepared silylated wood sponges showed excellent absorption capacity (≈16–41 g g⁻¹) and superhydrophobicity. Fu et al.^[173] also used a similar approach to fabricate delignified balsa wood for oil/water separation but they functionalized DW by a reactive epoxy-amine system to improve the mechanical strength and hydrophobicity. The epoxy functionalized DW showed excellent hydrophobic/oleophilic nature with 15 g g⁻¹ oil absorption capacity and high compressive strength and modulus of 18 and 263 MPa, respectively.

In another study, delignified basswood was prepared for crude oil/water separation^[206] with better anti-oil-fouling properties. The pure DW exhibited outstanding underwater (pre-hydrated state) anti-oil properties with an oil contact angle of <160°. This was due to its inbuilt vertical cell wall microstructure with pore size and porosity of ≈30 μm and 85%, respectively. However, DW in the dry state did not demonstrate similar behavior toward crude oil/water separation and could be easily fouled by crude oil. This may be due to the presence of residual lignin and hemicelluloses in DW,^[206] as well as the reduction of hydrophilic cellulose groups due to excessive drying. To overcome this problem, they spin-coated the DW by cellulose acetate solution (0.5 wt% in 10:1 volume ratio of acetone and dichloromethane). The prepared cellulose acetate coated-DW demonstrated excellent anti-oil behavior in both wet and dry state conditions. The water flux of DW increased from 20 779 to 35 341 L m⁻² h⁻¹ after cellulose acetate coating, which was measured during the crude oil/water separation experiment.

Huang et al.^[104] prepared rGO-coated hydrophobic delignified balsa wood sponges for viscous crude oil cleanup with electrothermal capabilities. First, the DW was vacuum infiltrated

with graphite via dip-coating. The sample was then chemically reduced by ascorbic acid as a reductant in an oven at 160 °C under air atmosphere for 2 h to obtain rGO wrapped wood sponge. Further, they achieved the hydrophobicity of rGO wood sponge treatment with perfluorinated octyltriethoxysilane. The rGO coating enhanced the capability of the DW sponge to clean up highly viscous crude oil by acting as an electrode through a power supply, heating the wood sponge, and reducing the viscosity of crude oil.

6.3.2. Membrane Distillation and Solar Steam Generation Membranes

According to a recent United Nations report, nearly 3.6 billion of the global population lived in water-scarce regions for at least one month in 2018. Furthermore, it was estimated that this number could increase to 4.8–5.7 billion by 2050.^[207] As fresh water is essential for survival as well as industrial and economic developments, the global fresh water demand has been accelerating exponentially. Therefore, an effective and sustainable desalination process is urgently required.^[208] Membrane-based desalination technologies that include pressure driven processes (e.g., nanofiltration, reverse osmosis, and pressure retarded osmosis) are mostly employed for water desalination from a range of saline or contaminated sources, including seawater and brackish groundwater.^[208] However, the energy consumption (2–4 kW h m⁻³) of these processes is not sustainable. Solar energy could provide an alternative power supply for the desalination process. Thermal processes such as membrane distillation (MD) have also been developed for this application.^[209] MD functions by water evaporation at the hot feed side of MD cells and diffusion through the porous hydrophobic membrane before condensing at the cold permeate side.^[210–212] In comparison to conventional processes, MD has lower hydrostatic pressure and operating temperatures.^[213] According to the literature, an ideal MD membrane should have a large pore size, low pore tortuosity, low thermal conductivity, high porosity, good mechanical strength, low cost, and low environmental impacts.^[209,213–217] DW could be an ideal material for MD membranes as it has an

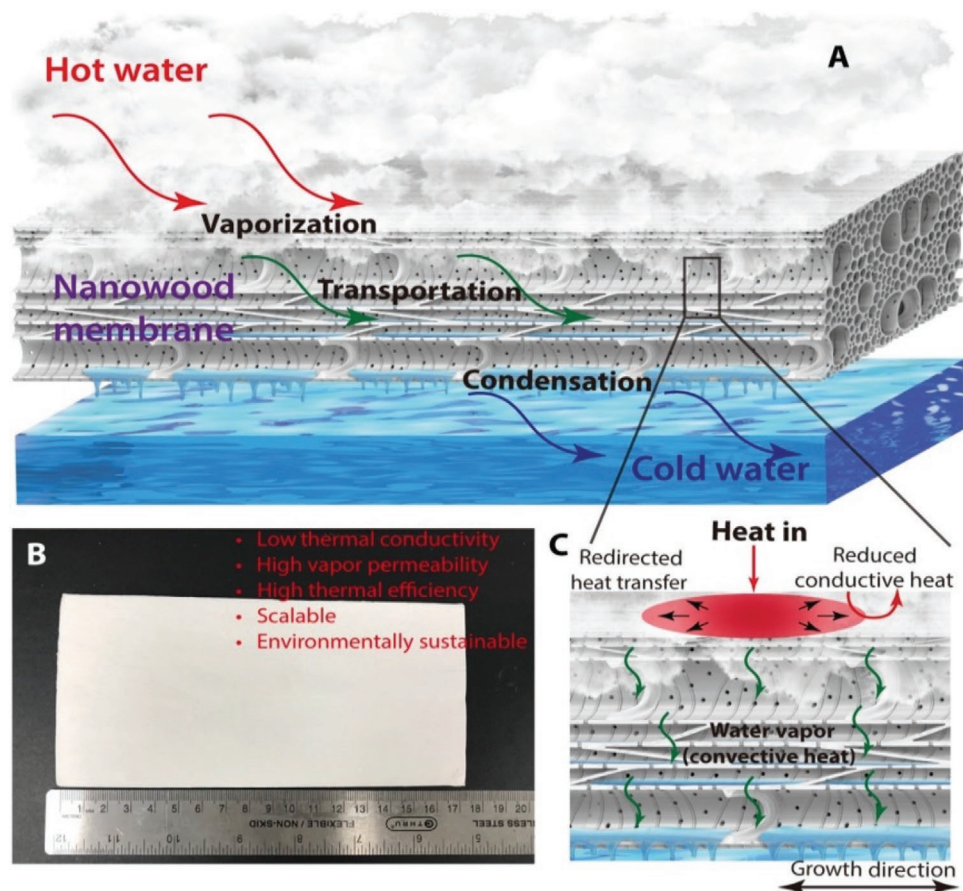


Figure 19. A) Schematic of MD using the DW membrane. B) Photograph of the DW membrane and its corresponding beneficial properties for MD applications. C) Schematic of the water (vapor) and heat transfer in the DW membrane during MD. Adapted with permission.^[218] Copyright 2019, American Association for the Advancement of Science.

inbuilt porous structure and suitable properties. Hou et al.^[218] explored the potential of DW as a MD membrane. The natural basswood slices (2 mm thickness) were delignified using the standard process of Kraft pulping (see **Figure 19**). The DW membrane was then treated with perfluorodecyltriethoxysilane (PFDS, $C_{16}H_{19}F_{17}O_3Si$) to achieve the hydrophobicity for mimicking the MD membrane. The prepared DW-based MD membrane had a pore size of 0.28 ± 0.03 mm, thickness of 502 ± 35 μm , porosity of $89 \pm 3\%$, water contact angle of 144° , liquid entry pressure (LEP) of 74.7 ± 0.5 kPa, intrinsic permeability of $1.44 \pm 0.09 \times 10^{-10}$ $kg\ m^{-1}\ s^{-1}\ Pa^{-1}$, thermal conductivity of $0.040\ W\ m^{-1}\ K^{-1}$, and thermal efficiency of $71 \pm 2\%$. DW membranes are a promising potential candidate to replace the petroleum-based ones currently used in MD. Additionally, this would also eliminate the complex fabrication process of commonly utilized MD membranes (e.g., polypropylene (PP) and polytetrafluorethylene). However, there are still many unanswered questions regarding the performance of DW membranes in water desalination under extreme conditions, such as how to control biofouling (e.g., the deposition of NaCl crystals in the porous structure of DW as it is highly reactive due to the presence of open OH groups). The long-term stability of the hydrophobic properties of DW membranes are also questionable.

A similar concept to MD was utilized to fabricate solar steam generation devices using DW for sea water desalination.^[219] A poplar wood sample was delignified in a mixture of choline chloride and lactic acid DESs. The surface layer of the DW was then carbonized using a scanning flame for 20 s (see **Figure 20**). The low thermal conductivity and porous structure of the sample led to the transportation of more water by controlling overheat losses during solar heat radiation. The carbonized upper layer helped to absorb more heat compared to the uncarbonized DW surface. The evaporation rate after 1 natural sun light irradiation of natural and DW was 1.0 and 1.3 $kg\ m^{-2}\ h^{-1}$, respectively. Chen et al.^[219] also conducted a real time experiment by utilizing the lab made setup to desalinate water using solar energy between 10:00 and 16:00. The water collected after desalination had two times lower concentrations of Na^+ , Mg^{2+} , K^+ , and Ca^{2+} ions.

He et al.^[220] prepared DW with infiltrated carbon nanotubes (CNTs) for solar steam generation and liquid water transportation. Compared to DW, the prepared DW/CNT composite was floatable with a 20% higher steam generation capacity and had better solar energy utilization due to an increased thermal efficiency of 8%. In another study,^[17] He et al. prepared a floatable 3D DW infiltrated with a titanium dioxide (TiO_2)-based photocatalyst for methylene blue photocatalytic degradation. The

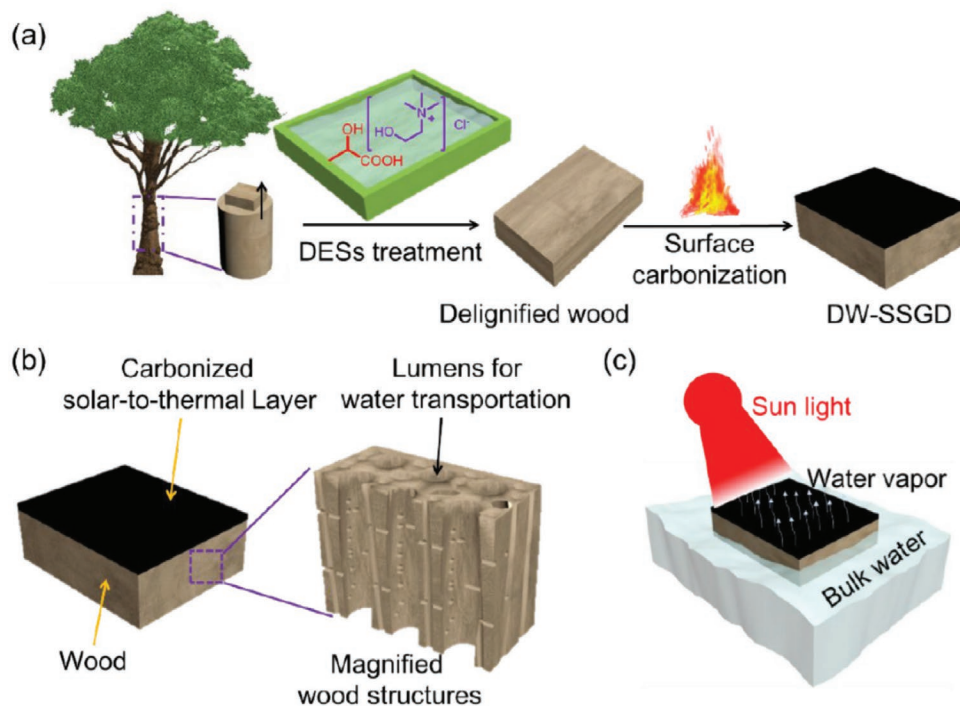


Figure 20. a–c) Schematic diagram of wood delignification in DESs and surface carbonization for application as steam generation devices. Adapted with permission.^[219] Copyright 2019, American Chemical Society.

porous and channeled structure of DW provided a passage for the uniform distribution of TiO_2 through the cell wall structure, in addition to providing an excellent uptake or transportation of methylene blue into DW for photocatalytic degradation. The prepared DW-based 3D photocatalyst could be a solution for the degradation of methylene blue or other environmental pollution from water sources.

6.3.3. Ionic Membranes

Naturally aligned cellulose nanofiber membranes were explored as a potential ion regulation membrane.^[221] The nanofluidic performance of DW and 2,2,6,6-tetramethylpiperidine-1-oxyl (TEMPO)-oxidized DW membranes were investigated using an ionic conductivity setup. The ionic conductivity of densified and undensified DW membranes were compared (see **Figure 21**). The TEMPO oxidation of DW significantly enhanced its zeta potential and ionic conductivity. This was because the oxidation process converts the primary free OH groups of DW into COOH groups.

6.4. Energy Storage Materials

6.4.1. PCMs

Dynamic energy storage materials are required to fulfil ever-increasing energy demands. PCMs are particularly attractive due to their high density storage of energy at a constant temperature. Within these materials, the stored thermal energy

(sensible, latent (PCMs), and chemical heat storage) can be discharged for later purposes.^[222,223] As the temperature increases, PCM change its phase from solid to liquid by an endothermic reaction and adsorbs heat. Conversely, when the temperature decreases, the material changes from a liquid to a solid phase by an exothermic reaction and releases heat. PCMs are usually mixed, dispersed, or injected into other materials for different applications. PCMs are mainly classified as organic (hydrocarbons, primary paraffins, and lipids), inorganic (salt hydrates), hygroscopic materials (natural materials due to their condensation and vaporization behavior), or solid–solid PCMs. The greatest disadvantage of PCMs is their shape-instability (leakage) during the charging and discharging processes. DW could be a potential candidate for a new PCM due to its extremely high hygroscopic behavior. The hierarchically aligned cellulosic structure of DW can easily become swollen in high moisture and also lose weight in dry conditions. Furthermore, it could provide stability during the charging and discharging process.

Ma et al.^[224] explored the potential use of DW in PCM composite preparation by vacuum impregnation with different weight percentages of capric–palmitic acid eutectic (CA–PA) mixtures for thermal energy storage. First, a stable mixture of capric acid (CA) and palmitic acid (PA) was formed (84.5% mass ratio of CA). The mixture was then vacuum impregnated into natural and DW. After impregnation, the CA–PA formed hydrogen bonds with open OH groups present in DW and filled the open pores and cell wall tracheids (see **Figure 22**). SEM images clearly show the difference between the natural and DW cell wall structure. After delignification, the cell wall became more porous with a wider cell lumen area.

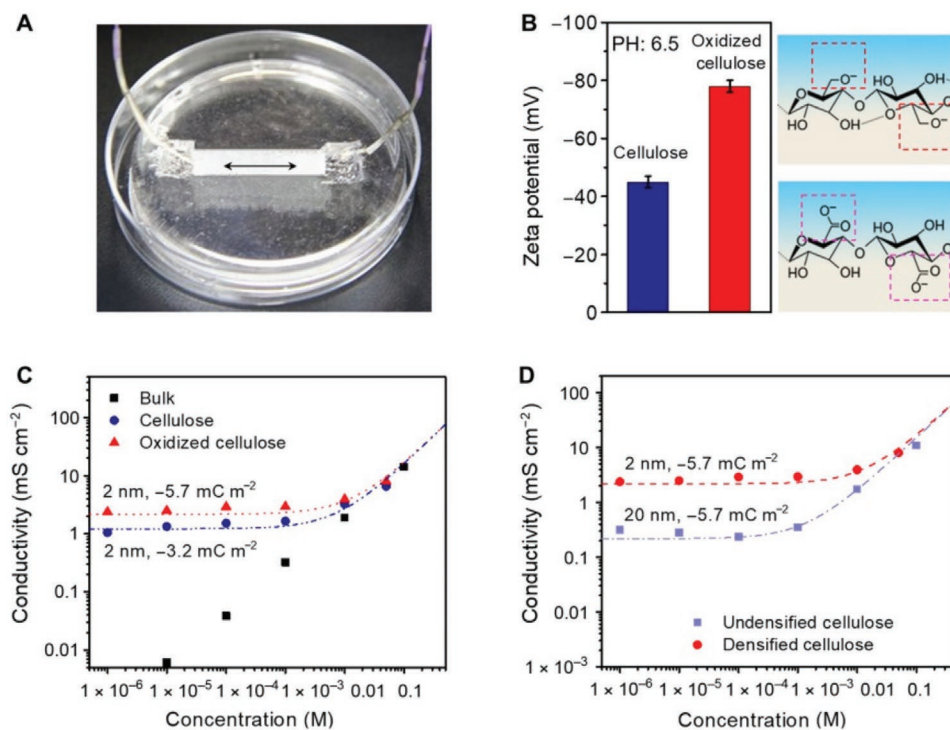


Figure 21. A) Ionic conductivity measurement setup. B) Zeta potential of the DW membrane and oxidized/DW membrane under neutral pH with a cellulose concentration of $\approx 0.1\%$. C) An ionic conductivity test with potassium chloride (KCl) solution. D) Ionic conductivity against concentration. Adapted with permission.^[221] Copyright 2019, American Association for the Advancement of Science.

Delignification opened the cellular structure of natural wood and provided sufficient passage for molten CA-PA penetration and homogenous deposition in the cell wall structures. This phenomenon is clearly visible in the SEM images shown in Figure 22. The thermal properties of the prepared natural and DW-based PCMs were analyzed by differential scanning calorimetry (DSC) by measuring the melting and cooling temperatures. The subsequent measurements of the heat of fusion (ΔH in J g^{-1}) for the melting (ΔH_m) and cooling (ΔH_c) phases were also measured. The CA-PA had a ΔH_m and melting temperature of $153.1 \pm 2.5 \text{ J g}^{-1}$ and $23.2 \pm 1.5 \text{ }^\circ\text{C}$, respectively, in the melting phase (endothermic process). In the cooling phase, the CA-PA had a ΔH_c and cooling temperature of $151.5 \pm 1 \text{ J g}^{-1}$ and $14.5 \pm 0.4 \text{ }^\circ\text{C}$, respectively. The DW/CA-PA showed a similar melting peak and cooling temperature, however, the ΔH was significantly lower with values of 94.4 ± 1 and $91.4 \pm 0.6 \text{ J g}^{-1}$ for the melting and cooling phases, respectively. The reason for this is because DW is not a natural phase-changing material like CA-PA. Despite this, DW could be a potential base material for PCM impregnation for various applications in energy systems, such as insulating systems for buildings.

In another study, a magnetic wood-based composite PCM was fabricated using delignified balsa wood as a base material due to its structural stability during phase-change progression.^[225] In this work, different weight percentages (1%, 2%, 5%, and 8%) of magnetic Fe_3O_4 nanoparticles ($>99.5\%$, average particle size of 20 nm) were mixed with melted tetradecanol (TD, $\geq 99\%$). The DW was then vacuum impregnated with TD and $\text{Fe}_3\text{O}_4/\text{TD}$ mixtures to obtain the magnetic wood-based

composite PCM. The Fe_3O_4 magnetic nanoparticles were mainly used because they can assist in converting solar energy to thermal energy. TD/DW have strong absorption in the ultraviolet region (wavelength range of 230–380 nm) and only weak absorption (≈ 0.3) in the visible region (wavelength range of 380–780 nm), as shown in Figure 23a. This illustrates that TD/DW exhibits a low solar-to-thermal energy conversion efficiency. Figure 23c shows photomicrographs of the prepared samples and demonstrates the shape stability at lower and higher temperatures. From the photomicrographs, it is apparent that the pure TD melted and lost its shape at $60 \text{ }^\circ\text{C}$. However, the TD/DW and $\text{Fe}_3\text{O}_4/\text{TD}/\text{DW}$ maintained very stable shapes of prepared magnetic PCM at low and high temperatures.

To further develop the TD/DW composite PCM, the same research group prepared a TD/DW composite PCM with a self-cleaning superhydrophobic surface.^[226] In this work, the TD/DW composite PCM surface was modified by three-step chemical coating. In the first step, epoxy resin/acetone solution (5% m/v) was sprayed on the sample. In the second step, a prepared mixture of hydrophilic SiO_2 (2 g), PFDS (2 mL), formic acid (2 mL), and acetone (100 mL) was coated on the precoated TD/DW sample and dried for 12 h at room temperature to obtain the superhydrophobic TD/DW composite PCM. The superhydrophobic treatment improves the leakage and shape stability of the PCM, which in turn improves its performance in humid conditions by maintaining a high thermal energy capacity. The prepared superhydrophobic TD/DW showed superior wear resistant properties over a wide range of temperatures (20–100 $^\circ\text{C}$) and chemical environments (pH 3–13).

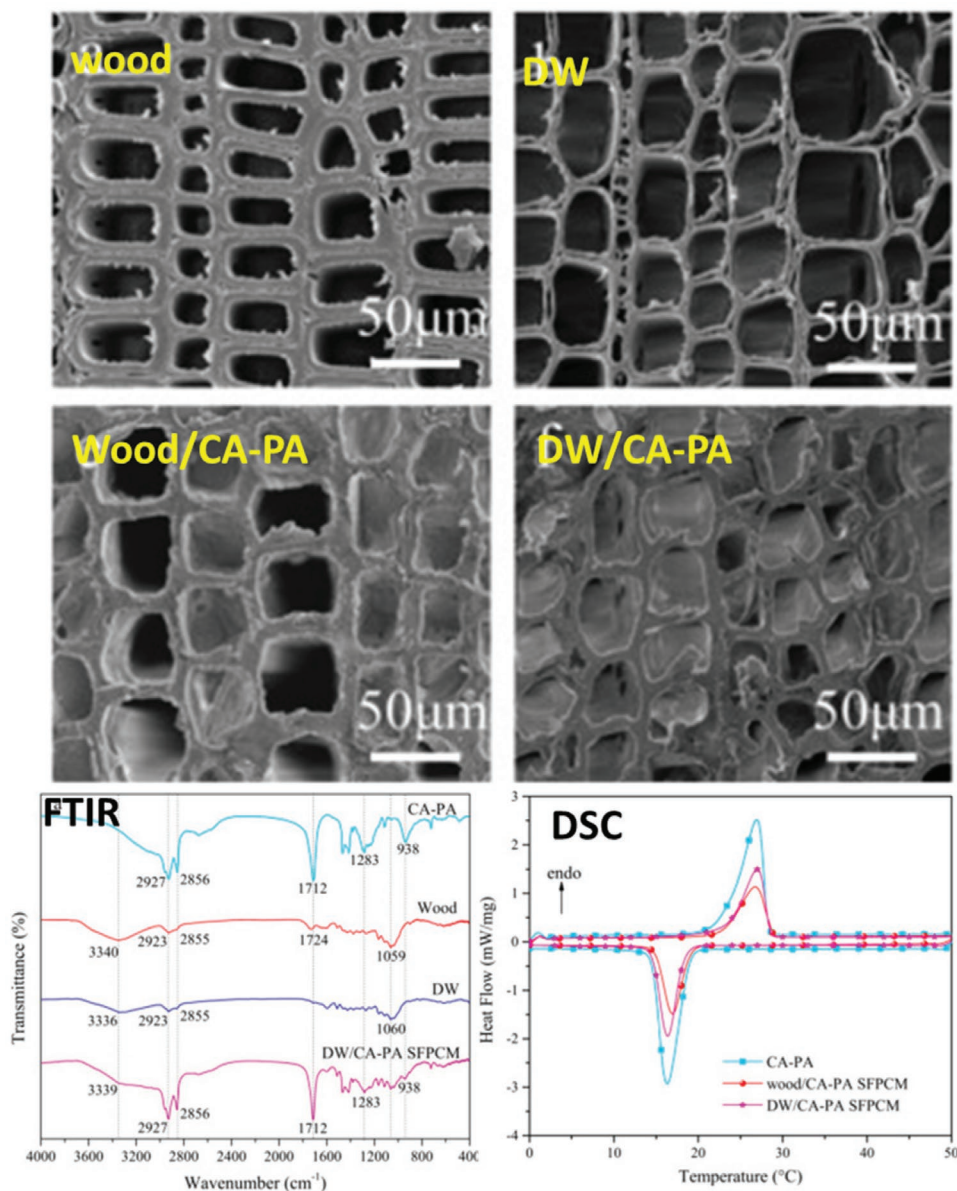


Figure 22. SEM images of natural and DW before and after CA-PA impregnation. Furthermore, FTIR spectra of CA-PA and composite materials are presented, in addition to DSC analysis of CA-PA, natural wood/CA-PA, and DW/CA-PA. Adapted with permission.^[224] Copyright 2019, Elsevier Ltd.

Furthermore, the superhydrophobic PCM demonstrated a superior thermal energy storage capacity (125.4 J g^{-1}) and slower energy release compared to TD/DW PCM (see Figure 24).

Wang et al.^[227] prepared a DW and microPCM (solid content 53.34%) emulsion-based composite PCM. Six different weight percentages (15%, 20%, 25%, 35%, and 40%) of microPCM emulsion were impregnated into DW via vacuum infusion and all the required properties of the PCMs were evaluated. Additionally, 0.2% of graphene was added to the sample with the 40% infusion of microPCM, which significantly improved the thermal conductivity of the composite PCM. Due to the superior energy storage capacity of phase change energy storage wood, it was considered for use as an indoor temperature regulating material for building energy conservation.

In another study, a ferromagnetic $\text{Fe}_3\text{O}_4/\text{ZIF-67}/\text{DW}$ aerogel^[228] was fabricated for efficient microwave absorption. The DW aerogel was used as the porous low-density compressible matrix and the $\text{Fe}_3\text{O}_4/\text{ZIF-67}$ dodecahedrons served as the absorbing agents. The Kraft pulping process was used for delignification to form the well-graded layered structure with uniform channels in the natural wood by removing the hemicellulose and lignin.^[228] After delignification, the wood samples were freeze-dried to maintain the structural integrity and dipped into a $\text{Co}^{2+}\text{-Fe}_3\text{O}_4$ nanoparticle dispersion (see ref. [228] for more details) multiple times to achieve homogeneous dispersion of the solution into the DW. The sample was then transferred into a methanol solution (40 mL) containing 2-methylimidazole (2.63 g) and aged for up to 12 h. The

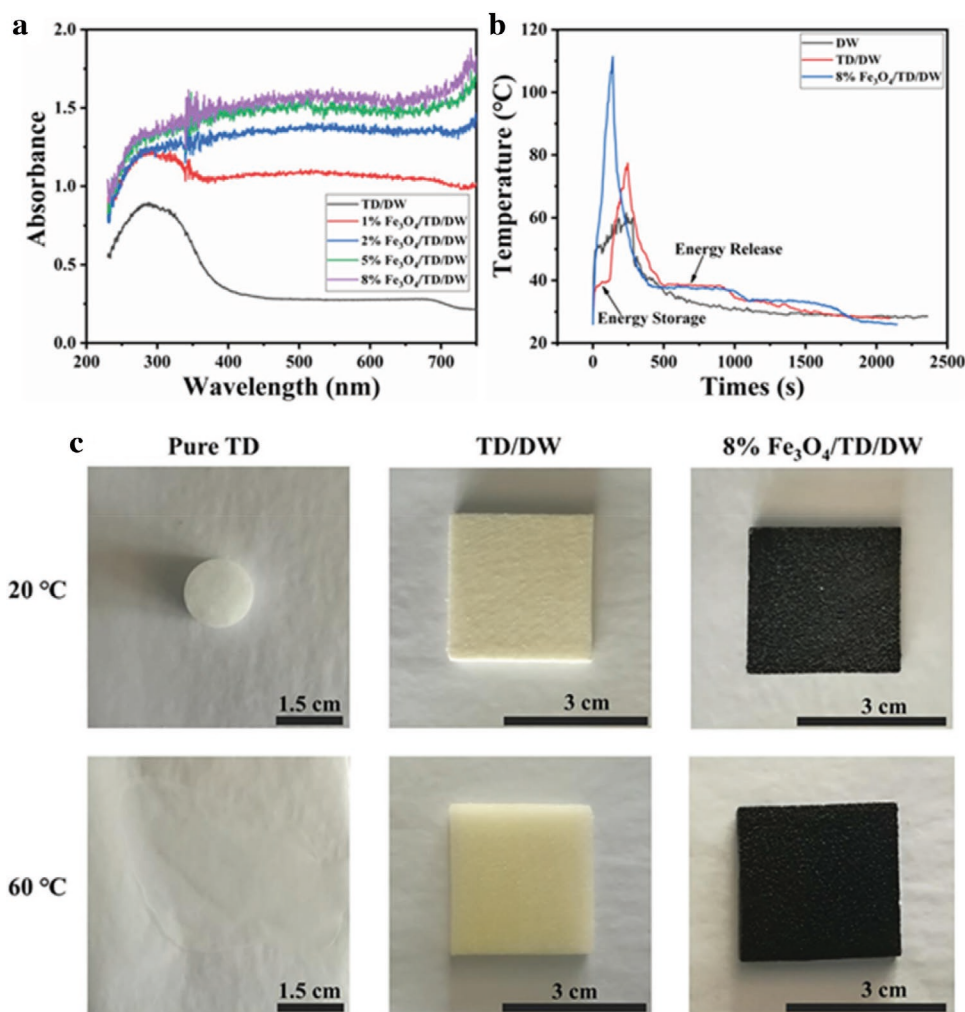


Figure 23. a) UV-vis absorption spectra of prepared PCMs. b) Solar-to-thermal energy conversion expressed with temperature-time curves of PCMs under a xenon light. c) Comparison of the shape stability of pure TD, TD/DW, and 8% Fe₃O₄/TD/DW at 20 and 60 °C. Adapted with permission.^[225] Copyright 2019, Elsevier Ltd.

sample was then washed with ethanol solution and freeze-dried (−50 °C, 24 h) to prepare the DW-Fe₃O₄/ZIF-67@WA magnetic composite for microwave adsorption. **Figure 25** demonstrates the microstructure differences of DW (Figure 25a–c) and Fe₃O₄/ZIF-67@WA-coated DW (Figure 25d–f), where dodecahedron-shaped magnetic Fe₂O₄ nanoparticles homogenously covered the layered cellulose structure. The Fe₂O₄ nanoparticle deposition significantly increased the density of DW from 49.5 to 150 mg cm^{−3}. As Fe₂O₄ concentration increased, the DW density reached a maximum value of 198 mg cm^{−3}. The magnetic composite exhibited excellent microwave absorption performance and resilience toward mechanical compression up to 60%.

Delignified wood flour (DWF) can be utilized in preparing composite PCMs for thermal bridging in buildings.^[229] Cheng and Feng^[229] prepared form-stable composite PCMs based on DWF that was vacuum impregnated with myristyl alcohol (MA). Further, they prepared the composite board using urea formaldehyde (UF) resin adhesive and thermal curing to enhance its applicability in building systems. Different weight ratios (65%, 70%, 75%, and 80%) of DWF and MA were prepared by heating

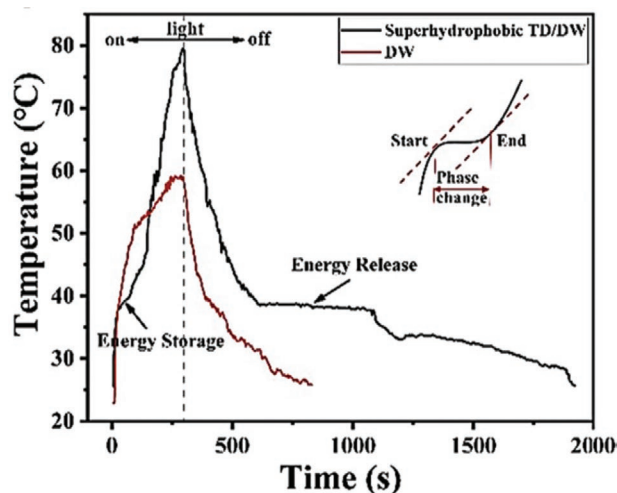


Figure 24. Solar-to-thermal energy conversion temperature-time curves of DW and superhydrophobic TD/DW composite PCM. Adapted with permission.^[226] Copyright 2020, Elsevier Ltd.

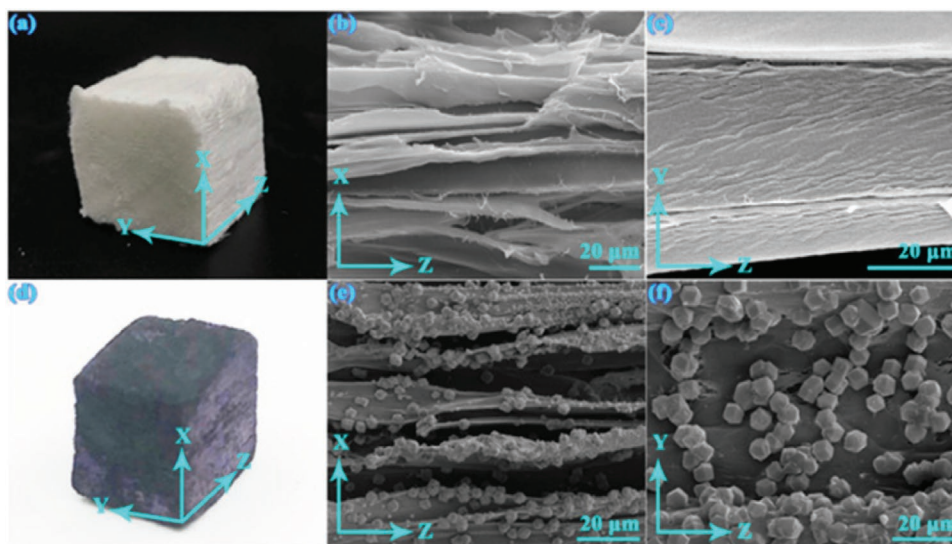


Figure 25. Structural characterization of DW aerogel and $\text{Fe}_3\text{O}_4/\text{ZIF-67@WA-2.0}$. a) Photograph of DW aerogel. b,c) SEM images of DW aerogel in the XZ and YZ planes. d) Photograph of $\text{Fe}_3\text{O}_4/\text{ZIF-67@WA-2.0}$. e,f) SEM images of $\text{Fe}_3\text{O}_4/\text{ZIF-67@WA-2.0}$ in the XZ and YZ planes. Adapted with permission.^[228] Copyright 2019, Elsevier Ltd.

in a vacuum oven at 70 °C. The prepared composite PCMs had the issue of leaking during phase changes, therefore UF resin was utilized as a binding agent. The UF resin improved the mechanical properties and thermal storage capability of the composite PCMs.

6.4.2. Self-Luminous Composite PCMs

Yang et al.^[230] prepared composite PCMs using a delignified poplar wood substrate with reversible thermochromic properties. Thermochromic composite PCMs were prepared by vacuum-assisted impregnation of a mixture of crystal violet lactone (CVL), bisphenol A (BPA), and TD into a delignified poplar

wood substrate with a weight ratio of 1:4:50 in a melted form at 90 °C for 12 h.^[230] To create the reversible thermochromic process, the equilibrium of the proton transfer phenomenon between CVL and BPA via ring-closed or ring-opening in response to the phase change properties of TD was utilized (i.e., when the phase of TD is liquid, the composite is colorless, otherwise it appears blue, see **Figure 26b**). The DW substrate provides a stable base for preparing the functional PCM with control over leaking during the discharging phase (see **Figure 26a**).

A DW-based self-luminous composite was prepared for both thermal and light energy storage.^[231] Melted TD and $\text{SrO} \cdot \text{Al}_2\text{O}_3 \cdot \text{SiO}_2 \cdot \text{Eu}^{2+}$ were mixed at different weight ratios (100:5, 100:10, 100:15, and 100:20) and uniformly dispersed

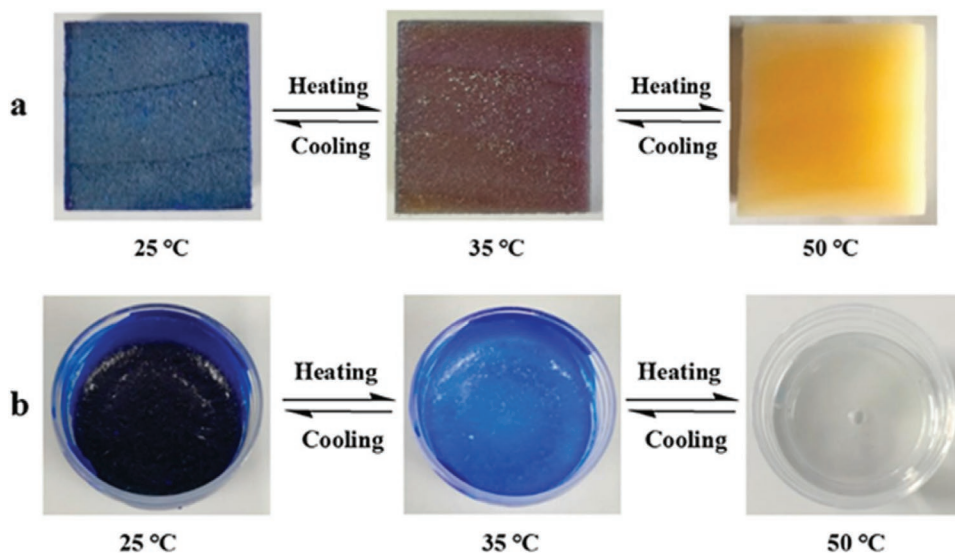


Figure 26. Thermochromic phenomenon. a) Composite PCM based on a delignified poplar wood substrate. b) A mixture of CVL and BPA in TD. Adapted with permission.^[230] Copyright 2018, Elsevier Ltd.

under stirring for 30 min. DW was immersed into the mixture at 70 °C for 4 h and then the excess mixture adhered on the wood surface was removed. After cooling to room temperature, the self-luminous wood was obtained.^[231] The prepared composite had a relatively high latent heat of fusion (146.7 J g⁻¹) and a phase change temperature of ≈37 °C. Furthermore, it could absorb ultraviolet and visible light, which emits the green light up to 11 h in dark.

6.5. Biomedical Applications

The hierarchical and porous structure of DW could become a biotemplate scaffold for various biomedical applications. The reactive nature of DW due to the presence of OH groups could be easily modified according to requirements in terms of functionality via polymer infusion and in situ deposition of functional particles or polymeric layers. The ideal scaffolds for biological applications should provide biocompatibility, porosity, favorable mechanical properties, and bioresorbability.^[232] Liu et al.^[233] prepared wood-derived hybrid scaffolds for bone tissue engineering. In this work, the aligned and porous DW was explored as a possible biomimetic scaffold via in situ deposition of hydroxyapatite (HAp) nanoparticles and vacuum inflated polycaprolactone (PCL). The prepared hybrid scaffold showed excellent mechanical anisotropic and capillary transport properties making it suitable for bone cell migration, proliferation, and alignment. The in situ HAp deposition into DW was achieved by immersion into a Ca(NO₃)₂ solution (0.5 M) for 8 h. This was followed by immersion in a (NH₄)₂HPO₄ solution (0.5 M) in order to fully form HAp particles in the microstructure. Further, the vacuum assisted infiltration of PCL (15% in dioxane solution) was applied. The mechanical anisotropic and capillary transport properties of the prepared DW, HAp deposited DW, and hybrid PCL infused into HAp-DW were measured. The compressive moduli of all the samples showed anisotropic behavior. The DW had a radial and longitudinal modulus of 39 and 2.27 MPa, respectively. After HAp coating and PCL infiltration, the radial compressive modulus increased to 221 and 420 MPa, respectively. The longitudinal compressive modulus also improved significantly to 3.60 and 20.50 MPa after HAp coating and PCL infiltration, respectively. Anisotropic behavior was also observed in the liquid transportation of all the samples (as shown in Figure 27). The DW and HAp deposited DW samples showed similar behavior of liquid transport in both R and L directions. However, liquid transportation decreased due to infiltration of hydrophobic PCL into the HAp deposited DW. Further, cell culture media transportation into prepared scaffolds and attachments, alignment, and proliferation were studied. Due to the highly aligned interconnected channels within the DW, cell media migrated to all parts of the scaffolds. The hydrophobic PCL together with HAp, improved the cell proliferation and osteogenic differentiation.

Wan et al.^[234] infiltrated copper sulfide (CuS) nanoparticles into DW for drug delivery in cancer treatment. DW was dipped into a copper sulfate (CuSO₄) solution (50 mL) and shaken gently for 3 h at room temperature. Further, ultrasonic treatment for 60 min at 80 W power was applied and the solution was again shaken for 1 h to ensure that the Cu²⁺ ions adequately

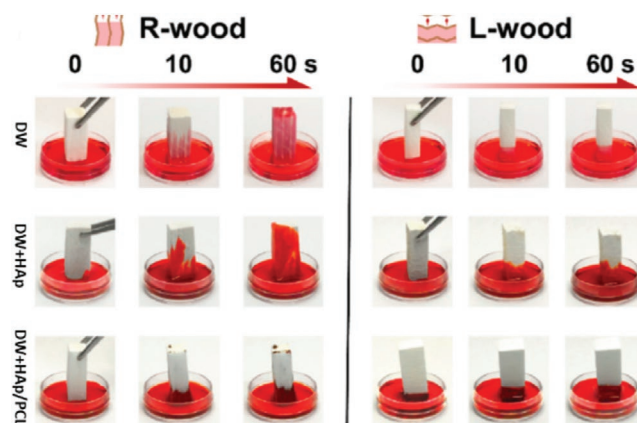


Figure 27. Liquid transport ability at different time intervals for different scaffolds along the radial and longitudinal directions. Adapted with permission.^[233] Copyright 2020, American Chemical Society.

entered into the wood's channels. In the last step, DW-Cu²⁺ was immersed into a 50 mL solution of sodium sulfide (Na₂S) (0.1 mol L⁻¹) until its color did not change from white to black. The prepared DW-CuS nanoparticles achieved ultrahigh inhibition ratios for *Escherichia coli* and *Staphylococcus aureus*, in addition to extremely low minimal inhibitory concentrations. Furthermore, the prepared functional composite was tested for doxorubicin hydrochloride (DOX) through regulating the pH of the solution. A maximum cumulative release capacity (78.3%) of DOX at pH of 2.2 was achieved. An in vivo mouse model was used to validate the cancer therapy capacity of DOX-loaded DW-CuS nanoparticles and H22 tumor growth was effectively reduced after 9 days of testing.

In another study, a superflexible wood scaffold was prepared using DW for medical applications.^[102] To achieve superflexibility in wet conditions, the wood membrane was treated with NaOH/Na₂SO₃⁻ at pH 7 and the lignin and hemicellulose were removed. The flexibility enables DW to act as a scaffold for biomedical applications as a flexible, wearable, biocompatible, and breathable biomaterial. Further, the biocompatibility of the prepared scaffold was tested by HEK293 cells cultured for 24–48 h. The results demonstrated that HEK293 cells were successfully adhered and proliferated on the surface of the flexible wood, indicating their excellent attachment and biocompatibility.

6.6. Other Functional Materials

6.6.1. Tunable Wood

Wood is a well-controlled hygroscopic material as its cell walls swell in high moisture and shrink in dry conditions.^[8,235] However, after delignification, wood becomes highly sensitive to moisture due to the presence of many OH groups, which abundantly react with moisture and change the DW cell wall structure. This phenomenon of DW hydrophilicity could be useful to fabricate tunable wood composites for diverse applications. In a recent study,^[100] water-triggered shaping of DW was investigated at a macroscopic level, where DW spruce veneer was shaped into varying radii of curvature (Figure 28). In the

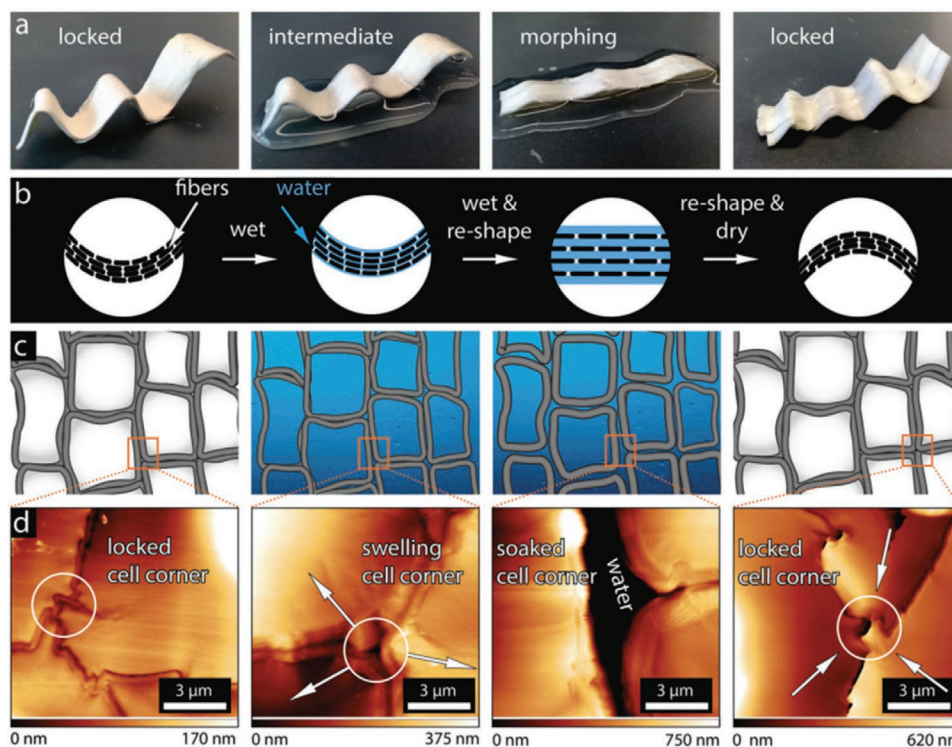


Figure 28. Shaping mechanism of DW using moisture induced reversible interlocks. a) DW samples in the locked, intermediate, morphing, and relocked (after reshaping) states. b) Corresponding scheme of a longitudinal section of DW in the four states, illustrating the swelling of DW fibers (black) by water (blue). c) Corresponding scheme of a DW sample cross-section. d) Atomic force microscopy images of the cell corner region showing the moisture induced interlocking mechanism. Adapted with permission.^[100] Copyright 2019, John Wiley & Sons, Inc.

first step, the delignified veneer curvature was locked by densification and drying. The tight interlocking occurred due to frictional forces and hydrogen bonding between the OH groups of cellulose (see Figure 28c,d). When the obtained shape was rewetted, the DW was softened due to the decreased interaction between neighboring fibers. This allowed repeated shaping of the material (see Figure 28a,b). Further, a permanently locked DW curvature with additional magnetic and superhydrophobic properties was achieved by TiO_2/PDMS coating.

6.6.2. Wood to Textiles

Jia et al.^[236] investigated the use of DW films in the preparation of wood-textile fibers (see Figure 29). First, balsa wood veneers (0.3–0.5 mm thickness) were delignified and cut into strips with a square cross-section along the longitudinal direction. They were then manually twisted in the opposite direction at both ends to form the textiles. The densely twisted and squeezed aligned wood-textiles exhibited a very high mechanical strength of 106.5 MPa, which was two times larger than natural wood. Furthermore, the prepared wood-textiles also exhibited ≈ 20 times higher toughness than natural wood. The functional wood-textiles were fabricated using a similar twisting process. The DW film was infiltrated with a solution of dispersed CNTs to prepare the conductive wood-textile. The sample was also infiltrated with methylene blue solution to dye the wood-textile. Further, to enhance the applicability

of the wood-textiles, glutaraldehyde-based crosslinking was employed. The flexibility of the wood-textile was improved further with a simultaneous rubber polymer coating and tetraethyl orthosilicate (TEOS)-based hydrophobic treatment. The methods presented in this study provide an alternative top-down approach to the typical preparation methods of nanocellulose textiles (e.g., dry-spinning, wet-spinning, and hydrodynamic alignment).

6.6.3. Wood Diaphragms for Speakers

Another very interesting study was carried out by Gan et al.^[237] on the fabrication of ultrathin partially delignified and densified flexible wood diaphragms for speakers (see Figure 30). First, a balsa wood sheet was partially delignified (10 cm \times 10 cm \times 0.3 mm) and then pressed at 100 °C and 10–15 MPa pressure for 24 h to obtain an ultrathin wood film. The densified wood film of DW had an exceptionally high tensile strength of 342 MPa and Young's modulus of 43.65 GPa, which were 20 and 35 times higher than those of natural wood, respectively. The acoustic and vibration behavior of the ultrathin wood film were measured and compared with the properties of a conventional polymer diaphragm. The results demonstrated that the wood film was a high performance acoustic transducer with 2.83 and 1.25 times increased resonance frequency and enhanced displacement amplitude, respectively, in comparison to a conventional polypropylene diaphragm.

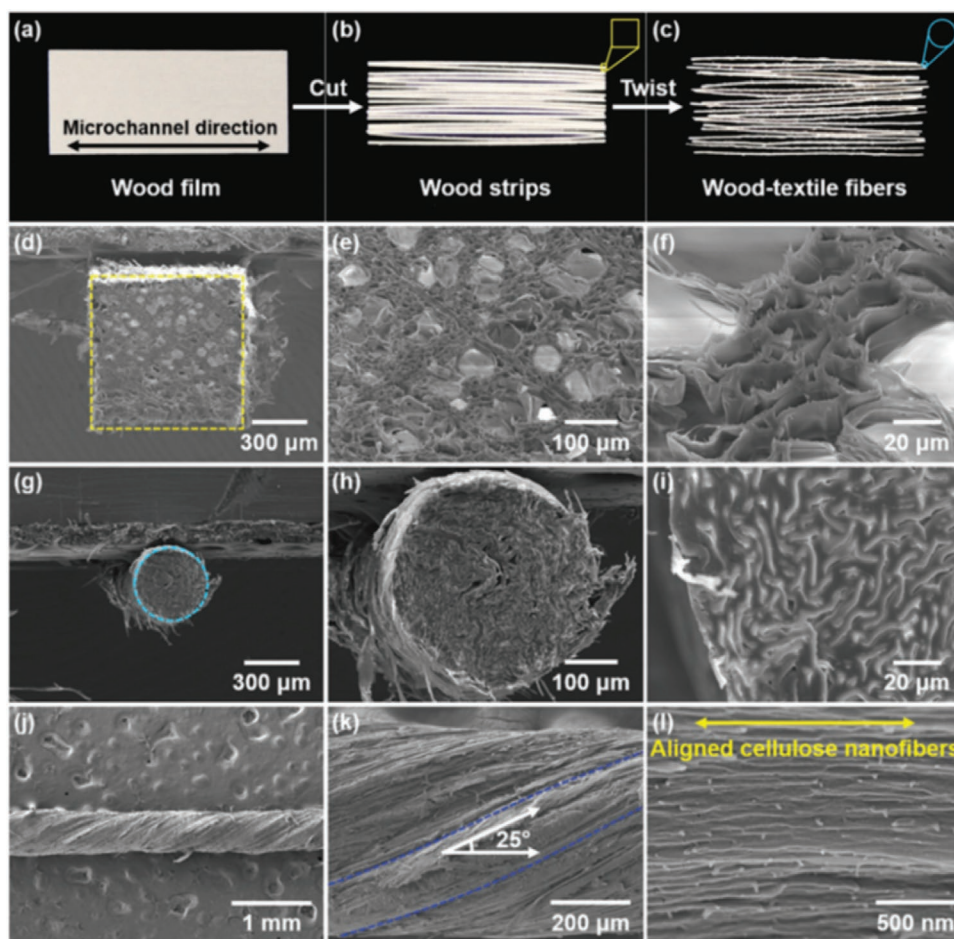


Figure 29. a–l) Fabrication process and microstructure characterization of wood-textile fibers. Adapted with permission.^[236] Copyright 2018, Wiley VCH.

6.6.4. Imprinted Wood

Huang et al.^[238] demonstrated a precise top-down approach for the preparation of imprinted wood (see **Figure 31**). First, the top surface of the wood substrate was partially delignified and then

pressed with a mold to form the imprinted wood. When the DW is pressed using a mold, it adopts the imprints of the mold in the dry condition, fixing the H-bonds (discussed in Section 5.4) between adjacent fibrils. Different shapes and sizes of imprints on the wood surface were achieved ranging from nanometers

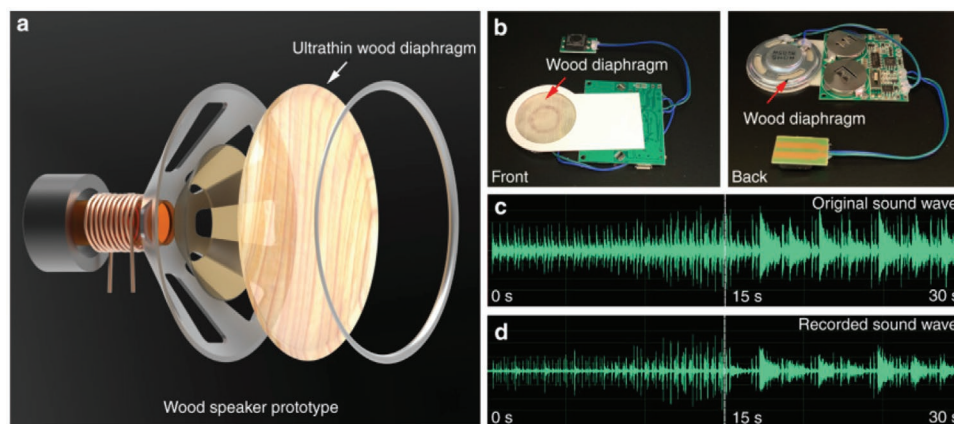


Figure 30. a) Schematic of the wood speaker prototype. b) Photographs of the speaker with the wood diaphragm. c) The sound wave of the original song (Spain Matador March). d) The recorded sound wave (Spain Matador March) of the speaker with the wood diaphragm. Adapted with permission.^[237] Copyright 2019, Nature Publishing Group.

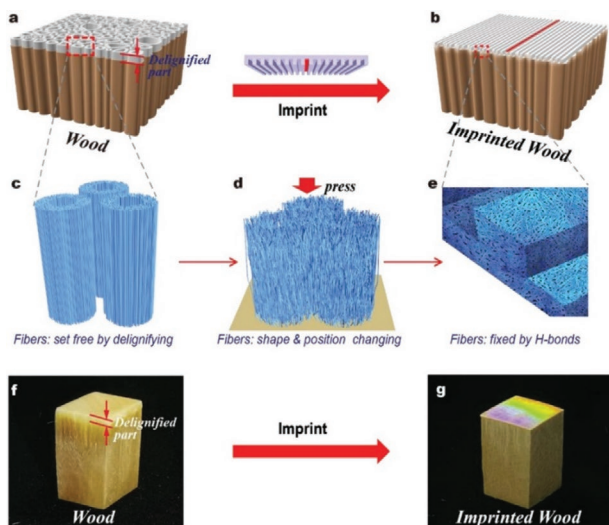


Figure 31. a–g) Schematic of the fabrication of imprinted wood with controllable surface microstructures. Adapted with permission.^[102] Copyright 2019, Wiley-VCH.

to tens of micrometers. To demonstrate the applicability of the imprinted wood, a wood microlens array (MLA) of 50–150 μm was prepared for potential applications in optical devices, which are useful in imaging and displaying. Both concave and convex MLAs were formed by imprinting the DW surface.

7. Concluding Remarks and Future Directions

Wood is a biobased, renewable, and mechanically robust scaffold with a hierarchical arrangement of cellulose fibrils bonded in the hemicellulose and lignin matrix. Lignin as a cementing material for wood cell walls limits potentials of chemical modification of wood for further applications. The removal of lignin from wood cell walls without altering the hierarchical arrangement of cellulose fibrils can lead to limitless opportunities in the area of biotemplated functional materials with an aligned cellulosic structure. So, the use of DW in the preparation of functional materials has become a leading scientific research topic in recent times. DW can be fabricated into different functional materials for a wide range of applications.

In preparation of DW scaffolds, alkaline pulping (e.g., Kraft pulping) methods are predominately used and NaClO_2 or NaClO , NaOH , and Na_2SO_3 are most commonly utilized for delignification, sometimes in combination with acetic acid, and the (additional) bleaching agent is by majority H_2O_2 . Until now, the most feasible and promising delignification method was H_2O_2 /acidic acid steam delignification, which fabricated DW samples with a maximum thickness of 40 mm.^[91] However, the sustainable and feasible delignification of solid wood samples with higher thicknesses and densities is vital for the future development of DW and its applications.

The delignification process significantly alters the physical, chemical, and mechanical structure of the wood cell wall and with this respect some fundamental questions still need to be addressed. For example, how the microfibril angles in the secondary wood cell wall are affected by delignification should be

investigated in more details, and the influence of the delignification on changes of the mechanical, physical, and chemical properties of wood should be additionally studied, as well.

To achieve complete lignin removal, which is needed for some functional applications, an additional bleaching step is required that removes hemicelluloses from the cell wall. Once the hemicellulose is removed, the robustness of the cellulosic structure is altered, which affects the mechanical properties of wood. The microscopic structure of the cell wall changes drastically upon lignin removal where visible voids are formed in the ML (which has the highest lignin content in the cell wall) and the cell wall corners. In mild delignification (22% lignin removal), the mesoporous pore size of wood decreases compared to natural wood. Conversely, the pore size increases with harsh delignification (94% lignin removal). The moisture sorption behavior of DW is different to natural wood because delignification increases the number of accessible OH groups in the wood cell wall, which attract more moisture. Delignification leads to the number of OH groups increasing from 8.5–9 mmol g^{-1} (natural wood) to 10.0–10.5 mmol g^{-1} . These reactive OH groups play a vital role in the fabrication of functional materials as various polymers possibly form bonds with them.

After delignification, it is very important to preserve the hierarchically aligned cellulosic structure, which can easily collapse during drying. Several methods have been tested to preserve the aligned cellulosic structure such as air-drying, solvent exchange-drying, and freeze-drying. Among them, freeze-drying stabilizes the structural integrity of DW scaffolds, and the porous structure formed due to lignin removal. However, during air- and solvent exchange-drying, the structural integrity is altered due rapid drying. The industrial applicability of freeze drying technique for DW might not be suitable for larger wooden samples and it limits to smaller size wood intended for specific applications.

The development of DW-based functional materials for a diverse range of applications (from building structural materials to biomimetic scaffolds) depends on how the DW fabrication is adapted via different strategies. These strategies are classified into five categories as mentioned in Figure 11: polymer infiltration, densification, surface treatments, and surface functionalization. The functional materials prepared from DW are classified according to their applications as structural materials, functional membranes, energy storage materials, electronics, biomedical materials, or other functional materials.

In the densification process, free OH groups play an important role in fixing the densified cellular structure to achieve maximum rigidity and stability via H-bonding (see Section 5.4 for explanations of different H-bond formations in DW). In the densification process, the DW should be in a moist or semi-moist conditions to obtain high quality densified products. In the polymer infiltration process, OH groups also play a significant role as they form bonds with the reactive sites of polymers.

The densification of DW is probably the most innovative way to obtain high performance wood materials for structural applications. The wood industry has historically struggled to obtain stable surface densified wood to improve the mechanical performance of low density timber species. The main challenge of fabricating densified wood is that the wood cell walls

return to their original shape after exposure to moisture (e.g., the spring-back effect and relaxation or shape recovery phenomena). Several methods have been employed to control the shape recovery of densified wood such as softening the wood using steam prior to densification or by using thermosetting polymers. Currently, partially and fully DW has been explored to obtain densified wood material (see Table 3 for more details). The highest mechanical properties (strength and work fracture of 586.8 MPa and 4 MJ m³, respectively) were achieved at 45% lignin removal and densification (100 °C under ≈5 MPa pressure for ≈1 day). The moisture content of DW prior to densification is very important as it influences the degree of densification and overall mechanical properties of the densified materials. This is because during densification, closed H-bonds are formed between the adjacent OH groups. The rehydration takes place prior to the compression and the mechanical properties of dry samples are compared. The densification approach is relatively new and its commercialization and bulk production will be challenging due to the limitations of chemical delignification, longer hot-pressing time for densification, and stability in moist conditions (without any further surface coatings). Although laboratory scale production of smaller densified DW samples is possible for specific applications, bulk structural material production has still not been achieved. Furthermore, in-depth scientific research is needed to optimize the delignification and densification processes (in terms of time and energy efficiency) to produce bulk quantities of such materials, as well as ensuring their stability against moisture. Furthermore, life cycle assessments of these materials should also be performed.

Transparent wood is a common application of polymer infiltrated DW. The DW used in transparent wood production is usually bleached with a H₂O₂ reaction system and the scaffold is then impregnated with a polymer (most commonly epoxy resin, PMMA, or PVA). Generally, the delignified and bleached substrate is impregnated with a liquid mixture containing the prepolymerized resin in a vacuum/pressure chamber. Afterward, the polymer is cured into a solid state within the wood cell walls by heating to an appropriate temperature. Transparent wood can be used as an alternative to glass as a conventional transparent material for windows. Transparent structural elements such as beams, façades, and wood rooftops have also been prepared from transparent wood. In such cases, the main challenge is to prepare thick transparent wood with maximal light transmittance. Li et al.^[145] made some advancement in this area by preparing 2–5 cm thick translucent (but not transparent) basswood composites for a wall material for a house model. Transparent wood can be further functionalized or upgraded to form transparent wood-based materials with other interesting properties. For instance, the UV resistance and IR heat shielding effect of transparent wood was increased by ATO nanoparticles.^[148] PCMs can also be incorporated into transparent wood for thermal energy storage applications. Furthermore, PCMs can improve the properties of transparent wood in order to fabricate optical transparent magnetic materials, light-emitting diodes, electrically conductive flexible green electronics, lasing and luminescent materials, electrochromic devices, and photochromic materials such as smart windows.

The properties of DW make it an ideal candidate for use as a thermally insulating material. These favorable properties

include low thermal energy absorbance/emissivity, low mass density, and good mechanical strength (could be achieved via densification). Furthermore, DW is sustainable, renewable, degradable, and cost-effective. DW can exhibit anisotropic thermal conductivity in the transverse and axial directions of cellulose fibers of 30 and 60 mW m⁻¹ K⁻¹, respectively. At the extremely low density of 13 kg m⁻³, the compressive strength of DW was 13 and 20 MPa in axial and transverse directions, respectively. These thermally insulating properties of DW are comparable to those of the best building materials such as mineral wool and polystyrene (see Table 4). Additionally, exceptional flame retardancy in DW-based thermal insulators can be achieved by in situ deposition of bentonite nanosheets. However, more research is needed, especially to reduce the moisture uptake and provide protection against microorganisms.

DW with an inbuilt hierarchical cellulosic porous structure has the potential to replace all existing fossil-based materials as a membrane in a diverse range of applications (e.g., oil spillage cleaning). DW-based 2D and 3D membranes have been explored in oil/water separation, membrane distillation for steam generation from seawater, and as ionic membranes for potential ion regulation. Different components and surface treatments have been employed to improve the performance of DW membranes, such as carbon nanomaterials (e.g., CNTs and GO), surface carbonization for solar steam generation, and superhydrophobic treatment to improve performance in oil spillage cleaning. The utilization of DW in membrane fabrication has a great potential to replace fossil-based polymeric membranes. However, more research is needed to improve the performance and durability of DW-based membranes and their applications in diverse areas.

Studies have demonstrated that DW can act as a scaffold for PCMs to improve their shape stability during charging and discharging processes. A CA–PA eutectic mixture was infused via vacuum impregnation into a DW scaffold in order to fabricate a thermal energy storage composite. Within the composite, the DW provided shape stability, in addition to maintaining the heat capture and discharge capacity of the PCM. Certain other features such as magnetic, photoluminescent, and superhydrophobic properties can also be added into PCM composites to enhance their wide range of applications.

Wood-based biomimetic scaffolds are an outstanding example of hierarchically organized natural materials with porous, biodegradable, and excellent mechanical properties. The delignification of wood further enhances their applicability as materials for biomedical applications. DW-based scaffolds have been employed as biomimetic materials for tissue engineering applications. For instance, DW was utilized to prepare the biomimetic scaffold for bone tissue regeneration via in situ Hap nanoparticle deposition and vacuum inflated PCL. The porous and aligned cellulose provided an excellent natural template for biomimicking the natural bone structure. Further, the flexibility of DW enables its application as a scaffold for biomedical applications as flexible, wearable, biocompatible, and breathable biomaterials. The application of DW as a biomedical material is at an early stage and substantially more scientific research, in addition to a wide range of application exploration is needed. This includes the testing of biocompatibility both in vitro and in vivo. DW-based biomedical materials have

a wide range of potential medical applications such as tissue engineering, drug delivery, dental applications, and in the fabrication of biomedical equipment. Other DW-based functional materials also include tunable wood (moisture induced tunability), textiles from wood (via mechanical rolling of DW strips), wood diaphragms of speakers, surface imprinting of wood, and some other functional materials to replace synthetic plastics.

In spite of the described benefits of DW and its great potential as a renewable biomaterial, its possible influence on the environment should be regarded with great care. It is common for DW-based materials to be described as an environmentally friendly alternative to conventional materials for certain products and devices.^[164–167] This idea is based on the utilization of wood, which is undoubtedly environmentally friendly and sustainable. However, in the manufacturing of DW-based materials, the delignification process, utilization of various impregnating polymers, and manufacturing process of the final products (e.g., transparent wood) are not ecologically benign. Therefore, we believe that it is necessary to carry out a life cycle assessment of DW-based materials and products, including transparent wood. Only when these assessment results are obtained, can one claim that DW has a better environmental profile than conventional materials (e.g., comparing ordinary glass with transparent wood for windows). Feifel et al.^[239] carried out a life cycle assessment study of two different types of wood–polymer composites (WPCs) with different compositions and geometries. Assessments were also performed on two wood decking materials, consisting either of *Bilinga* (tropical wood) or pressure-impregnated pine (regional wood) with identical geometries. Under the assumption of identical lifespans, the results showed that for all impact categories, the decking made of pine was the most environmentally benign. However, to our best knowledge, there are no scientific papers that perform a life cycle assessment of any DW-based products including transparent wood. Even if it was proven that the environmental profile of DW is better than conventional materials for the same purposes, the cost analysis should also be performed. DW can only become a serious alternative to conventional products and transfer into bulk production when both life cycle assessments and cost analyses provide promising results.

In the authors' opinion, transparent wood can be also regarded as a new type of WPC. As explained by Xu et al.,^[240] the use of natural fibers in such composite materials does not automatically make them “sustainable.” For example, the term “natural” may not necessarily equal “environmentally friendly.” Therefore, because transparent wood is a sort of WPC, some environmental analyses of this material could also be applied in the research of transparent wood. For instance, Teaca et al.^[241] presented the challenge of utilizing WPC after its service life. It is stated that repeated exploitation of plastics and wood is not possible over a certain limit without a severe reduction of properties. Consequently, this limits the range of applications and unbalances the costs-effectiveness. The best long-range approach would be selective separation of components and their appropriate disposal. For example, wood can be used for energy purposes or in compost formulations while plastics can be further recycled. However, the overall costs associated with such hi-tech disposal strategies are prohibitive.

To conclude, DW provides an extraordinary natural template for the development of various functional materials, which can be easily altered for different specifications via chemical, physical, and mechanical processes. Most of these functional materials are still only produced at laboratory scales. However, this is a growing area of development using novel materials from sustainable and renewable resources. Consequently, there is immense potential to provide alternate solutions to fossil-based plastics products.

Acknowledgements

The authors would like to acknowledge the financial support of the Natural Resources Institute Finland strategic funding in the form of AspenWillow, UBWGI, and VALUEPOT projects. WoodCircus (wood industry and wood construction in circular economy): H2020 European funding is also acknowledged by the authors. The authors also acknowledge the financial support from the Slovenian Research Agency (Research Programme Funding No. P4-0015, “Wood and lignocellulose composites”). The authors would like to acknowledge the courtesy images provided by Dr. Jussi-Petteri Suuronen, Prof. Sangeeta Gupta, Dr. Tiina Belt, and Urbano Tenorio Fernando. The authors would like to thank Dr. Anna Kärkönen for fruitful discussion and comments on wood lignification process. Various fruitful discussions with Prof. Jan Tywoniak and Prof. Korada Viswanatha Sharma are also acknowledged.

Conflict of Interest

The authors declare no conflict of interest.

Keywords

aligned-porous cellulose structure, delignification, delignified wood, functional materials, structural materials, transparent wood

Received: October 30, 2020

Revised: February 12, 2021

Published online:

- [1] J. Keckes, I. Burgert, K. Frühmann, M. Müller, K. Kölln, M. Hamilton, M. Burghammer, S. V. Roth, S. Stanzl-Tschegg, P. Fratzl, *Nat. Mater.* **2003**, *2*, 810.
- [2] P. Fratzl, R. Weinkamer, *Prog. Mater. Sci.* **2007**, *52*, 1263.
- [3] A. Payen, *Acad. Sci., Paris, C. R.* **1839**, *8*, 169.
- [4] L. A. Berglund, I. Burgert, *Adv. Mater.* **2018**, *30*, 1704285.
- [5] R. M. Rowell, *Handbook of Engineering Biopolymers, Homopolymers, Blends, and Composites*, Hanser Gardner Publications, Inc., Cincinnati, OH **2007**, pp. 673–691.
- [6] A. Kumar, P. Ryparová, A. S. Škapin, M. Humar, M. Pavlič, J. Tywoniak, P. Hajek, J. Žigon, M. Petrič, *Cellulose* **2016**, *23*, 3249.
- [7] A. Kumar, J. Richter, J. Tywoniak, P. Hajek, S. Adamopoulos, U. Šegedin, M. Petrič, *Holzforchung* **2017**, *72*, 45.
- [8] C. A. Hill, *Wood Modification: Chemical, Thermal and Other Processes*, Vol. 5, John Wiley & Sons, Chichester, UK **2007**.
- [9] V. Merk, M. Chanana, N. Gierlinger, A. M. Hirt, I. Burgert, *ACS Appl. Mater. Interfaces* **2014**, *6*, 9760.
- [10] W. Gan, L. Gao, Q. Sun, C. Jin, Y. Lu, J. Li, *Appl. Surf. Sci.* **2015**, *332*, 565.
- [11] V. Merk, J. K. Berg, C. Krywka, I. Burgert, *Cryst. Growth Des.* **2017**, *17*, 677.

- [12] S. Fink, *Holzforschung* **1992**, 46, 403.
- [13] Y. Li, E. Vasileva, I. Sychugov, S. Popov, L. Berglund, *Adv. Opt. Mater.* **2018**, 6, 1800059.
- [14] M. Zhu, J. Song, T. Li, A. Gong, Y. Wang, J. Dai, Y. Yao, W. Luo, D. Henderson, L. Hu, *Adv. Mater.* **2016**, 28, 5181.
- [15] T. Li, J. Song, X. Zhao, Z. Yang, G. Pastel, S. Xu, C. Jia, J. Dai, C. Chen, A. Gong, *Sci. Adv.* **2018**, 4, eaar3724.
- [16] C. Montanari, Y. Li, H. Chen, M. Yan, L. A. Berglund, *ACS Appl. Mater. Interfaces* **2019**, 11, 20465.
- [17] Y. He, H. Li, X. Guo, R. Zheng, *Catalysts* **2019**, 9, 115.
- [18] W. Huang, D. Restrepo, J. Jung, F. Y. Su, Z. Liu, R. O. Ritchie, J. McKittrick, P. Zavattieri, D. Kisailus, *Adv. Mater.* **2019**, 31, 1901561.
- [19] F. Chen, A. S. Gong, M. Zhu, G. Chen, S. D. Lacey, F. Jiang, Y. Li, Y. Wang, J. Dai, Y. Yao, *ACS Nano* **2017**, 11, 4275.
- [20] Z. Yu, N. Yang, L. Zhou, Z. Ma, Y. Zhu, Y. Lu, B. Qin, W. Xing, T. Ma, S. Li, *Sci. Adv.* **2018**, 4, eaat7223.
- [21] S. Wang, A. Lu, L. Zhang, *Prog. Polym. Sci.* **2016**, 53, 169.
- [22] A. Dufresne, *Mater. Today* **2013**, 16, 220.
- [23] T. Mokhena, M. John, *Cellulose* **2020**, 27, 1149.
- [24] Z. Fang, G. Hou, C. Chen, L. Hu, *Curr. Opin. Solid State Mater. Sci.* **2019**, 23, 100764.
- [25] R. J. Moon, A. Martini, J. Nairn, J. Simonsen, J. Youngblood, *Chem. Soc. Rev.* **2011**, 40, 3941.
- [26] S. H. Osong, S. Norgren, P. Engstrand, *Cellulose* **2016**, 23, 93.
- [27] N. Grishkewich, N. Mohammed, J. Tang, K. C. Tam, *Curr. Opin. Colloid Interface Sci.* **2017**, 29, 32.
- [28] W. Chen, H. Yu, S. Lee, T. Wei, J. Li, Z. Fan, *Chem. Soc. Rev.* **2018**, 47, 2837.
- [29] X. Du, Z. Zhang, W. Liu, Y. Deng, *Nano Energy* **2017**, 35, 299.
- [30] C. Calvino, N. Macke, R. Kato, S. J. Rowan, *Prog. Polym. Sci.* **2020**, 103, 101221.
- [31] D. Klemm, E. D. Cranston, D. Fischer, M. Gama, S. A. Kedzior, D. Kralisch, F. Kramer, T. Kondo, T. Lindström, S. Nietzsche, *Mater. Today* **2018**, 21, 720.
- [32] K. De France, Z. Zeng, T. Wu, G. Nyström, *Adv. Mater.* **2020**, 2000657.
- [33] T. Abitbol, A. Rivkin, Y. Cao, Y. Nevo, E. Abraham, T. Ben-Shalom, S. Lapidot, O. Shoseyov, *Curr. Opin. Biotechnol.* **2016**, 39, 76.
- [34] Y. Yang, Y. Lu, K. Zeng, T. Heinze, T. Groth, K. Zhang, *Adv. Mater.* **2020**, 2000717.
- [35] F. Jiang, T. Li, Y. Li, Y. Zhang, A. Gong, J. Dai, E. Hitz, W. Luo, L. Hu, *Adv. Mater.* **2018**, 30, 1703453.
- [36] I. Burgert, E. Cabane, C. Zollfrank, L. Berglund, *Int. Mater. Rev.* **2015**, 60, 431.
- [37] L. A. Berglund, I. Burgert, *Adv. Mater.* **2018**, 30, 1704285.
- [38] H. Zhu, W. Luo, P. N. Ciesielski, Z. Fang, J. Zhu, G. Henriksson, M. E. Himmel, L. Hu, *Chem. Rev.* **2016**, 116, 9305.
- [39] J. Huang, B. Zhao, T. Liu, J. Mou, Z. Jiang, J. Liu, H. Li, M. Liu, *Adv. Funct. Mater.* **2019**, 29, 1902255.
- [40] C. Chen, L. Hu, *Acc. Chem. Res.* **2018**, 51, 3154.
- [41] Y. Dong, K. Wang, J. Li, S. Zhang, S. Q. Shi, *ACS Sustainable Chem. Eng.* **2020**, 8, 3532.
- [42] M. Yu, G. Zhang, T. Saunders, *Ceram. Int.* **2019**, 46, 5536.
- [43] Z. Wang, M. S. Ganewatta, C. Tang, *Prog. Polym. Sci.* **2019**, 101, 101197.
- [44] S. Rongpipi, D. Ye, E. D. Gomez, E. W. Gomez, *Front. Plant Sci.* **2019**, 9, 1894.
- [45] C. Chen, Y. Kuang, S. Zhu, I. Burgert, T. Keplinger, A. Gong, T. Li, L. Berglund, S. J. Eichhorn, L. Hu, *Nat. Rev. Mater.* **2020**, 5, 642.
- [46] C. Huang, H. Lindström, R. Nakada, J. Ralston, *Holz Roh- Werkst.* **2003**, 61, 321.
- [47] R. H. Atalla, U. P. Agarwal, *Science* **1985**, 227, 636.
- [48] O. Hamant, J. Traas, *New Phytol.* **2010**, 185, 369.
- [49] J. Barnett, G. Jeronimidis, *Wood Quality and Its Biological Basis*, John Wiley & Sons, Oxford **2009**.
- [50] L. Donaldson, *IAWA J.* **2008**, 29, 345.
- [51] A. Rafsanjani, M. Stiefel, K. Jefimovs, R. Mokso, D. Derome, J. Carmeliet, *J. R. Soc., Interface* **2014**, 11, 20140126.
- [52] J. R. Barnett, V. A. Bonham, *Biol. Rev.* **2004**, 79, 461.
- [53] N. Chaffey, *Trends Plant Sci.* **2000**, 5, 360.
- [54] R. M. Rowell, R. Pettersen, J. S. Han, J. S. Rowell, M. A. Tshabalala, *Handbook of Wood Chemistry and Wood Composites*, Vol. 2, CRC Press, Boca Raton, FL **2005**.
- [55] R. A. Parham, R. L. Gray, *The Chemistry of Solid Wood*, ACS Publications, Washington, DC **1984**.
- [56] R. Alén, *For. Prod. Chem.* **2000**, 3, 11.
- [57] A. Panshin, C. De Zeeuw, McGraw-Hill, New York, USA **1980**.
- [58] D. Fengel, *Wood Sci. Technol.* **1969**, 3, 203.
- [59] I. M. Saxena, R. M. Brown Jr., *Ann. Bot.* **2005**, 96, 9.
- [60] R. M. Brown Jr., *J. Macromol. Sci., Part A: Pure Appl. Chem.* **1996**, 33, 1345.
- [61] S. K. Cousins, R. M. Brown Jr., *Polymer* **1995**, 36, 3885.
- [62] E. Sjöström, *Wood Chemistry: Fundamentals and Applications*, Gulf Professional Publishing, New York **1993**.
- [63] H. Pereira, J. Graça, J. C. Rodrigues, *Wood Quality and Its Biological Basis*, CRC Press, Boca Raton, FL **2003**, p. 53.
- [64] A. R. Barceló, *International Review of Cytology*, Vol. 176, Elsevier, Amsterdam **1997**, pp. 87–132.
- [65] J. Barros, H. Serk, I. Granlund, E. Pesquet, *Ann. Bot.* **2015**, 115, 1053.
- [66] C. Liu, *Mol. Plant* **2012**, 5, 304.
- [67] Y. Wang, M. Chantreau, R. Sibout, S. Hawkins, *Front. Plant Sci.* **2013**, 4, 220.
- [68] A. Kärkönen, S. Koutaniemi, *J. Integr. Plant Biol.* **2010**, 52, 176.
- [69] W. Boerjan, J. Ralph, M. Baucher, *Annu. Rev. Plant Biol.* **2003**, 54, 519.
- [70] R. Vanholme, B. Demedts, K. Morreel, J. Ralph, W. Boerjan, *Plant Physiol.* **2010**, 153, 895.
- [71] R. Hatfield, W. Vermeris, *Plant Physiol.* **2001**, 126, 1351.
- [72] R. Sibout, H. Höfte, *Curr. Biol.* **2012**, 22, R533.
- [73] Z. Xu, D. Zhang, J. Hu, X. Zhou, X. Ye, K. L. Reichel, N. R. Stewart, R. D. Syrenne, X. Yang, P. Gao, W. Shi, C. Doepcke, R. W. Sykes, J. N. Burris, J. J. Bozell, M. Z.-M. Cheng, D. G. Hayes, N. Labbe, M. Davis, C. N. Stewart Jr., J. S. Yuan, *BMC Bioinf.* **2009**, 10, S3.
- [74] L. Donaldson, *Wood Sci. Technol.* **1994**, 28, 111.
- [75] L. Donaldson, *Wood Sci. Technol.* **1995**, 29, 51.
- [76] L. A. Donaldson, *Phytochemistry* **2001**, 57, 859.
- [77] R. Zhong, D. Cui, Z. Ye, *New Phytol.* **2019**, 221, 1703.
- [78] R. Vanholme, B. De Meester, J. Ralph, W. Boerjan, *Curr. Opin. Biotechnol.* **2019**, 56, 230.
- [79] W. Schutyser, T. Renders, S. Van den Bosch, S. Koelewijn, G. Beckham, B. F. Sels, *Chem. Soc. Rev.* **2018**, 47, 852.
- [80] T. Renders, E. Cooreman, S. Van den Bosch, W. Schutyser, S. Koelewijn, T. Vangeel, A. Deneyer, G. Van den Bossche, C. Courtin, B. Sels, *Green Chem.* **2018**, 20, 4607.
- [81] P. Bajpai, *Biermann's Handbook of Pulp and Paper: Paper and Board Making*, Vol. 2, Elsevier, Amsterdam **2018**.
- [82] J. S. Kim, Y. Lee, T. H. Kim, *Bioresour. Technol.* **2016**, 199, 42.
- [83] R. A. Ribeiro, S. Vaz Junior, H. Jameel, H. Chang, R. Narron, X. Jiang, J. L. Colodette, *ACS Sustainable Chem. Eng.* **2019**, 7, 10274.
- [84] J. J. Klemes, *Handbook of Process Integration (PI): Minimisation of Energy and Water Use, Waste and Emissions*, Elsevier, Amsterdam **2013**.
- [85] Y. Li, X. Yang, Q. Fu, R. Rojas, M. Yan, L. Berglund, *J. Mater. Chem. A* **2018**, 6, 1094.
- [86] J. Wu, Y. Wu, F. Yang, C. Tang, Q. Huang, J. Zhang, *Composites, Part A* **2019**, 117, 324.
- [87] K. E. Foster, K. M. Hess, G. M. Miyake, W. V. Srubar, *Materials* **2019**, 12, 2256.
- [88] J. Qin, X. Li, Y. Shao, K. Shi, X. Zhao, T. Feng, Y. Hu, *Vacuum* **2018**, 158, 158.

- [89] M. Zhu, J. Song, T. Li, A. Gong, Y. Wang, J. Dai, Y. Yao, W. Luo, D. Henderson, L. Hu, *Adv. Mater.* **2016**, *28*, 5181.
- [90] W. Zou, D. Sun, Z. Wang, R. Li, W. Yu, P. Zhang, *RSC Adv.* **2019**, *9*, 21566.
- [91] H. Li, X. Guo, Y. He, R. Zheng, *J. Mater. Res.* **2019**, *34*, 932.
- [92] Z. Bi, T. Li, H. Su, Y. Ni, L. Yan, *ACS Sustainable Chem. Eng.* **2018**, *6*, 9314.
- [93] T. Feng, J. Qin, Y. Shao, L. Jia, Q. Li, Y. Hu, *Coatings* **2019**, *9*, 433.
- [94] S. Zhang, C. Wang, B. Fei, Y. Yu, H. Cheng, G. Tian, *BioResources* **2013**, *8*, 2376.
- [95] Y. Li, Q. Fu, S. Yu, M. Yan, L. Berglund, *Biomacromolecules* **2016**, *17*, 1358.
- [96] R. Mi, T. Li, D. Dalgo, C. Chen, Y. Kuang, S. He, X. Zhao, W. Xie, W. Gan, J. Zhu, *Adv. Funct. Mater.* **2020**, *30*, 1907511.
- [97] M. Zhu, T. Li, C. S. Davis, Y. Yao, J. Dai, Y. Wang, F. AlQatari, J. W. Gilman, L. Hu, *Nano Energy* **2016**, *26*, 332.
- [98] M. Frey, D. Widner, J. S. Segmehl, K. Casdorff, T. Keplinger, I. Burgert, *ACS Appl. Mater. Interfaces* **2018**, *10*, 5030.
- [99] M. Frey, L. Schneider, K. Masania, T. Keplinger, I. Burgert, *ACS Appl. Mater. Interfaces* **2019**, *11*, 35305.
- [100] M. Frey, G. Biffi, M. Adobes-Vidal, M. Zirkelbach, Y. Wang, K. Tu, A. M. Hirt, K. Masania, I. Burgert, T. Keplinger, *Adv. Sci.* **2019**, *6*, 1802190.
- [101] J. Segmehl, V. Studer, T. Keplinger, I. Burgert, *Materials* **2018**, *11*, 517.
- [102] J. Song, C. Chen, C. Wang, Y. Kuang, Y. Li, F. Jiang, Y. Li, E. Hitz, Y. Zhang, B. Liu, *ACS Appl. Mater. Interfaces* **2017**, *9*, 23520.
- [103] T. Yang, J. Cao, E. Ma, *Ind. Crops Prod.* **2019**, *135*, 91.
- [104] W. Huang, L. Zhang, X. Lai, H. Li, X. Zeng, *Chem. Eng. J.* **2019**, *386*, 123994.
- [105] X. Han, Y. Ye, F. Lam, J. Pu, F. Jiang, *J. Mater. Chem. A* **2019**, *7*, 27023.
- [106] A. Khakalo, A. Tanaka, A. Korpela, L. K. Hauru, H. Orelma, *ACS Sustainable Chem. Eng.* **2019**, *7*, 3195.
- [107] S. He, C. Chen, T. Li, J. Song, X. Zhao, Y. Kuang, Y. Liu, Y. Pei, E. Hitz, W. Kong, *Small Methods* **2020**, *4*, 1900747.
- [108] Z. Li, C. Chen, R. Mi, W. Gan, J. Dai, M. Jiao, H. Xie, Y. Yao, S. Xiao, L. Hu, *Adv. Mater.* **2020**, *32*, 1906308.
- [109] R. Liang, Y. Zhu, L. Wen, W. Zhao, B. Kuai, Y. Zhang, L. Cai, *Cellulose* **2020**, *27*, 1921.
- [110] L. Cheng, J. Feng, *Composites, Part A* **2020**, *129*, 105690.
- [111] L. Salmén, A. Olsson, *J. Pulp Pap. Sci.* **1998**, *24*, 99.
- [112] L. Salmén, *C. R. Biol.* **2004**, *327*, 873.
- [113] L. Salmén, *J. Mater. Sci.* **1984**, *19*, 3090.
- [114] Y. Yin, L. Berglund, L. Salmén, *Biomacromolecules* **2011**, *12*, 194.
- [115] M. Maaß, S. Saleh, H. Militz, C. A. Volkert, *Adv. Mater.* **2020**, *32*, 1907693.
- [116] L. Salmén, I. Burgert, *Holzforschung* **2009**, *63*, 121.
- [117] L. H. Thomas, A. Martel, I. Grillo, M. C. Jarvis, *Cellulose* **2020**, *27*, 4249.
- [118] S. Vitas, J. S. Segmehl, I. Burgert, E. Cabane, *Materials* **2019**, *12*, 416.
- [119] P. Grönquist, M. Frey, T. Keplinger, I. Burgert, *ACS Omega* **2019**, *4*, 12425.
- [120] T. Endo, F. Zhang, R. Kitagawa, T. Hirotsu, J. Hosokawa, *Polym. J.* **2000**, *32*, 182.
- [121] M. Nogi, H. Yano, *Adv. Mater.* **2008**, *20*, 1849.
- [122] Y. Okahisa, A. Yoshida, S. Miyaguchi, H. Yano, *Compos. Sci. Technol.* **2009**, *69*, 1958.
- [123] H. Abrial, J. Arikas, M. Mahardika, D. Handayani, I. Aminah, N. Sandrawati, A. B. Pratama, N. Fajri, S. Sapuan, R. Ilyas, *Food Hydrocolloids* **2020**, *98*, 105266.
- [124] V. Karl'a, *IOP Conf. Ser.: Mater. Sci. Eng.* **2019**, *566*, 012015.
- [125] J. Huang, B. Zhao, T. Liu, J. Mou, Z. Jiang, J. Liu, H. Li, M. Liu, *Adv. Funct. Mater.* **2019**, *29*, 1902255.
- [126] Y. Li, Q. Fu, X. Yang, L. Berglund, *Philos. Trans. R. Soc., A* **2018**, *376*, 20170182.
- [127] Y. Li, M. Cheng, E. Jungstedt, B. Xu, L. Sun, L. Berglund, *ACS Sustainable Chem. Eng.* **2019**, *7*, 6061.
- [128] Y. Li, Q. Fu, S. Yu, M. Yan, L. Berglund, *Biomacromolecules* **2016**, *17*, 1358.
- [129] H. S. Yaddanapudi, N. Hickerson, S. Saini, A. Tiwari, *Vacuum* **2017**, *146*, 649.
- [130] Y. Li, Q. Fu, R. Rojas, M. Yan, M. Lawoko, L. Berglund, *ChemSusChem* **2017**, *10*, 3445.
- [131] Y. Wu, J. Zhou, Q. Huang, F. Yang, Y. Wang, X. Liang, J. Li, *ACS Omega* **2020**, *5*, 1782.
- [132] Y. Wu, J. Wu, F. Yang, C. Tang, Q. Huang, *Polymers* **2019**, *11*, 776.
- [133] A. N. S. Rao, G. B. Nagarajappa, S. Nair, A. M. Chathoth, K. K. Pandey, *Compos. Sci. Technol.* **2019**, *182*, 107719.
- [134] L. Wang, Y. Liu, X. Zhan, D. Luo, X. Sun, *J. Mater. Chem. C* **2019**, *7*, 8649.
- [135] Q. Fu, M. Yan, E. Jungstedt, X. Yang, Y. Li, L. A. Berglund, *Compos. Sci. Technol.* **2018**, *164*, 296.
- [136] P. A. Dias, J. A. Alves, D. P. Fagg, M. S. Reis, M. H. Gil, *J. Vinyl Addit. Technol.* **2012**, *18*, 95.
- [137] Y. Nishiwaki-Akine, S. Kanazawa, T. Uneyama, K. Nitta, R. Yamamoto-Ikemoto, T. Watanabe, *ACS Sustainable Chem. Eng.* **2017**, *5*, 11536.
- [138] M. Zhu, C. Jia, Y. Wang, Z. Fang, J. Dai, L. Xu, D. Huang, J. Wu, Y. Li, J. Song, *ACS Appl. Mater. Interfaces* **2018**, *10*, 28566.
- [139] R. J. Tilley, *Colour and the Optical Properties of Materials*, John Wiley & Sons, Chichester, UK **2020**.
- [140] C. Preston, Y. Xu, X. Han, J. N. Munday, L. Hu, *Nano Res.* **2013**, *6*, 461.
- [141] E. Vasileva, H. Chen, Y. Li, I. Sychugov, M. Yan, L. Berglund, S. Popov, *Adv. Opt. Mater.* **2018**, *6*, 1800999.
- [142] H. Chen, A. Baitenov, Y. Li, E. Vasileva, S. Popov, I. Sychugov, M. Yan, L. Berglund, *ACS Appl. Mater. Interfaces* **2019**, *11*, 35451.
- [143] T. Keplinger, X. Wang, I. Burgert, *J. Mater. Chem. A* **2019**, *7*, 2981.
- [144] E. Jungstedt, C. Montanari, S. Östlund, L. Berglund, *Composites, Part A* **2020**, *133*, 105853.
- [145] H. Li, X. Guo, Y. He, R. Zheng, *Eur. J. Wood Wood Prod.* **2019**, *77*, 843.
- [146] Y. Li, Q. Fu, X. Yang, L. Berglund, *Philos. Trans. R. Soc., A* **2018**, *376*, 20170182.
- [147] A. W. Lang, Y. Li, M. De Keersmaecker, D. E. Shen, A. M. Österholm, L. Berglund, J. R. Reynolds, *ChemSusChem* **2018**, *11*, 854.
- [148] Z. Qiu, Z. Xiao, L. Gao, J. Li, H. Wang, Y. Wang, Y. Xie, *Compos. Sci. Technol.* **2019**, *172*, 43.
- [149] R. Mi, T. Li, D. Dalgo, C. Chen, Y. Kuang, S. He, X. Zhao, W. Xie, W. Gan, J. Zhu, *Adv. Funct. Mater.* **2020**, *30*, 1907511.
- [150] Z. Yu, Y. Yao, J. Yao, L. Zhang, Z. Chen, Y. Gao, H. Luo, *J. Mater. Chem. A* **2017**, *5*, 6019.
- [151] C. Jia, C. Chen, R. Mi, T. Li, J. Dai, Z. Yang, Y. Pei, S. He, H. Bian, S. Jang, *ACS Nano* **2019**, *13*, 9993.
- [152] X. Wang, T. Zhan, Y. Liu, J. Shi, B. Pan, Y. Zhang, L. Cai, S. Q. Shi, *ChemSusChem* **2018**, *11*, 4086.
- [153] W. Gan, L. Gao, S. Xiao, W. Zhang, X. Zhan, J. Li, *J. Mater. Sci.* **2017**, *52*, 3321.
- [154] Q. Tang, L. Fang, Y. Wang, M. Zou, W. Guo, *Nanoscale* **2018**, *10*, 4344.
- [155] S. Popov, A. Marinins, I. Sychugov, M. Yan, E. Vasileva, Y. Li, L. Berglund, A. Udalcovs, O. Ozolins, in *2018 17th Workshop on Information Optics (WIO)*, IEEE, Piscataway, NJ **2018**.
- [156] E. Vasileva, Y. Li, I. Sychugov, M. Mensi, L. Berglund, S. Popov, *Adv. Opt. Mater.* **2017**, *5*, 1700057.
- [157] M. Koivurova, E. Vasileva, Y. Li, L. Berglund, S. Popov, *Opt. Express* **2018**, *26*, 13474.

- [158] T. Zhang, P. Yang, M. Chen, K. Yang, Y. Cao, X. Li, M. Tang, W. Chen, X. Zhou, *ACS Appl. Mater. Interfaces* **2019**, *11*, 36010.
- [159] T. Zhang, P. Yang, Y. Li, Y. Cao, Y. Zhou, M. Chen, Z. Zhu, W. Chen, X. Zhou, *ACS Sustainable Chem. Eng.* **2019**, *7*, 11464.
- [160] Q. Fu, F. Ansari, Q. Zhou, L. A. Berglund, *ACS Nano* **2018**, *12*, 2222.
- [161] W. Gan, S. Xiao, L. Gao, R. Gao, J. Li, X. Zhan, *ACS Sustainable Chem. Eng.* **2017**, *5*, 3855.
- [162] J. Song, C. Chen, S. Zhu, M. Zhu, J. Dai, U. Ray, Y. Li, Y. Kuang, Y. Li, N. Qisppe, *Nature* **2018**, *554*, 224.
- [163] B. Jiang, C. Chen, Z. Liang, S. He, Y. Kuang, J. Song, R. Mi, G. Chen, M. Jiao, L. Hu, *Adv. Funct. Mater.* **2019**, *30*, 1906307.
- [164] C. Chen, Z. Li, R. Mi, J. Dai, H. Xie, Y. Pei, J. Li, H. Qiao, H. Tang, B. Yang, L. Hu, *ACS Nano* **2020**, *14*, 5194.
- [165] A. Kumar, K. Staněk, P. Ryparová, P. Hajek, J. Tywoniak, *Composites, Part B* **2016**, *106*, 285.
- [166] S. Schiavoni, F. Bianchi, F. Asdrubali, *Renewable Sustainable Energy Rev.* **2016**, *62*, 988.
- [167] B. P. Jelle, *Energy Build.* **2011**, *43*, 2549.
- [168] B. Wicklein, A. Kocjan, G. Salazar-Alvarez, F. Carosio, G. Camino, M. Antonietti, L. Bergström, *Nat. Nanotechnol.* **2015**, *10*, 277.
- [169] H. M. Duong, S. T. Nguyen, *Nano and Biotech Based Materials for Energy Building Efficiency*, Springer, Cham **2016**, pp. 411–427.
- [170] P. Gupta, B. Singh, A. K. Agrawal, P. K. Maji, *Mater. Des.* **2018**, *158*, 224.
- [171] F. Liebner, E. Haimer, M. Wendland, M. Neouze, K. Schlufte, P. Miethe, T. Heinze, A. Potthast, T. Rosenau, *Macromol. Biosci.* **2010**, *10*, 349.
- [172] L. Long, Y. Weng, Y. Wang, *Polymers* **2018**, *10*, 623.
- [173] N. Lavoine, L. Bergström, *J. Mater. Chem. A* **2017**, *5*, 16105.
- [174] J. Zhang, B. Li, L. Li, A. Wang, *J. Mater. Chem. A* **2016**, *4*, 2069.
- [175] K. Uetani, K. Hatori, *Sci. Technol. Adv. Mater.* **2017**, *18*, 877.
- [176] P. L. Hurtado, A. Rouilly, V. Vandenbossche, C. Raynaud, *Build. Environ.* **2016**, *96*, 170.
- [177] A. M. Papadopoulos, *Energy Build.* **2005**, *37*, 77.
- [178] A. Demilecamps, C. Beauger, C. Hildenbrand, A. Rigacci, T. Budtova, *Carbohydr. Polym.* **2015**, *122*, 293.
- [179] C. Jiménez-Saelices, B. Seantier, B. Cathala, Y. Grohens, *Carbohydr. Polym.* **2017**, *157*, 105.
- [180] P. Munier, V. Apostolopoulou-Kalkavoura, M. Persson, L. Bergström, *Cellulose* **2020**, *27*, 10825.
- [181] H. Sun, H. Bi, X. Lin, L. Cai, M. Xu, *Polymers* **2020**, *12*, 165.
- [182] G. Chen, C. Chen, Y. Pei, S. He, Y. Liu, B. Jiang, M. Jiao, W. Gan, D. Liu, B. Yang, L. Hu, *Chem. Eng. J.* **2020**, *383*, 123109.
- [183] T. Li, Y. Zhai, S. He, W. Gan, Z. Wei, M. Heidarinejad, D. Dalgo, R. Mi, X. Zhao, J. Song, *Science* **2019**, *364*, 760.
- [184] H. Yano, *J. Mater. Sci. Lett.* **2001**, *20*, 1127.
- [185] S. Xiong, H. Long, G. Tang, J. Wan, H. Li, *Mar. Pollut. Bull.* **2015**, *96*, 7.
- [186] J. H. Paul, D. Hollander, P. Coble, K. L. Daly, S. Murasko, D. English, J. Basso, J. Delaney, L. McDaniel, C. W. Kovach, *Environ. Sci. Technol.* **2013**, *47*, 9651.
- [187] H. Sai, R. Fu, L. Xing, J. Xiang, Z. Li, F. Li, T. Zhang, *ACS Appl. Mater. Interfaces* **2015**, *7*, 7373.
- [188] Z. Zhang, G. Sèbe, D. Rentsch, T. Zimmermann, P. Tingaut, *Chem. Mater.* **2014**, *26*, 2659.
- [189] M. Khosravi, S. Azizian, *ACS Appl. Mater. Interfaces* **2015**, *7*, 25326.
- [190] L. Wu, L. Li, B. Li, J. Zhang, A. Wang, *ACS Appl. Mater. Interfaces* **2015**, *7*, 4936.
- [191] V. H. Pham, J. H. Dickerson, *ACS Appl. Mater. Interfaces* **2014**, *6*, 14181.
- [192] Y. Pan, K. Shi, C. Peng, W. Wang, Z. Liu, X. Ji, *ACS Appl. Mater. Interfaces* **2014**, *6*, 8651.
- [193] N. Zhang, W. Jiang, T. Wang, J. Gu, S. Zhong, S. Zhou, T. Xie, J. Fu, *Ind. Eng. Chem. Res.* **2015**, *54*, 11033.
- [194] L. Chen, R. Du, J. Zhang, T. Yi, *J. Mater. Chem. A* **2015**, *3*, 20547.
- [195] H. Hu, Z. Zhao, Y. Gogotsi, J. Qiu, *Environ. Sci. Technol. Lett.* **2014**, *1*, 214.
- [196] D. Li, F. Z. Zhu, J. Y. Li, P. Na, N. Wang, *Ind. Eng. Chem. Res.* **2012**, *52*, 516.
- [197] V. Singh, S. Jinka, K. Hake, S. Parameswaran, R. J. Kendall, S. Ramkumar, *Ind. Eng. Chem. Res.* **2014**, *53*, 11954.
- [198] Y. Jin, P. Jiang, Q. Ke, F. Cheng, Y. Zhu, Y. Zhang, *J. Hazard. Mater.* **2015**, *300*, 175.
- [199] A. W. Carpenter, C. de Lannoy, M. R. Wiesner, *Environ. Sci. Technol.* **2015**, *49*, 5277.
- [200] K. J. De France, T. Hoare, E. D. Cranston, *Chem. Mater.* **2017**, *29*, 4609.
- [201] X. Yang, E. D. Cranston, *Chem. Mater.* **2014**, *26*, 6016.
- [202] B. Wang, W. Liang, Z. Guo, W. Liu, *Chem. Soc. Rev.* **2015**, *44*, 336.
- [203] F. Liu, M. Ma, D. Zang, Z. Gao, C. Wang, *Carbohydr. Polym.* **2014**, *103*, 480.
- [204] K. Wang, X. Liu, Y. Tan, W. Zhang, S. Zhang, J. Li, *Chem. Eng. J.* **2019**, *371*, 769.
- [205] H. Guan, Z. Cheng, X. Wang, *ACS Nano* **2018**, *12*, 10365.
- [206] M. Wu, Y. Hong, C. Liu, J. Yang, X. Wang, S. Agarwal, A. Greiner, Z. Xu, *J. Mater. Chem. A* **2019**, *7*, 16735.
- [207] P. Burek, Y. Satoh, G. Fischer, M. T. Kahil, A. Scherzer, S. Tramberend, L. F. Nava, Y. Wada, S. Eisner, M. Flörke, N. Hanasaki, P. Magnuszewski, B. Cosgrove, D. Wiberg, *Water Futures and Solution - Fast Track Initiative (Final Report)*, I IASA, Laxenburg, Austria: WP-16-006, **2016**.
- [208] P. Goh, W. Lau, M. Othman, A. Ismail, *Desalination* **2018**, *425*, 130.
- [209] A. Deshmukh, C. Boo, V. Karanikola, S. Lin, A. P. Straub, T. Tong, D. M. Warsinger, M. Elimelech, *Energy Environ. Sci.* **2018**, *11*, 1177.
- [210] A. Alkudhiri, N. Darwish, N. Hilal, *Desalination* **2012**, *287*, 2.
- [211] K. W. Lawson, D. R. Lloyd, *J. Membr. Sci.* **1997**, *124*, 1.
- [212] R. Schofield, A. Fane, C. Fell, *J. Membr. Sci.* **1987**, *33*, 299.
- [213] N. Hilal, C. J. Wright, *npj Clean Water* **2018**, *1*, 8.
- [214] A. Deshmukh, M. Elimelech, *J. Membr. Sci.* **2017**, *539*, 458.
- [215] M. Khayet, *Adv. Colloid Interface Sci.* **2011**, *164*, 56.
- [216] J. Vanneste, J. A. Bush, K. L. Hickenbottom, C. A. Marks, D. Jassby, C. S. Turchi, T. Y. Cath, *J. Membr. Sci.* **2018**, *548*, 298.
- [217] D. Hou, D. Jassby, R. Nerenberg, Z. J. Ren, *Environ. Sci. Technol.* **2019**, *53*, 11618.
- [218] D. Hou, T. Li, X. Chen, S. He, J. Dai, S. A. Mofid, D. Hou, A. Iddya, D. Jassby, R. Yang, *Sci. Adv.* **2019**, *5*, eaaw3203.
- [219] Z. Chen, B. Dang, X. Luo, W. Li, J. Li, H. Yu, S. Liu, S. Li, *ACS Appl. Mater. Interfaces* **2019**, *11*, 26032.
- [220] Y. He, H. Li, X. Guo, R. Zheng, *BioResources* **2019**, *14*, 3758.
- [221] T. Li, S. X. Li, W. Kong, C. Chen, E. Hitz, C. Jia, J. Dai, X. Zhang, R. Briber, Z. Siwy, *Sci. Adv.* **2019**, *5*, eaau4238.
- [222] F. Kuznik, J. Virgone, *Appl. Energy* **2009**, *86*, 2038.
- [223] Y. Hong, G. Xin-Shi, *Sol. Energy Mater. Sol. Cells* **2000**, *64*, 37.
- [224] L. Ma, Q. Wang, L. Li, *Sol. Energy Mater. Sol. Cells* **2019**, *194*, 215.
- [225] H. Yang, W. Chao, X. Di, Z. Yang, T. Yang, Q. Yu, F. Liu, J. Li, G. Li, C. Wang, *Energy Convers. Manage.* **2019**, *200*, 112029.
- [226] H. Yang, S. Wang, X. Wang, W. Chao, N. Wang, X. Ding, F. Liu, Q. Yu, T. Yang, Z. Yang, *Appl. Energy* **2020**, *261*, 114481.
- [227] W. Wang, H. Cao, J. Liu, S. Jia, L. Ma, X. Guo, W. Sun, *RSC Adv.* **2020**, *10*, 8097.
- [228] L. Xu, Y. Xiong, B. Dang, Z. Ye, C. Jin, Q. Sun, X. Yu, *Mater. Des.* **2019**, *182*, 108006.
- [229] L. Cheng, J. Feng, *Composites, Part A* **2019**, *129*, 105690.
- [230] H. Yang, Y. Wang, Q. Yu, G. Cao, R. Yang, J. Ke, X. Di, F. Liu, W. Zhang, C. Wang, *Appl. Energy* **2018**, *212*, 455.
- [231] H. Yang, W. Chao, S. Wang, Q. Yu, G. Cao, T. Yang, F. Liu, X. Di, J. Li, C. Wang, *Energy Storage Mater.* **2019**, *18*, 15.
- [232] S. Chahal, A. Kumar, F. S. J. Hussain, *J. Biomater. Sci., Polym. Ed.* **2019**, *30*, 1308.
- [233] J. Liu, P. Yu, D. Wang, Z. Chen, Q. Cui, B. Hu, D. Zhang, Y. Li, H. Chu, J. Li, *ACS Appl. Mater. Interfaces* **2020**, *12*, 17957.

- [234] C. Wan, Y. Jiao, W. Tian, L. Zhang, Y. Wu, J. Li, X. Li, *Chem. Eng. J.* **2020**, 393, 124637.
- [235] E. E. Thybring, L. G. Thygesen, I. Burgert, *Cellulose* **2017**, 24, 2375.
- [236] C. Jia, C. Chen, Y. Kuang, K. Fu, Y. Wang, Y. Yao, S. Kronthal, E. Hitz, J. Song, F. Xu, *Adv. Mater.* **2018**, 30, 1801347.
- [237] W. Gan, C. Chen, H. Kim, Z. Lin, J. Dai, Z. Dong, Z. Zhou, W. Ping, S. He, S. Xiao, *Nat. Commun.* **2019**, 10, 5084.
- [238] D. Huang, J. Wu, C. Chen, X. Fu, A. H. Brozena, Y. Zhang, P. Gu, C. Li, C. Yuan, H. Ge, *Adv. Mater.* **2019**, 31, 1903270.
- [239] S. Feifel, O. Stübs, K. Seibert, J. Hartl, *European J. Wood and Wood Products* **2015**, 73, 829.
- [240] X. Xu, K. Jayaraman, C. Morin, N. Pecqueur, *J. Mater. Proc. Tech.* **2008**, 198, 168.
- [241] C. A. Teaca, F. Tanasa, M. Zanoaga, *BioResources* **2018**, 13, 4728.



Anuj Kumar works as a senior scientist at the Natural Resources Institute Finland. He received his B.Sc. in Mathematics and Chemistry from Meerut University (2007), M.Sc. in Wood Science and Technology at Forest Research Institute Deemed University (2009), India, and Ph.D. in Chemical Engineering at Universiti Malaysia Pahang (2013). His research areas are wood composites, wood modification, biotemplated scaffolds, adhesives, coatings, and biobased building materials. He has working experience of postdoctoral research at Czech Technical University in Prague and Linnaeus University Sweden and visiting scientist at Fraunhofer Institute for Wood Research (WKI) and University of Ljubljana.



Tuula Jyske works as a senior scientist and group manager at the Natural Resources Institute Finland. Her research interests include the properties and formation of woody biomass as part of tree growth processes, as well as the potential of woody biomass and forest industry byproducts for various applications. She graduated with a master's degree in environmental sciences in 2003 from the University of Kuopio in Finland. She received her doctoral degree in wood science at the University of Helsinki in Finland in 2008 and achieved the title of docent (equal to the title of associate professor) in 2016.



Marko Petrič received his B.Sc., M.Sc., and Ph.D. degrees in chemistry at the University of Ljubljana, Faculty for Science and Technology, Ljubljana, Slovenia. His B.Sc. and M.Sc. theses were in the field of materials and with his Ph.D., he oriented toward wood protection. He is currently a full professor at the Biotechnical Faculty of the University of Ljubljana, Slovenia. His research interests are related to the field of wood science and technology, more specifically to wood surfaces and their treatments, wood coatings, surface finishing of wood, and protection of wood to abiotic degradation factors.